UNCLASSIFIED

FOR INTERNAL USE ONLY
ORNL
Central Files Number
56-8-206

OAK RIDGE SCHOOL OF REACTOR TECHNOLOGY

REACTOR DESIGN AND FEASIBILITY PROBLEM

HIGH FLUX RESEARCH REACTOR

(HFRR)

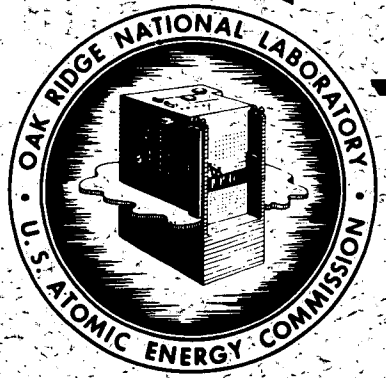

NOTICE

This document contains information of a preliminary nature and was prepared primarily for internal use at the Oak Ridge National Laboratory. It is subject to revision or correction and therefore does not represent a final report.

OAK RIDGE NATIONAL LABORATORY
OPERATED BY
UNION CARBIDE NUCLEAR COMPANY
A Division of Union Carbide and Carbon Corporation
UCC
POST OFFICE BOX X · OAK RIDGE, TENNESSEE

UNCLASSIFIED

DISCLAIMER

UNCLASSIFIED

OAK RIDGE SCHOOL OF REACTOR TECHNOLOGY

Reactor Design and Feasibility Study

"HIGH FLUX RESEARCH REACTOR"
(HFRR)

Prepared by:

R. D. Cheverton, Group Leader
A. W. Charmatz
R. L. Crowther
R. J. Feinberg
G. A. Mortensen
T. G. Schleiter

August 1956

UNCLASSIFIED

Distribution:

1. A. M. Weinberg
2. J. A. Swartout
3. R. A. Charpie
4. Lewis Nelson
5. D. C. Hamilton
6. J. Kerrebrock
7. R. K. Osborn
8. M. E. Whatley
9. P. G. Lafyatis
10. H. Pomerance
11. H. Lurie
12. R. W. Peelle
13. A. Robeson
14. C. O. Smith
15. R. D. Cheverton
16. R. B. Briggs
17. J. A. Lane
18-19. Central Research Library
20-26. ORSORT Files
27-55. Laboratory Records

PREFACE

In September, 1955, a group of men experienced in various scientific and engineering fields embarked on the twelve months of study which culminated in this report. For nine of those months, formal classroom and student laboratory work occupied their time. At the end of that period, these six students were presented with a problem in reactor design. They studied it for ten weeks, the final period of the school term.

This is a summary report of their effort. It must be realized that, in so short a time, a study of this scope can not be guaranteed complete or free of error. This "thesis" is not offered as a polished engineering report, but rather as a record of the work done by the group under the leadership of the group leader. It is issued for use by those persons competent to assess the uncertainties inherent in the results obtained in terms of the preciseness of the technical data and analytical methods employed in the study. In the opinion of the students and faculty of ORSORT, the problem has served the pedagogical purpose for which it was intended.

The faculty joins the authors in an expression of appreciation for the generous assistance which various members of the Oak Ridge National Laboratory gave. In particular, the guidance of the group consultant, J. A. Lane, is gratefully acknowledged.

Lewis Nelson

for

The Faculty of ORSORT

ACKNOWLEDGMENTS

The authors wish to acknowledge the assistance of Drs. Lewis Nelson and R. K. Osborn of the Oak Ridge School of Reactor Technology, Mr. W. E. Kinney of the Applied Nuclear Physics Division, Dr. M. Tobias of the Reactor Experimental Engineering Division, Mr. J. E. Cunningham of the Metallurgy Division, and the staff of the ORACLE. The authors are particularly grateful to the project advisor, Mr. J. A. Lane of the Reactor Experimental Engineering Division, for his valuable aid and advice.

ABSTRACT

This project was initiated for the purpose of determining the feasibility of a high flux, solid fuel research reactor. The following report describes by means of a parameter study a reactor consisting of a cylindrical fuel annulus submerged in heavy water. The thermal neutron flux peaks in the heavy water adjacent to the annulus and is a maximum in the region surrounded by the fuel annulus, while the minimum thermal flux occurs in the annulus. The fast flux has the opposite shape. Calculations indicate that practical peaking factors, ratios of maximum thermal flux in the heavy water to average thermal flux in the fuel annulus, as high as eight can be obtained.

The report also describes a typical reactor in which the maximum thermal and fast fluxes are greater than 10^{15} n/cm^2-sec. 28 References

TABLE OF CONTENTS

LIST OF FIGURES

LIST OF TABLES

INTRODUCTION

The purpose of this study was to investigate the design of an advanced reactor for research and materials testing. The reactor analyzed consisted of an annular array of fuel elements surrounded by heavy water. The thermal neutron flux was expected to peak in the heavy water region surrounded by the fuel annulus and in the heavy water reflector. These regions of high flux surrounding the fuel annulus were to be used for experimental purposes. The following paragraphs summarize the preliminary analysis which led to the selection of this type reactor.

A reactor to be used for research and for testing materials is optimized by maximizing the neutron fluxes. For purposes of analysis the neutron flux can be divided into a fast or fission spectrum flux, an intermediate or dE/E flux, and a thermal flux. Several important experimental uses of neutron fluxes characterized by these spans of energy are as follows: a fast flux is desirable for radiation damage experiments involving non-fissionable materials; an intermediate flux is desirable for experiments with time-of-flight spectrometers and for studying the effects of resonance capture; and a thermal flux is desirable for studying effects of thermal neutron capture on reactor materials, for studying radiation effects on reactor fuel elements, and for studying characteristics of circulating reactor fuels in reactor environment. Many experiments such as the study of transuranic buildup in fertile materials require a combination of thermal and intermediate fluxes.

Fluxes of large magnitude are needed for several reasons. Some experiments involving the measurement of nuclear quantities cannot be performed

accurately without a high flux. A high flux provides a high nvt in a short time which allows one to predict what will happen to certain reactor materials after long irradiation times in lower flux reactors and also provides additional information necessary for determining the effects of the rate of irradiation on materials. One must remember, however, that reactor experiment time involves preparation time as well as irradiation time. Thus, if a testing reactor designed for a high neutron flux is so complicated as to require long down time for experiment preparation, little time has been saved by use of the high flux.

As the thermal flux is increased to higher levels, the power and the burn-up rate increase rapidly. Thus it seems reasonable that the ultimate reactor for research and materials testing may be a circulating fuel type reactor since fuel can be added continuously and heat transfer from the fuel atoms is not such an important problem. However, the various fluid fuel reactors which could be constructed using existing technology have some limitations and require additional development work. Since solid fuel research reactors may involve a lesser development effort, the objectives of this summer study were limited to the analysis of such reactors.

For the reasons discussed above it was concluded that to design a heterogeneous reactor with a flux considerably greater than now available it would be necessary for the high thermal flux region of the reactor to be located other than in the fuel. Preliminary investigations suggested that a possible means of achieving such a design would be by arranging the fuel elements in an annular ring submerged in a low neutron absorbing moderator such as D_2O. The annular ring of fuel acts as a source of fast and intermediate neutrons which are converted into thermal neutrons in the regions external to the fuel annulus.

If the metal to water ratio in the fuel zone is high so as to give adequate leakage of neutrons from the fuel annulus and if there is poor moderation and high thermal absorption in the annulus so as to give a large ratio of fast to thermal flux in the annulus, then appreciable peaking of the thermal flux occurs in the region surrounded by the fuel annulus (hereafter referred to as the moderator) and in the reflector. Since the multiplication constant decreases rapidly with increasing metal to water ratio and since the moderation in the annulus depends largely on the space required for the coolant, the main objective from a nuclear point of view was to maximize the ratio of fast to thermal flux in the fuel annulus.

The thermal flux is proportional to the power per unit mass of fuel, while the fast flux is proportional to the power per unit volume. Therefore, the desired condition in the annulus is obtained by maximizing the fuel concentration and power density. From the heat transfer point of view this meant maximizing the surface area to volume ratio in the fuel elements.

A design study was initiated on a reactor incorporating the concepts summarized in the above paragraph. This reactor was designated the High Flux Research Reactor (HFRR).

SUMMARY OF RESULTS

In summarizing the results of this study it may be beneficial to give a general description of a typical reactor based on the analysis found in this report. References should be made to Figure 1.

A cylindrical fuel annulus, surrounded by D_2O is the basic concept by which a high thermal neutron flux is obtained in a region other than the fuel. The D_2O region in the center of the reactor is called the moderator. In this region a maximum thermal flux peaking exists. Another peak, not so great, exists in the D_2O reflector on the outside of the fuel annulus. The fast flux peaks in the fuel region, where the thermal flux is a minimum. Axial distortion of the flux is reduced by D_2O end reflectors 200 cm thick. The flux distributions are shown in Figure 2.

The highly enriched fuel, in the form of a uranium-aluminum alloy, is incorporated in aluminum clad, plate-type fuel elements. Each elements is three feet long and is in the form of a spiral. Other design features make it possible for each element to rotate continuously during operation of the reactor, resulting in more uniform burnup of the fuel. Pairs of elements are located in aluminum fuel element housings which are grouped to form the fuel annulus. They are secured by plugging into a plenum chamber at the bottom of the reactor tank.

Cooling of the reactor is accomplished with heavy water that enters through the bottom of the reactor tank. Water is directed through the fuel element housings as well as against the outer surfaces of the housings. The latter is accomplished by means of baffle plates which may also serve to direct coolant flow for experiments suspended in the moderator and reflector regions. Pressurization of the coolant in the fuel element housing is obtained by means of the circulating pump head and the pressure drop across an orifice at the outlet end of the housing. The hot water discharges from the orifice into the moderator

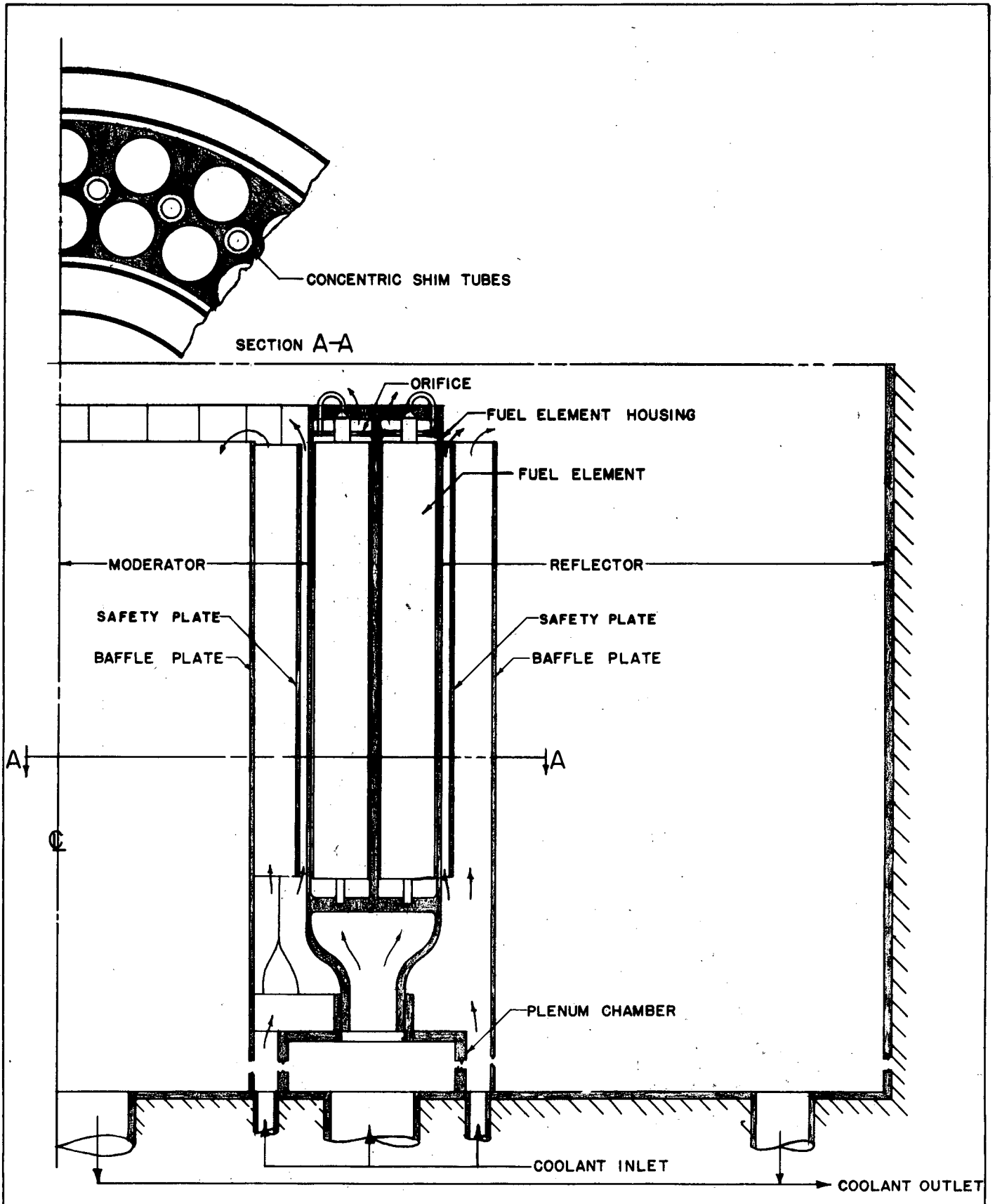

FIG. 1 QUARTER SECTION OF HFRR CORE

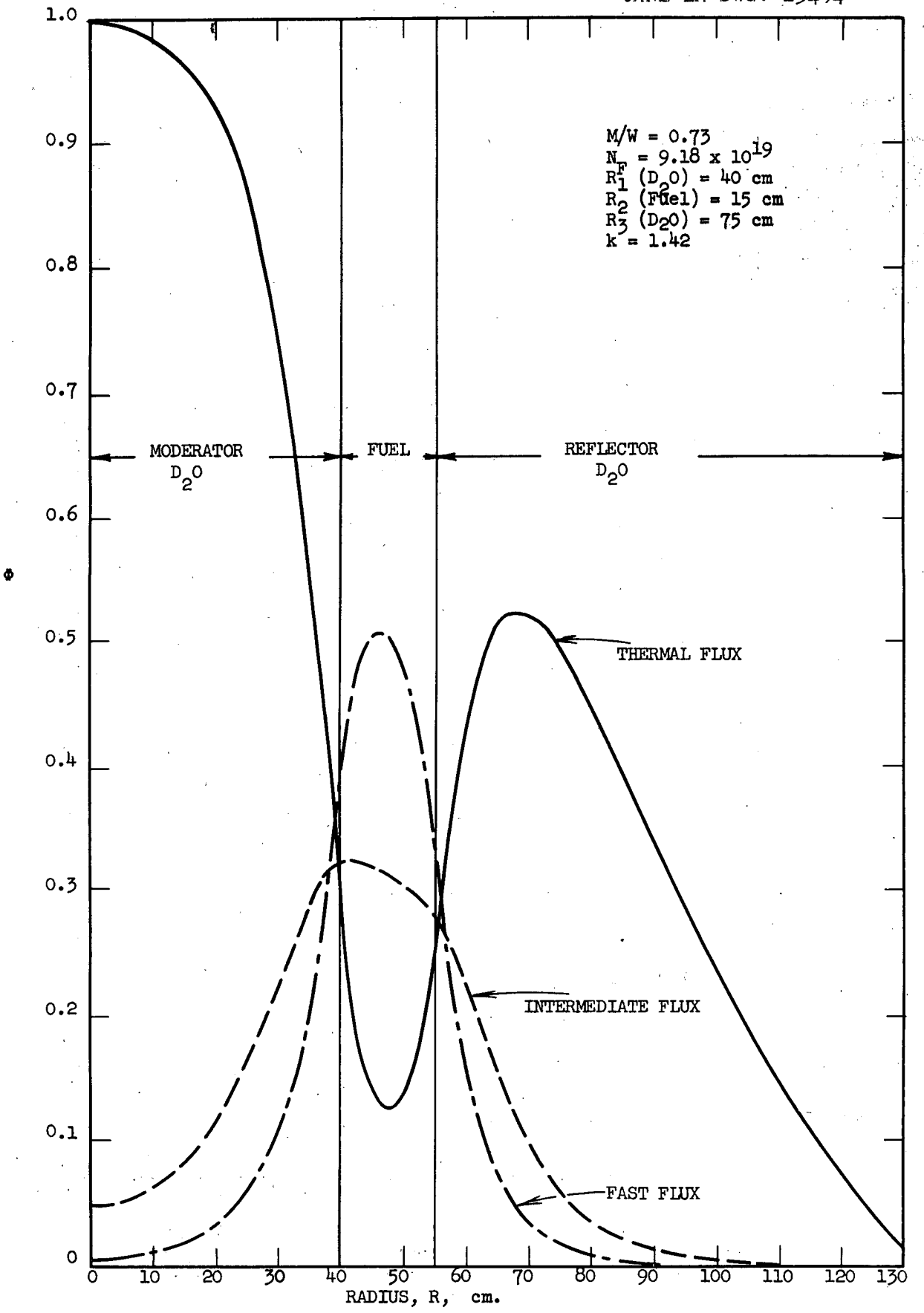

Fig. 2 FAST, INTERMEDIATE, AND THERMAL FLUXES VS. RADIUS FOR THE REFERENCE CASE.

and reflector regions which are at essentially atmospheric pressure and is then circulated through heat exchangers. A secondary system of light water removes the heat from the heavy water to cooling towers or some other suitable sink.

Complete control of the reactor is accomplished by means of: two one-quarter inch thick steel or aluminum clad cadmium segmented cylindrical safety elements adjacent to the inside and outside circumferences of the fuel annulus; twenty-one stainless steel shim tubes, located between fuel element housings which contain a continuously circulating aqueous boric acid solution for shim control and burnable poison, the concentration of which can be varied during reactor operation; and four or more steel or aluminum clad cadmium regulating rods located in empty shim tubes. Safety and regulating elements are driven from the bottom of the reactor. Each safety shell is worth seventy percent reactivity, each boric acid tube zero to two percent reactivity, and each regulating rod one half percent reactivity.

Shielding directly above the reactor consists of 200 cm of D_2O, 18 cm of iron thermal shield and 295 cm of concrete. One day after shutdown remote handling of experiments through holes in the concrete is required and is accomplished inside a cylindrical tank, purged with helium. During operation of the reactor at 500 Mw power, a person can stand on the concrete over the reactor.

A small inert gas space is provided above the D_2O for continuous removal of deuterium and oxygen produced by radiolytic decomposition.

Based on the analysis in this report, the following detailed information approximately represents the maximum conditions for the reactor just described:

Average thermal flux in fuel annulus	6.12×10^{14}
Maximum thermal flux in center region	4.81×10^{15}
Maximum thermal flux in reflector	2.45×10^{15}
Average fast flux in fuel annulus	2.36×10^{15}
Average intermediate flux in fuel annulus	1.46×10^{15}
U-235 concentration in the fuel elements	1.3×10^{20} atoms/cm^3
	9.8 mg/cm^2
Fuel loading	14.5 kg
Reactor power	425 Mw
Fuel cycle time	10 days
Average power density	1500 watts/cm^3
	1.45×10^8 Btu/hr ft^3
Specific power	31,000 Kw/Kg
Maximum power density	3.48×10^8 Btu/hr ft^3
Average heat flux	4.69×10^5 Btu/hr ft^2
Maximum heat flux	1.13×10^6 Btu/hr ft^2
Coolant velocity	30 ft/sec
Maximum fuel element surface temperature	350°F
Coolant inlet temperature	100°F
Average coolant exit temperature	200°F
Pressure drop across orifice	260 psi
Moderator radius, R_1	40 cm
Annulus width, R_2	21 cm
Reflector width, R_3	75 cm
Length of fuel zone, 2H	3 ft

Diameter of fuel elements	3.5 in.
Number of fuel elements	50
Total volume of fuel elements	$2.85 \times 10^5 cm^3$
Thickness of fuel plate, W	.030 in.
Thickness of coolant channel, E	.045 in.
Coolant circulation rate	62,000 gpm
Pressure drop across fuel element	62 psi
Wt.% of U in U-Al alloy	12.5%
M/W in fuel elements	.667
Average thermal flux in ten cm diameter experiment placed at center of reactor	
Thorium	5.8×10^{14}
Iron	5.2×10^{14}
MTR fuel element (9×10^{19} atoms U-235/cm^3)	2.2×10^{15}
Aluminum, sodium	2.8×10^{15}
Beryllium	3.9×10^{15}

It should be emphasized that the reactor described above has not necessarily been optimized because of the many variables involved.

Research reactors which have been designed for materials testing have generally been of one type -- light water moderated and cooled, highly enriched reactors, using plate-type fuel elements. The Materials Testing Reactor, the Oak Ridge Research Reactor, the Low Intensity Test Reactor, the Bulk Shielding or Swimming Pool Reactor, the Westinghouse Test Reactor, and the Engineering Test Reactor are reactors of this type. An exception is the CP-5 type reactor which is heavy water moderated and cooled. In contrast to the HFRR design these

reactors have been designed to attain a combination of fast and thermal fluxes, and the experimental volume of these reactors is generally located within the fuel zone. In Table 1 some of the important features of these reactor designs are summarized for comparison with the typical design which was completed on the HFRR.

TABLE 1

Comparison of Reactor Parameters

Reactor Designation	Power	Max. Thermal Flux	Max. Inter. Flux	Max. Fast Flux	Specific Power	Power Density	Max. Heat Flux
	Kw	$n/cm^2/sec$	$n/cm^2/sec$	$n/cm^2/sec$	Kw/Kg 25	Kw/l	$Btu/hr\ ft^2$
LITR	3,000	$4x10^{13}$			880	31	
BSR	100	$2x10^{12}$	$3x10^{11}$	$1x10^{11}$	30	1.1	
MTR	40,000	$5.3x10^{14}$			8,900	390	
ETR	175,000	$6.05x10^{14}$	$8.5x10^{14}$	$1.7x10^{14}$	10,000	590	$1.15x10^6$
CP-5	1,000	$1.7x10^{13}$	$1x10^{13}$	$1x10^{12}$	870	6	
HFRR	425,000	$4.81x10^{15}$	$1.55x10^{15}$	$2.59x10^{15}$	31,000	1500	$1.13x10^6$

REACTOR PHYSICS

The purpose of the nuclear analysis of the HFRR was to determine the more important variables leading to a maximum thermal neutron flux in the center region or "flux trap." A parameter study was undertaken in an effort to optimize the design and gain a preliminary insight to the more important problems associated with this reactor. The effect of the size of the regions and the concentrations of various components in each region on the critical mass and the flux distribution was studied. Approximate flux perturbations resulting from experiment insertion were determined.

Calculations were made to determine a feasible control system for the HFRR. Xenon instability, burnup, and the temperature coefficient of reactivity were investigated as they appeared to be possible limitations to a high flux reactor design.

A three-group, three region ORACLE[a] code (1)[b] was used extensively to evaluate many of the nuclear characteristics of the HFRR. Two-group calculations were used for some of the systems investigated which employed light water. The regions were assumed to be homogeneous, and corrections were not made for self-shielding in the fuel assemblies. Thirty-group "Eyewash"(2) cross-sections were flux averaged to determine the three-group constants. Integrated fluxes versus lethargy were obtained from previous UNIVAC calculations(3) for somewhat similar systems and were assumed to be correct. Critical experiments were calculated to determine the adequacy of the method of preparing group constants. These calculations indicated that within the assumptions made the HFRR calculations were

---

a Oak Ridge Automatic Computer and Logical Engine.

b Refers to List of References.

accurate within about 15 percent. A detailed summary of the nuclear analysis is presented in Appendix II.

An optimum HFRR was not determined as a result of the calculations which were completed. The nuclear analysis indicated that the criteria for maximum thermal flux peaking in the experimental zones was a maximum ratio of fast and intermediate flux to thermal flux in the fuel zone. The thermal flux in the fuel region is proportaional to P/M (specific power), where P is the total power, and M is the mass of U^{235}. The fast and intermediate fluxes are proportional to P/V (power density), where V is the fuel annulus volume[4]. Therefore, in order to maximize the ratio of fast and intermediate flux to thermal flux in the fuel region, M/V or the ratio of mass of U^{235} to the fuel element volume should be maximized. From the heat transfer standpoint this requires maximizing the power density which is the same as requiring a maximum surface area to volume ratio in the fuel elements. From the nuclear standpoint this means minimizing the specific power or power output per kilogram of U^{235}. This requires a maximum fuel concentration which, if not fixed by power removal considerations, is determined by the amount of excess reactivity which can be controlled. Because of the many variables involved in fuel element design and because of the strong dependance of the heat transfer on the thermal flux distributions within the fuel region, it is very difficult and time consuming to determine the balance of materials, reactor size, heat transfer, and physics which results in peak performance. The flux shapes of the HFRR will continuously change with time, which further complicates the problem. Considerable error can be introduced by assuming homogeneous regions and uniform burnup, and neglecting effects of regulating rods. Therefore, in order to optimize this reactor one should make use of a two

or three-dimensional reactor code. Such an analysis was beyond the scope of this summer study. The calculations which were completed should give an adequate indication of the general trend to be expected from the variation of the many variables associated with the HFRR. The results of the calculations are summarized in the following paragraphs.

Materials and Size Selection

The primary object of investigating variations in the materials to be used in the moderator, fuel, and reflector regions was to determine the proper materials and concentrations necessary to give a maximum ratio of the maximum thermal flux in the experimental regions to the average thermal flux in the fuel region.

Fuel Region: Initial analysis concerning selection of a coolant for the fuel region indicated that light water would be desirable from the standpoint of minimizing D_2O holdup, and D_2O would be desirable from the standpoint of not requiring a leak tight system between the fuel region and the heavy water regions. The decision as to which was to be used was based on the criteria of maximizing the thermal neutron flux peaking in the experimental zones. It appeared that the central and reflector regions would serve as a source of thermal neutrons for the fuel region. Since the thermal neutrons in the regions external to the fuel originate as fast and intermediate neutrons in the fuel, the fast and intermediate neutron leakage out of the fuel region should be made as high as possible. Also, the thermal neutron gradient within the fuel is important from the standpoint of making the average thermal neutron flux in the fuel small with respect to the thermal flux in the experimental zone. Heavy water has a greater slowing down length than light water; and hence, the fast leakage should be greater for a D_2O cooled system. However, light water has a higher absorption cross-section than

heavy water and hence, the thermal neutron gradient in the fuel region should be steeper for light water. Thus, the question was whether the high fast leakage of the heavy water system or the high thermal absorption of the light water system was more desirable from the standpoint of achieving maximum thermal flux peaking.

This was investigated using the 3G3R ORACLE code and it was found that in terms of thermal flux peaking heavy water was a better coolant for the fuel region. This is illustrated in Figure 3. Figures 5 and 6 show that in the fuel region the ratio of the maximum to the average thermal flux is greater and the ratio of the average fast to the average thermal flux is smaller for light water coolant. Thus, although the gradient of the thermal flux in the fuel region was greater for the H_2O cooled system, the greater fast leakage of the D_2O cooled system produced higher peaking. It should also be mentioned that a large thermal flux gradient in the fuel results in a greater degree of non-uniform fuel burnup and in more difficult power removal problems. Therefore, the lower thermal flux gradient of the D_2O cooled reactor is an added advantage of this system.

As a result of this preliminary analysis pertaining to coolant selection it was concluded that the important criteria for maximum thermal flux peaking in the experimental regions was a maximum ratio of fast and intermediate flux in the fuel region to thermal flux in the fuel region.

Parameters which can be varied in the fuel region are metal to water ratio, thickness and volume of the fuel region, and fuel concentration. An increase in the metal to water ratio in the fuel region decreases the moderating properties of this region. Therefore, based on the previous analysis, the thermal flux peaking should increase with metal to water ratio. This was verified by ORACLE calculations and is illustrated in Figures 7 and 8. However, it must be

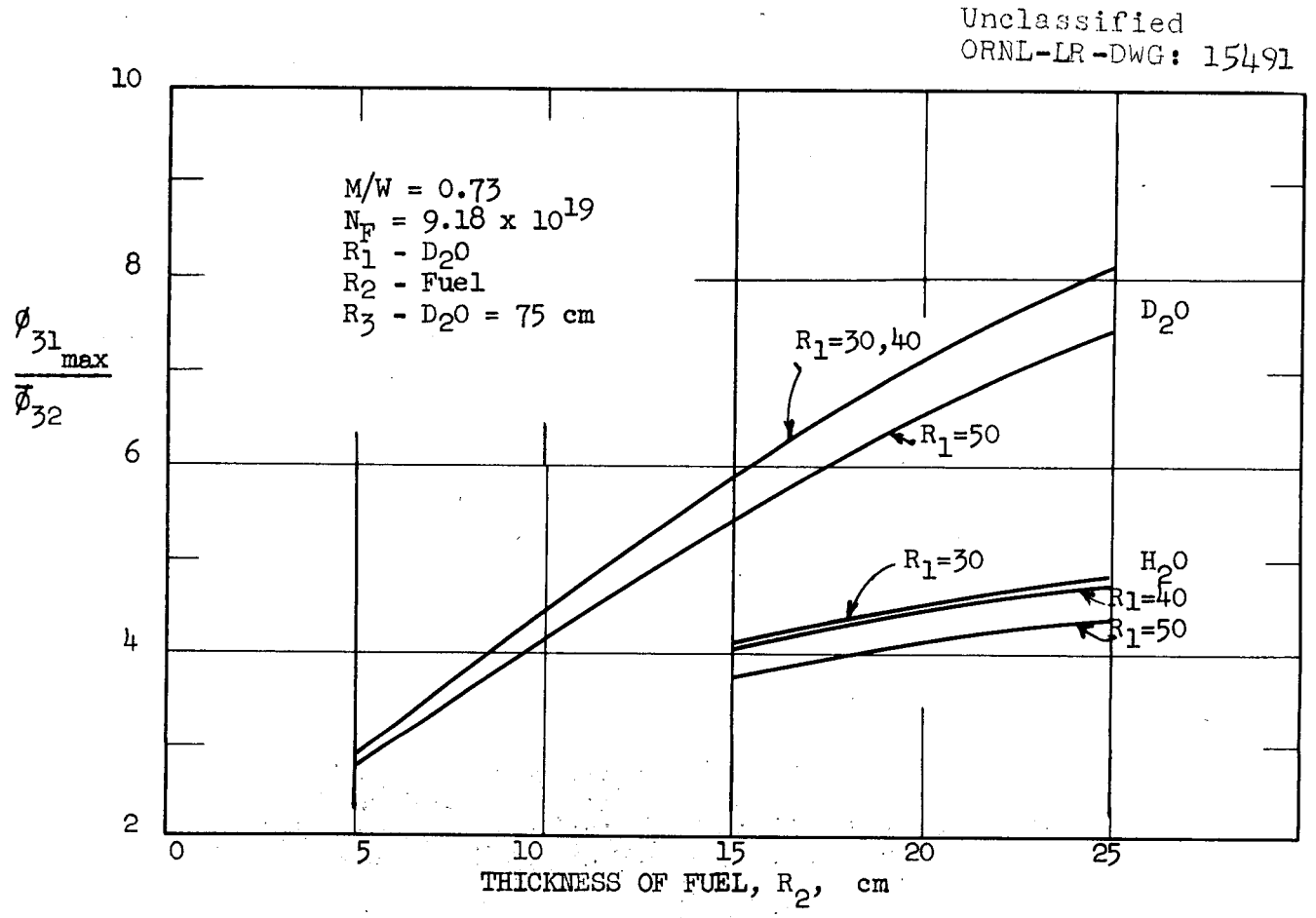

Fig. 3 RATIO OF MAXIMUM THERMAL FLUX IN CENTER REGION TO AVERAGE THERMAL FLUX IN THE FUEL, FOR DIFFERENT DIAMETERS OF CENTER REGION AND FOR LIGHT AND HEAVY WATER

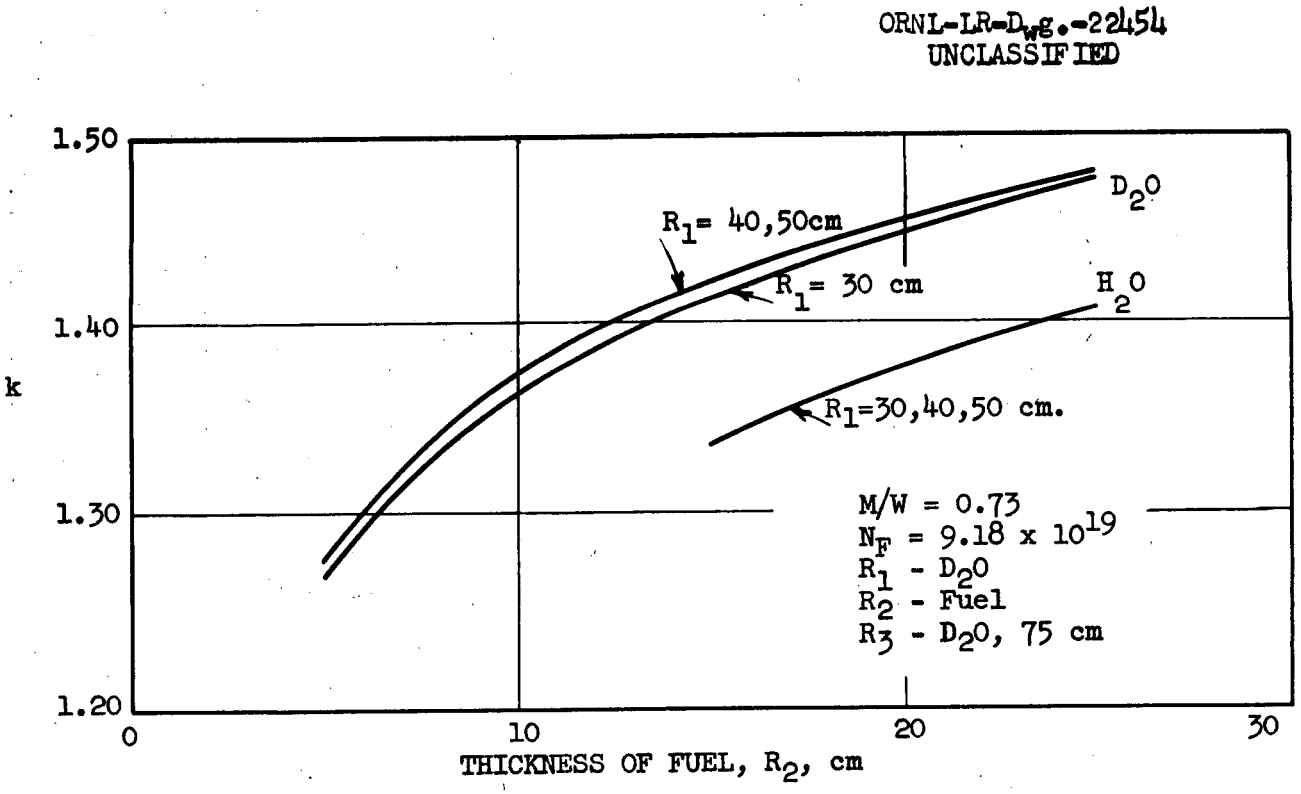

Fig. 4 MULTIPLICATION CONSTANT VS. THICKNESS OF FUEL ANNULUS FOR VARIOUS INSIDE DIAMETERS AND LIGHT AND HEAVY WATER

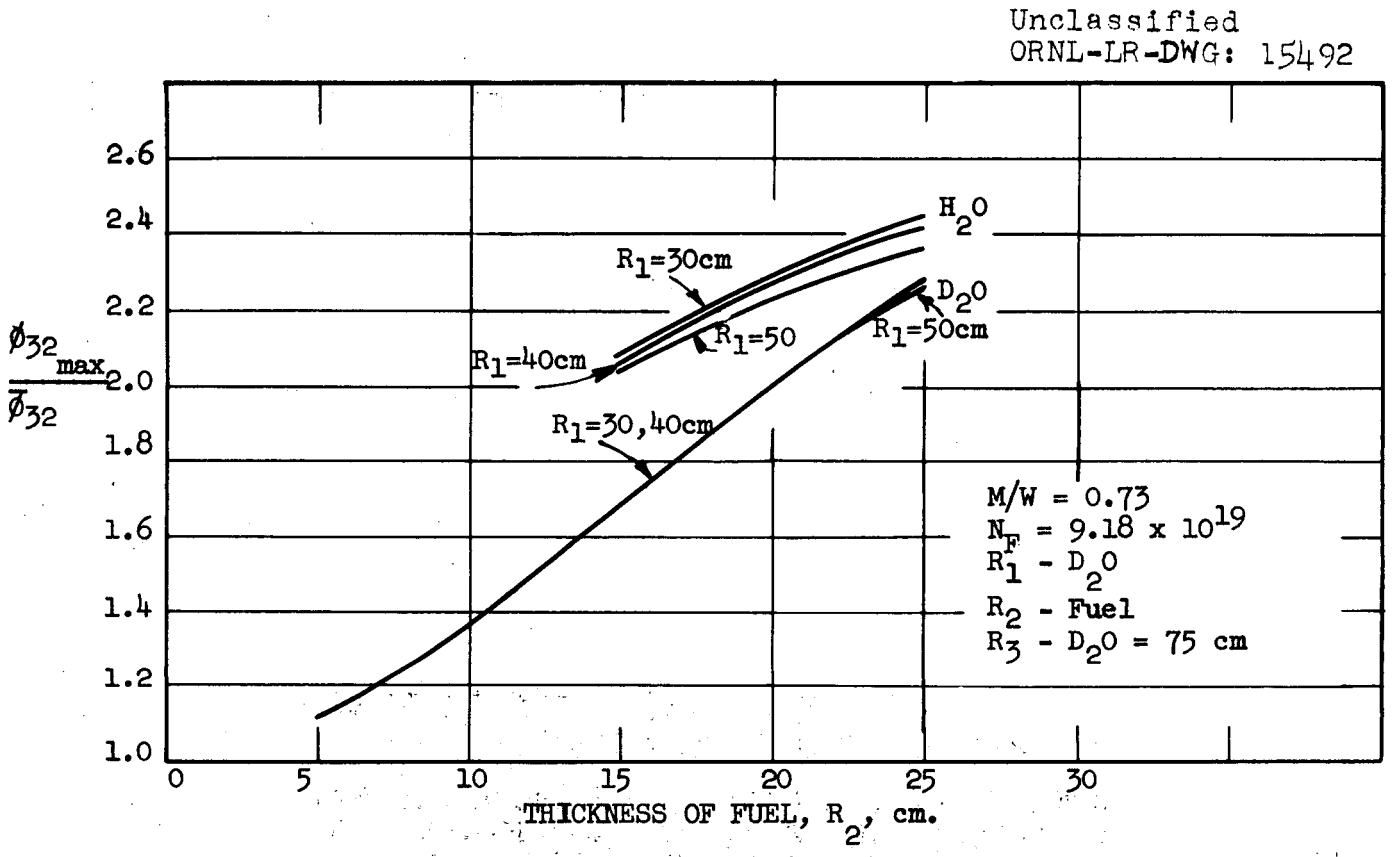

Fig. 5 RATIO OF MAXIMUM THERMAL FLUX IN FUEL TO AVERAGE THERMAL FLUX IN FUEL, VS. THICKNESS OF FUEL REGION FOR VARIOUS INSIDE DIAMETERS AND LIGHT AND HEAVY WATER IN FUEL REGION

ORNL-LR-Dwg.-22455
UNCLASSIFIED

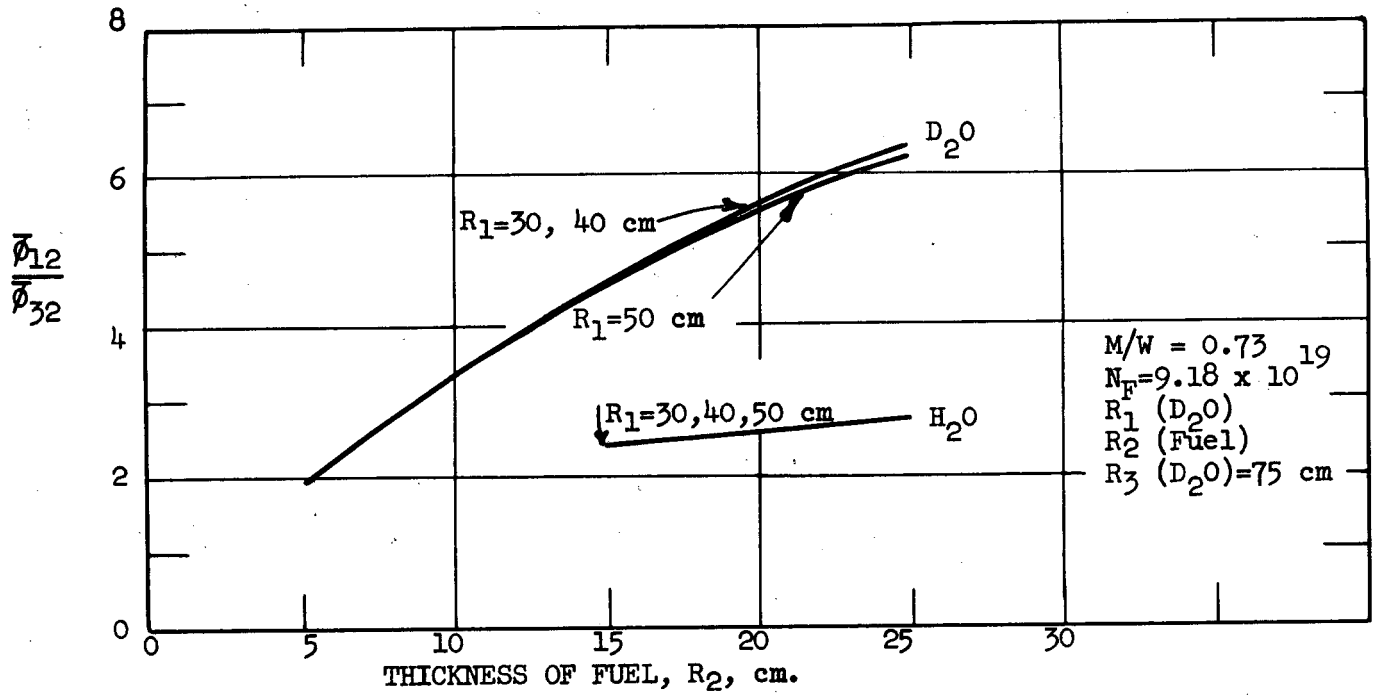

Fig. 6 RATIO OF AVERAGE FAST FLUX IN FUEL TO AVERAGE THERMAL FLUX IN FUEL VS. THICKNESS OF FUEL REGION FOR VARIOUS INSIDE DIAMETERS AND HEAVY AND LIGHT WATER IN FUEL REGION

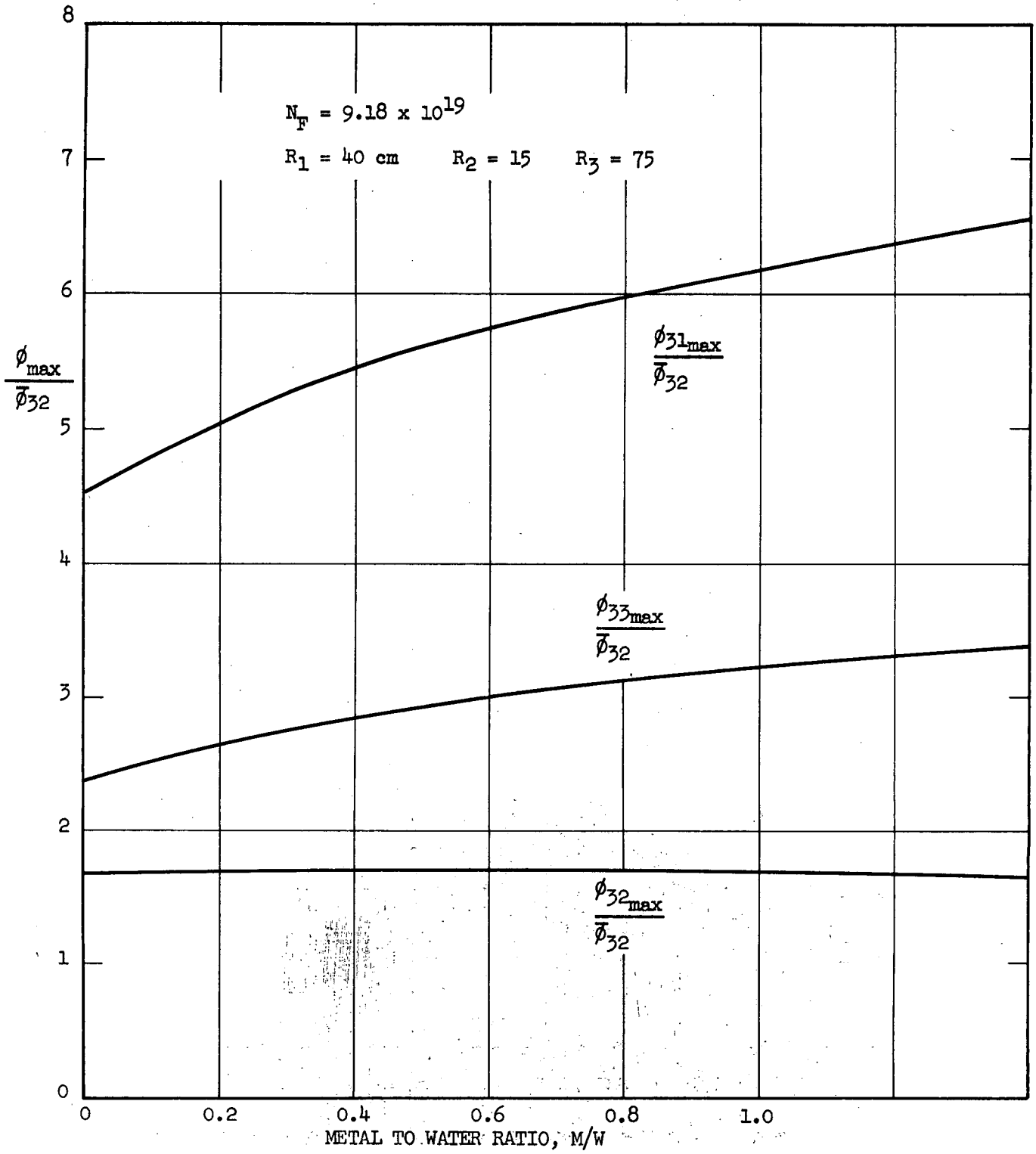

Fig. 7 RATIOS OF PEAK THERMAL FLUX IN CENTRAL REGION, IN FUEL ANNULUS, AND IN REFLECTOR TO AVERAGE THERMAL FLUX IN FUEL VS. METAL TO WATER RATIO

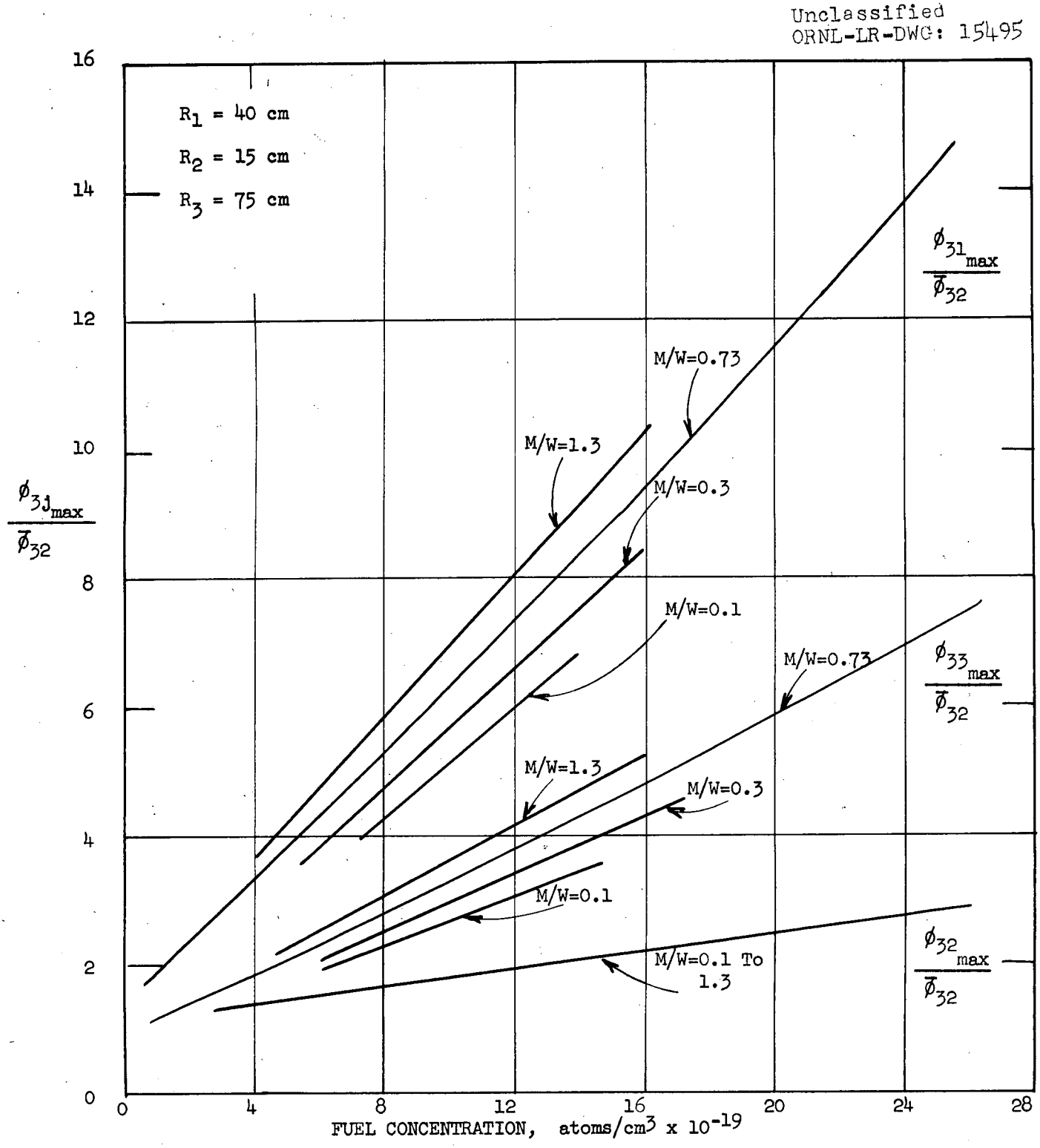

Fig. 8 RATIOS OF MAXIMUM THERMAL FLUX IN CENTRAL REGION, IN FUEL ANNULUS, AND IN REFLECTOR TO AVERAGE THERMAL FLUX IN FUEL, VS. FUEL CONCENTRATION FOR VARIOUS METAL TO WATER RATIOS

remembered that the effective multiplication constant is rapidly reduced by an increase in the metal to water ratio as shown in Figure 9.

The effect of varying the fuel zone thickness is shown in Figures 3, 4, 5, and 6. For a constant fuel concentration, an increase in fuel zone thickness increases the multiplication constant, the ratio of the maximum thermal flux in the center region to the average thermal flux in the fuel, the ratio of the maximum thermal flux in the fuel to the average thermal flux in the fuel, and the ratio of the average fast flux in the fuel to the average thermal flux in the fuel. It appears that for the D_2O system the primary effect of an increase in fuel annulus thickness is to increase the fast and intermediate leakage out of the fuel zone because of the increased total mass of U^{235}.

If the fuel concentration in the fuel zone is increased, the thermal flux peaking increases. This is illustrated in Figure 8. It is interesting to note that the ratio of the maximum to average thermal flux in the fuel does not change as rapidly with an increase in fuel concentration, indicating that increased leakage of fast and intermediate neutron flux out of the fuel zone rather than the change in thermal flux gradient is the primary cause of the increased peaking.

The effect of decreasing fuel concentration with time on the thermal, intermediate, and fast flux spacial distributions is illustrated in Figures 10, 11, and 12. Constant power operation and uniform radial fuel burnup were assumed. Even though the thermal flux peaking decreases with a decrease in fuel concentration, the increase in the thermal flux in the fuel zone more than compensates. If there were non-uniform fuel burnout, the fuel at the edges of the fuel zone would be depleted more rapidly than the fuel in the center. This would effectively decrease the thickness of the fuel zone with time. In Figure 3 it was shown that

ORNL-LR-Dwg.-22457
UNCLASSIFIED

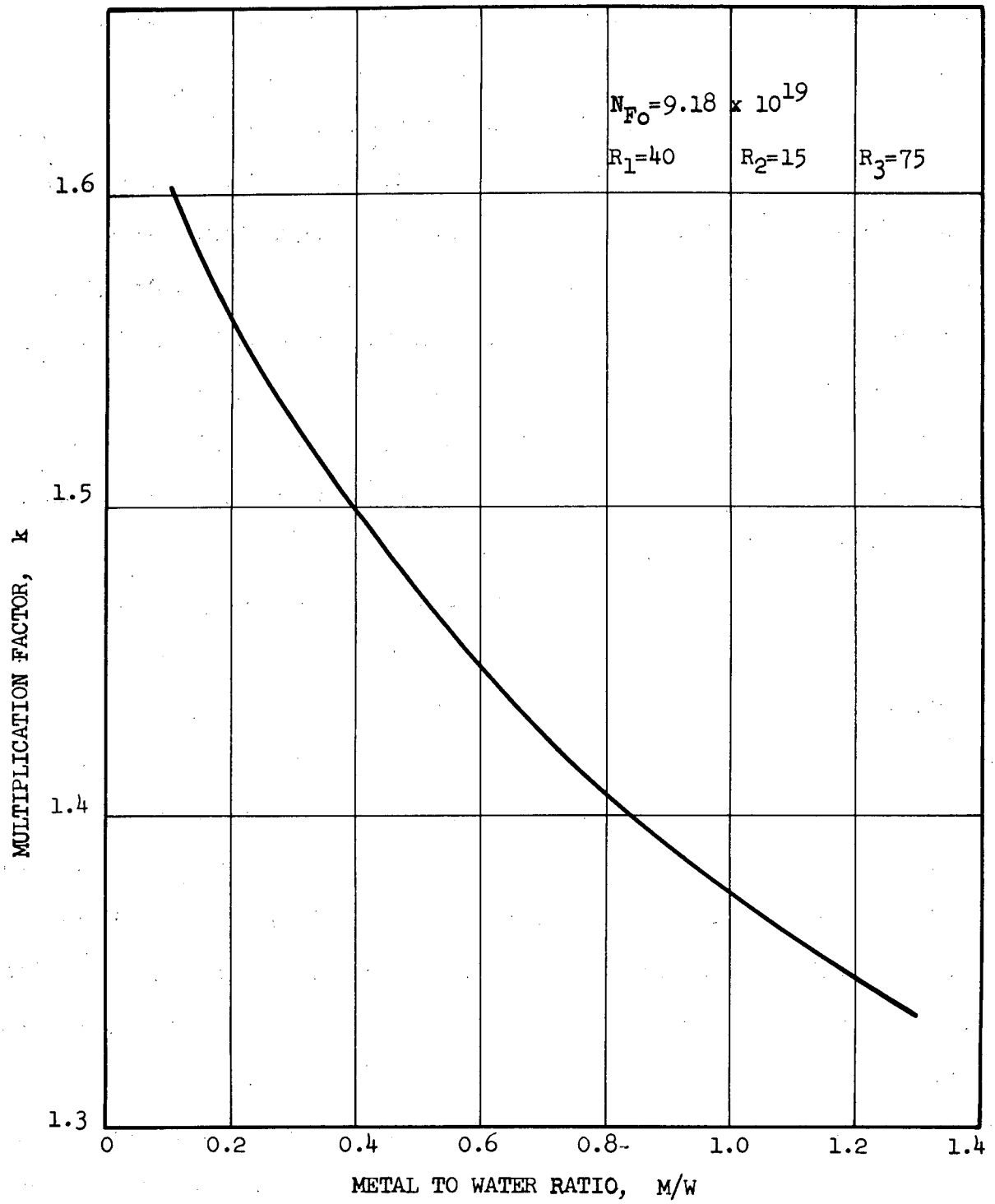

Fig. 9 METAL TO WATER RATIO Vs. MULTIPLICATION FACTOR

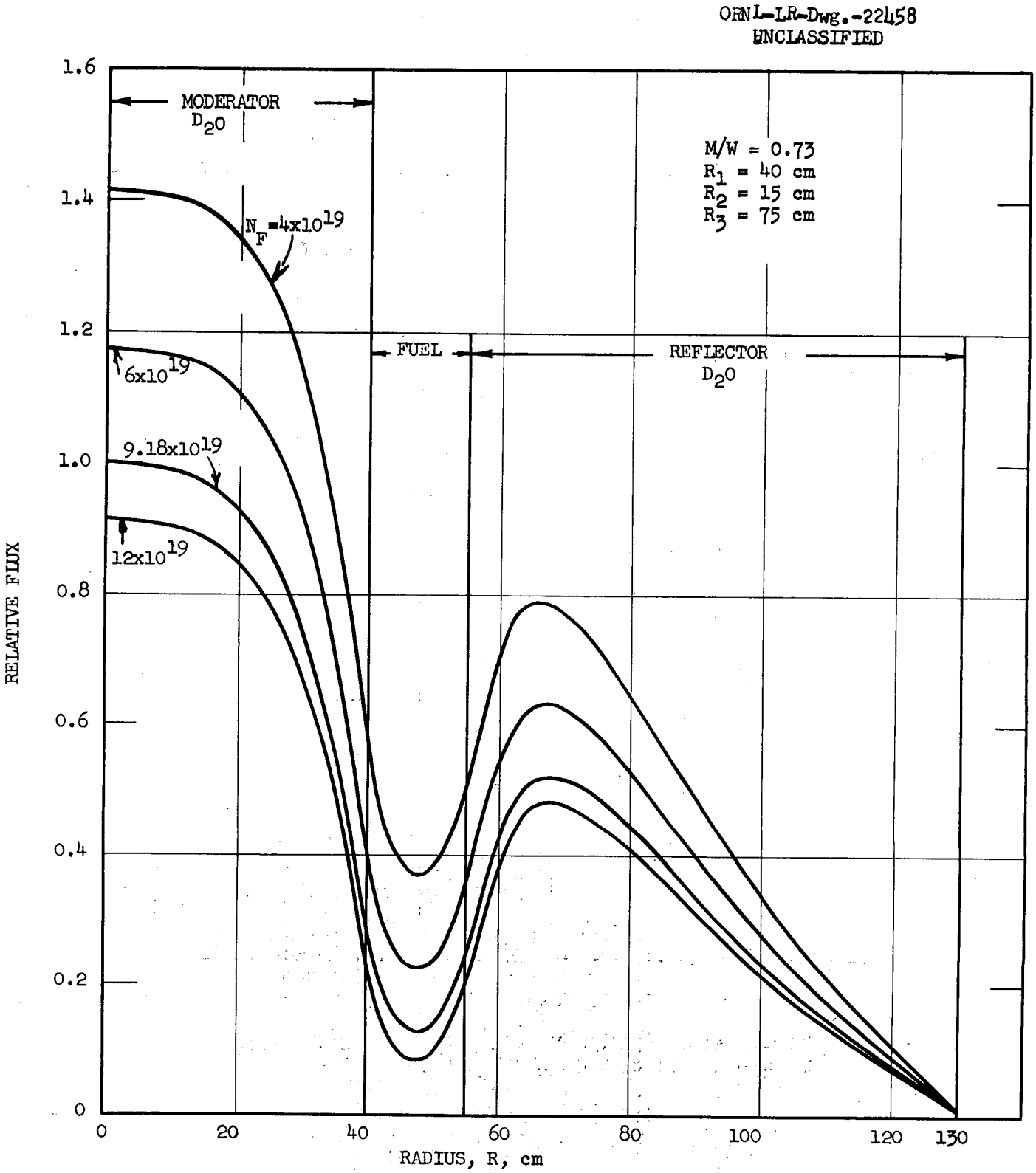

Fig. 10 CONSTANT POWER SPATIAL THERMAL NEUTRON FLUX DISTRIBUTIONS FOR VARIOUS FUEL CONCENTRATIONS

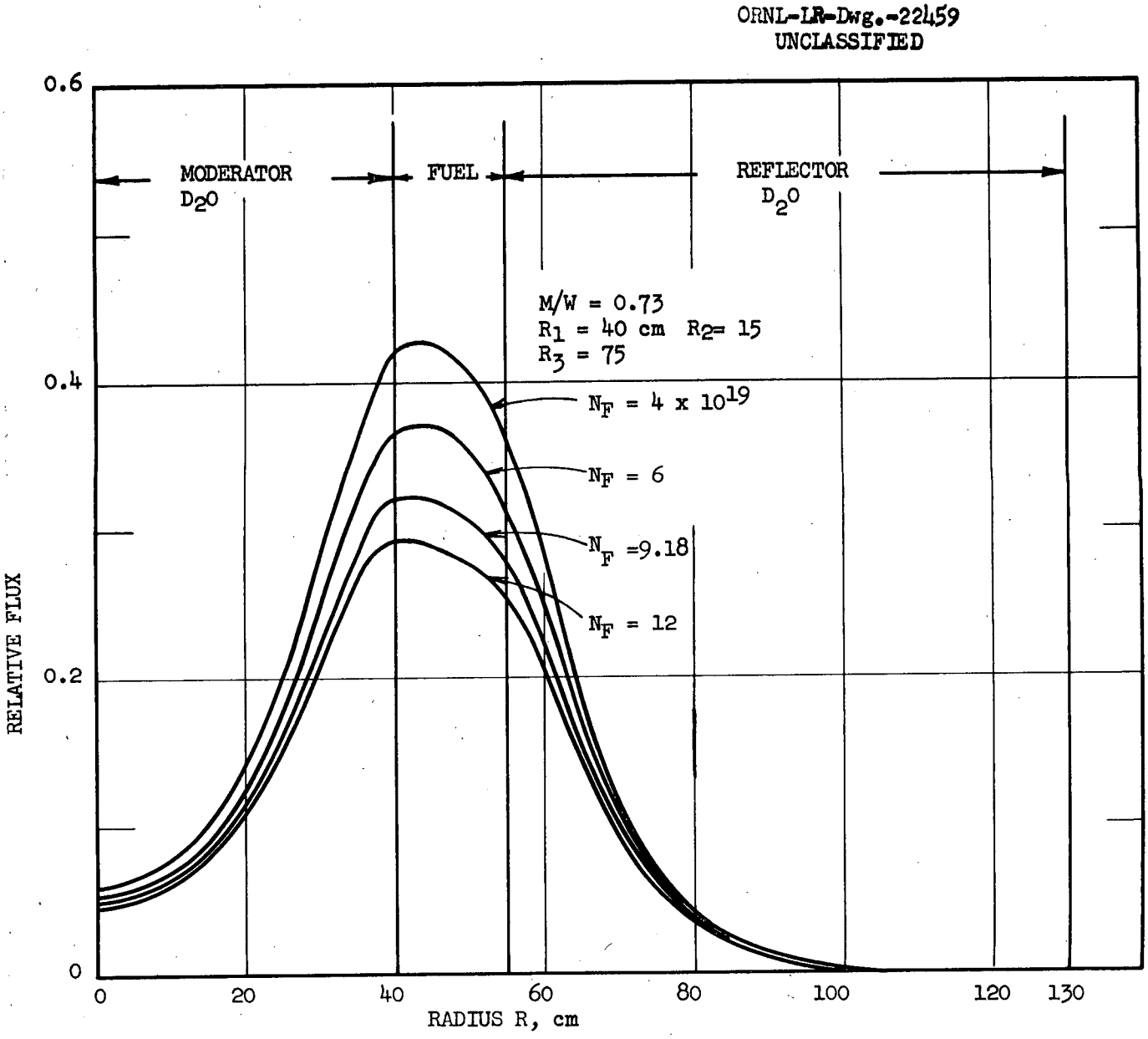

Fig. 11 CONSTANT POWER INTERMEDIATE NEUTRON FLUX SPATIAL DISTRIBUTION FOR VARIOUS FUEL CONCENTRATIONS

ORNL-LR-Dwg.-22460
UNCLASSIFIED

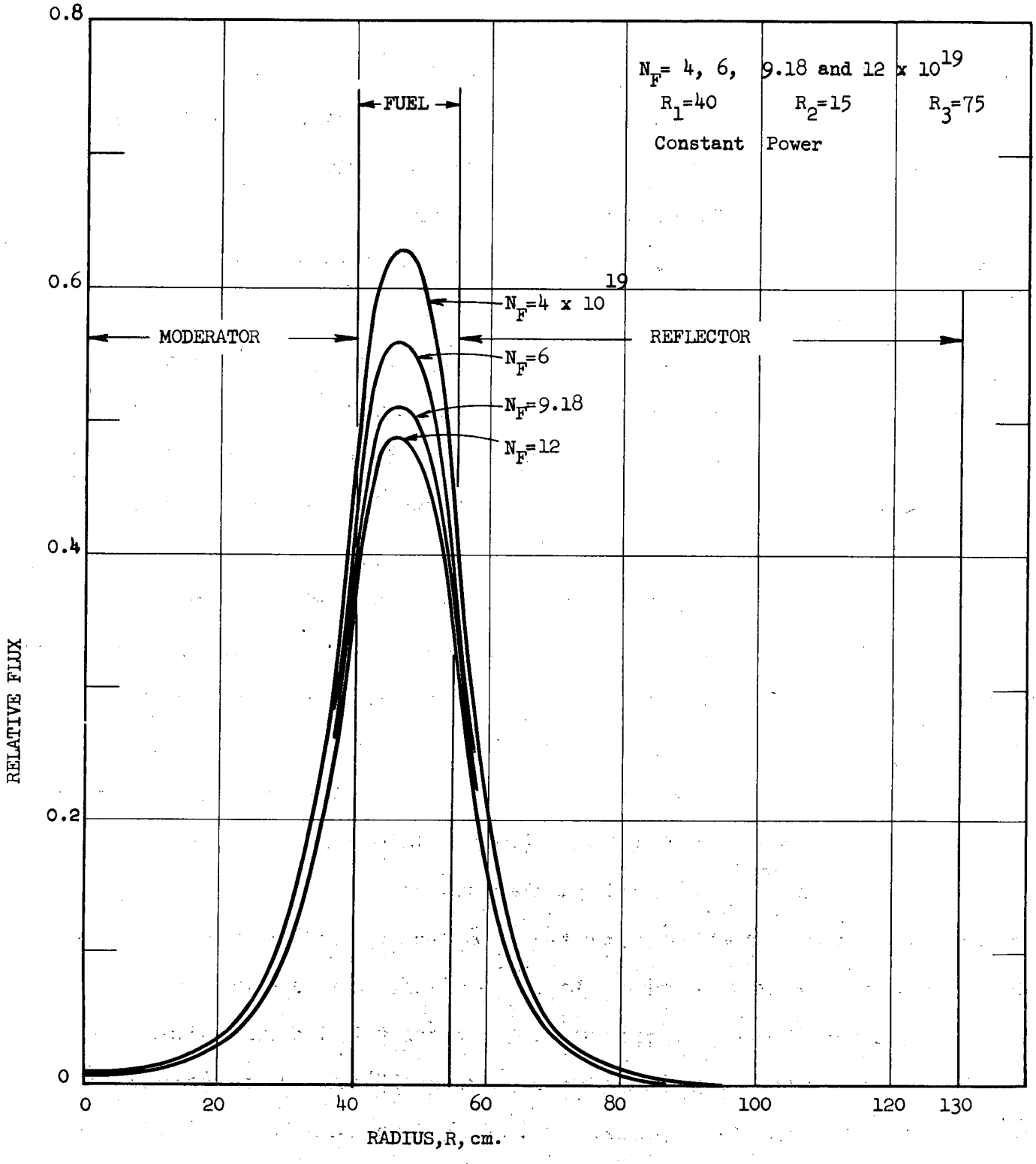

Fig. 12 CONSTANT POWER FAST NEUTRON FLUX SPATIAL DISTRIBUTION FOR VARIOUS FUEL CONCENTRATIONS

a decrease in fuel region thickness decreases the thermal flux peaking. This indicates that uniform burnout is desirable in order to obtain the maximum nvt in the experimental zones. The effect of the fuel zone thickness becomes less important with decreasing fuel concentration so that a multi-region code would be desirable to evaluate all the ramifications of the change in thermal flux peaking with time.

A possible method of obtaining uniform radial fuel burnup would be to continuously rotate fuel elements in the fuel zone, during operation of the reactor. However, it would be necessary to balance the engineering difficulties of this type of fuel element with the gain in thermal flux peaking in order to determine its feasibility.

The variation of the multiplication constant with fuel concentration is shown in Figure 13. The cold clean critical mass for the particular core considered is about 3.2 kilograms which corresponds to a fuel concentration of 2×10^{19} atoms per cm^3. For these calculations, the uranium in the fuel region was assumed to be distributed homogeneously. In the practical reactor the U^{235} would be lumped in fuel plates and then these plates would be arranged in separate cylindrical assemblies. In order to maintain the same mass of uranium the fuel concentration in the assemblies would be higher than in the homogeneous annulus. This decreases the effectiveness of the U^{235} and results in a higher critical mass.

As previously shown the increased concentration in the cylindrical fuel assemblies, as compared to the homogeneous annulus with the lower concentration but the same mass, results in an increased ratio of maximum thermal flux in the experimental zones to the average thermal flux in the fuel. This peaking will not be as high as for a homogeneous annulus of the same fuel concentration because

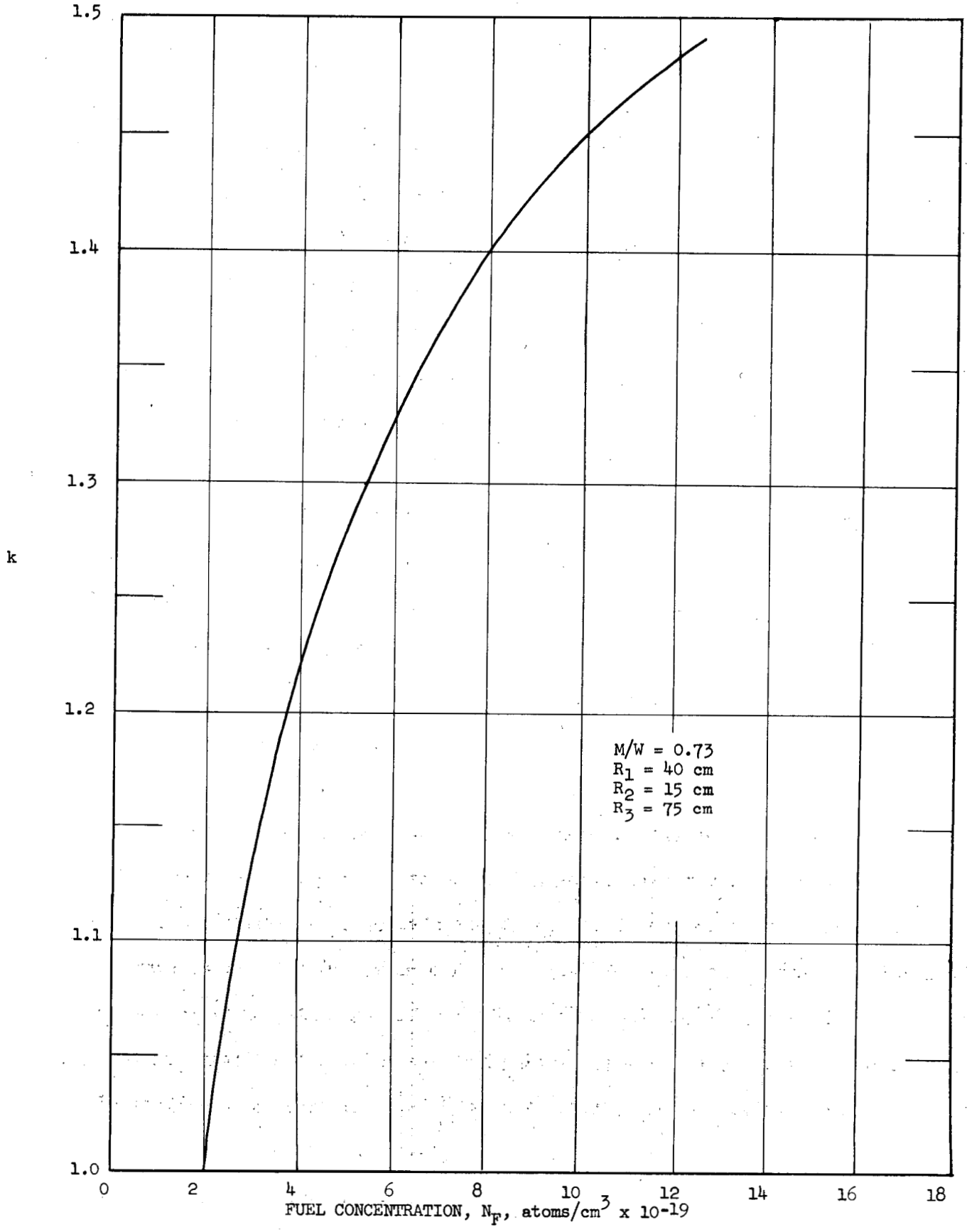

Fig. 13 MULTIPLICATION FACTOR VS. FUEL CONCENTRATION

the circular fuel assemblies expose more surface area to the neutron current available at their boundaries. For the same reason the ratio of the maximum to average thermal flux in the fuel zone will be lower for the heterogeneous assembly as compared to a homogeneous annulus of the same concentration.

In summarizing the preceding discussion, it is concluded that, in order to attain maximum thermal flux peaking the fuel concentration, the metal to water ratio and the width of the fuel zone should be maximized. To attain a maximum multiplication constant for a given fuel loading the metal to water ratio should be decreased.

Central Region or "Moderator": Heavy water appeared to be an obvious choice for the central region because of its low neutron absorption cross-section. For comparison purposes calculations were made using D_2O, beryllium, and aluminum. Figure 14 shows the variation of the spatial thermal flux distribution with varying percentages of heavy water and beryllium in the center region. These curves are normalized to constant power in the fuel region. The effect of the beryllium on the multiplication constant is shown in Figure 15. Figures 16, 17, and 18 show a comparison of the spatial distributions of fast, intermediate, and thermal fluxes for beryllium, D_2O, and aluminum in the center region. If a high thermal flux is desired, heavy water is the ideal material for the central region. If a high intermediate or fast flux is desired, then heavy water could be partially replaced with carbon, aluminum, or some other material with poorer moderating properties. Figure 19 shows the variation of the ratios of the maximum thermal fluxes to the average thermal flux in the fuel for varying concentrations of D_2O and Al in the center region. Figure 20 illustrates the ratio of the fast and intermediate fluxes in the center region to the fast and intermediate fluxes

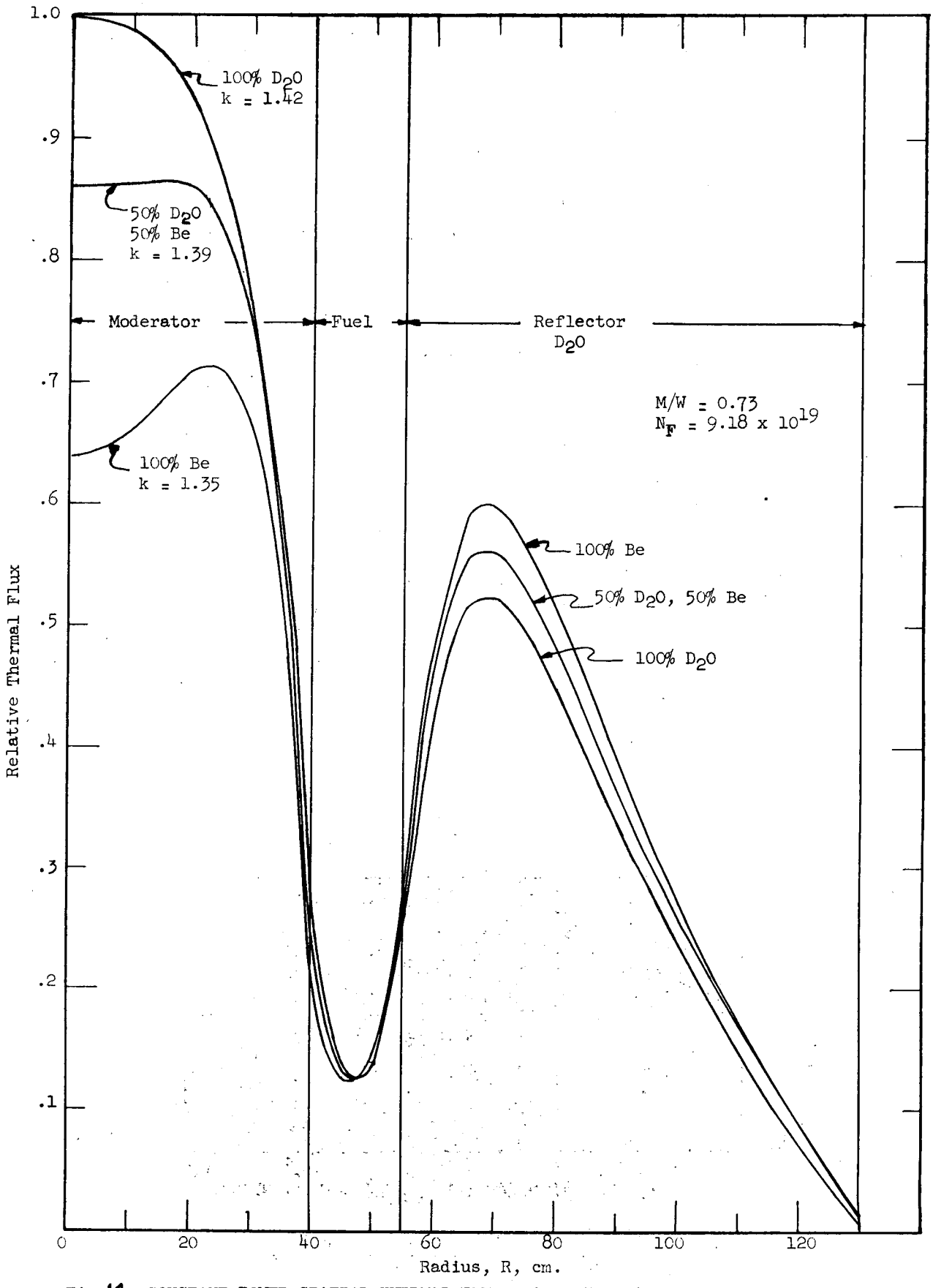

Fig. 14 CONSTANT POWER SPATIAL THERMAL FLUX DISTRIBUTIONS FOR VARIOUS CONCENTRATIONS OF HEAVY WATER AND BERYLLIUM IN THE CENTER REGION

ORNL-LR-Dwg.-22463
UNCLASSIFIED

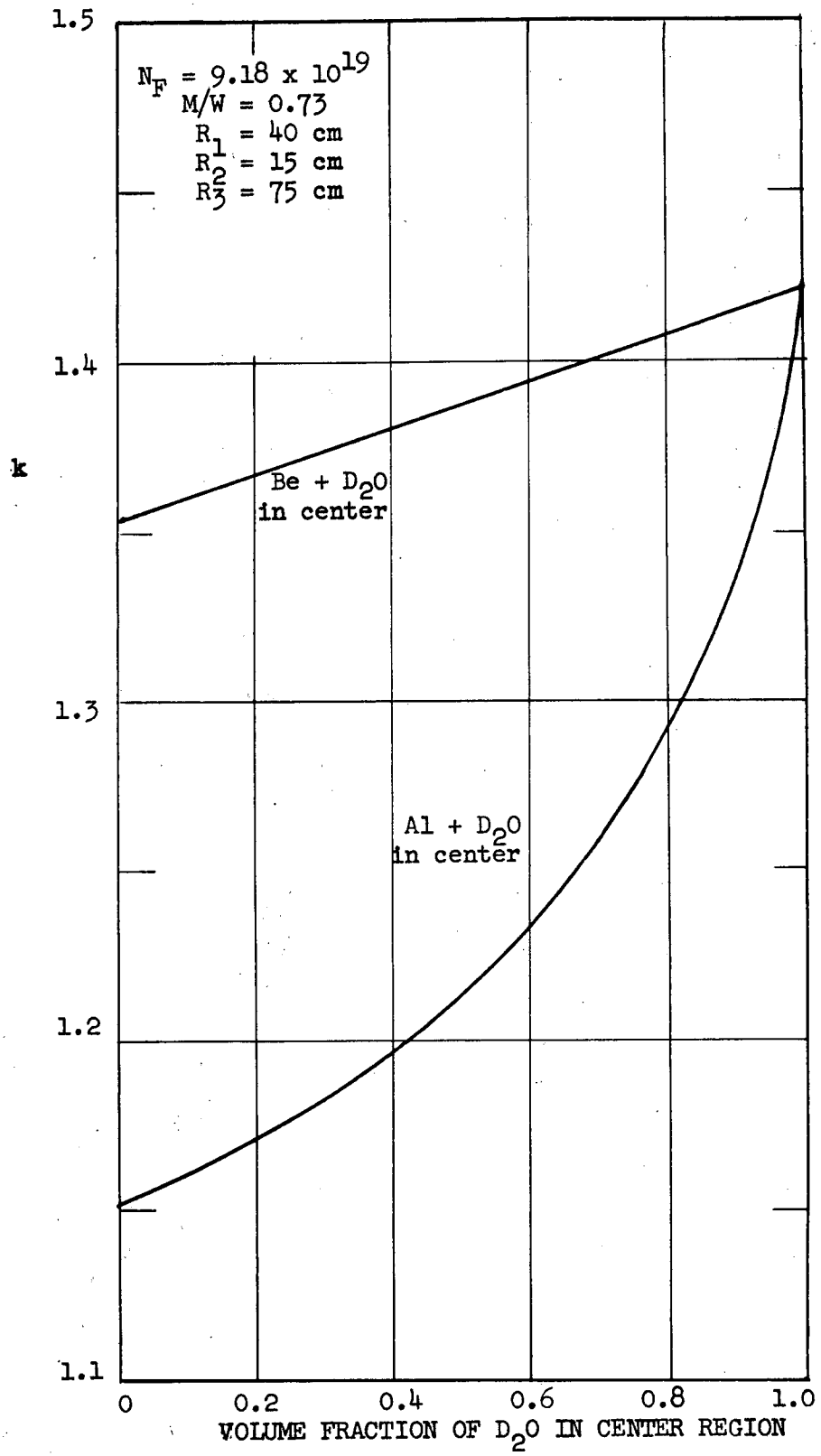

Fig. 15 EFFECT OF ADDITIONS OF ALUMINUM AND BERYLLIUM TO CENTER REGION: k VS. VOLUME FRACTION OF D_2O

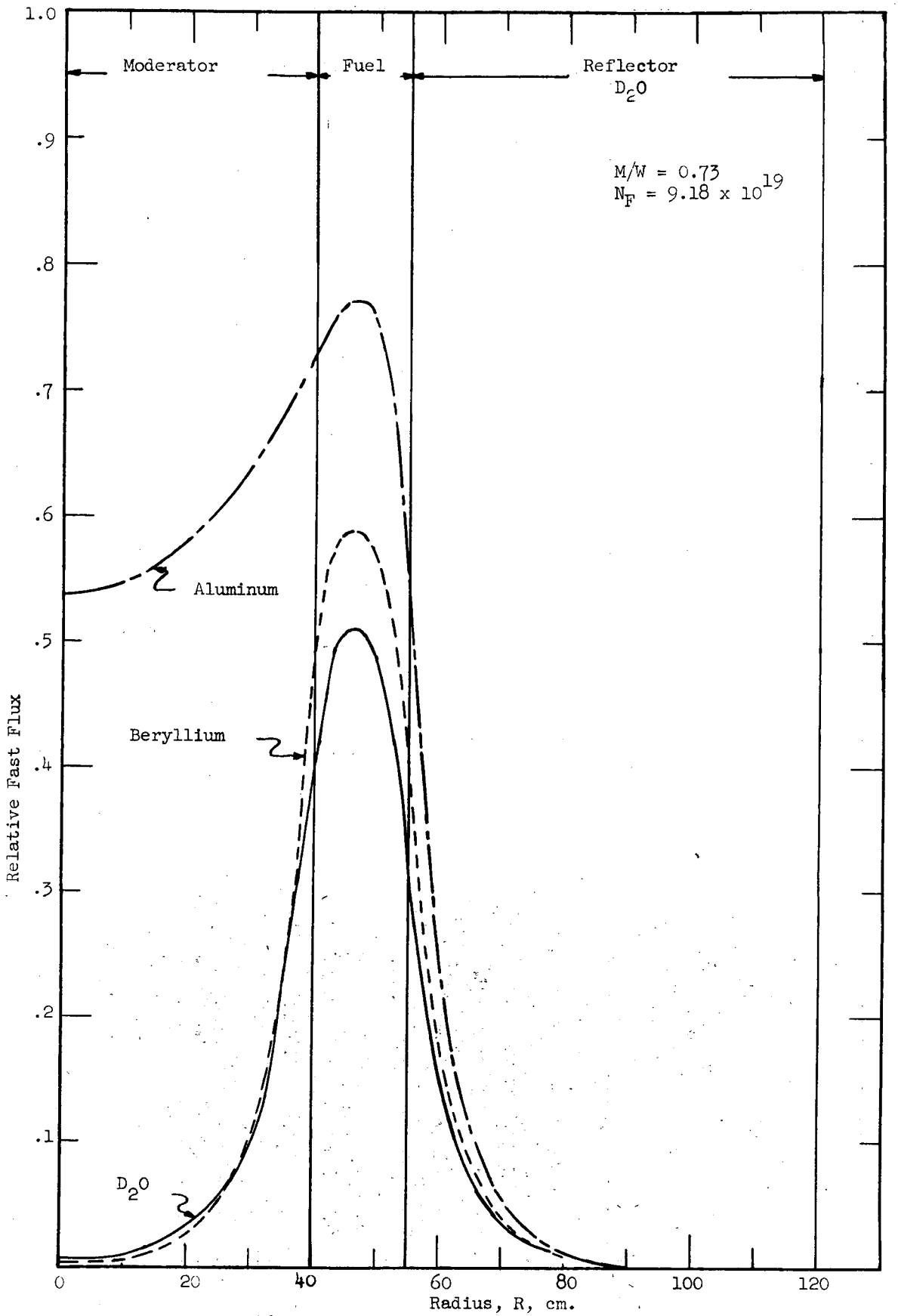

Fig. 16 CONSTANT POWER FAST FLUX DISTRIBUTIONS FOR D_2O, Al AND Be IN CENTER REGION

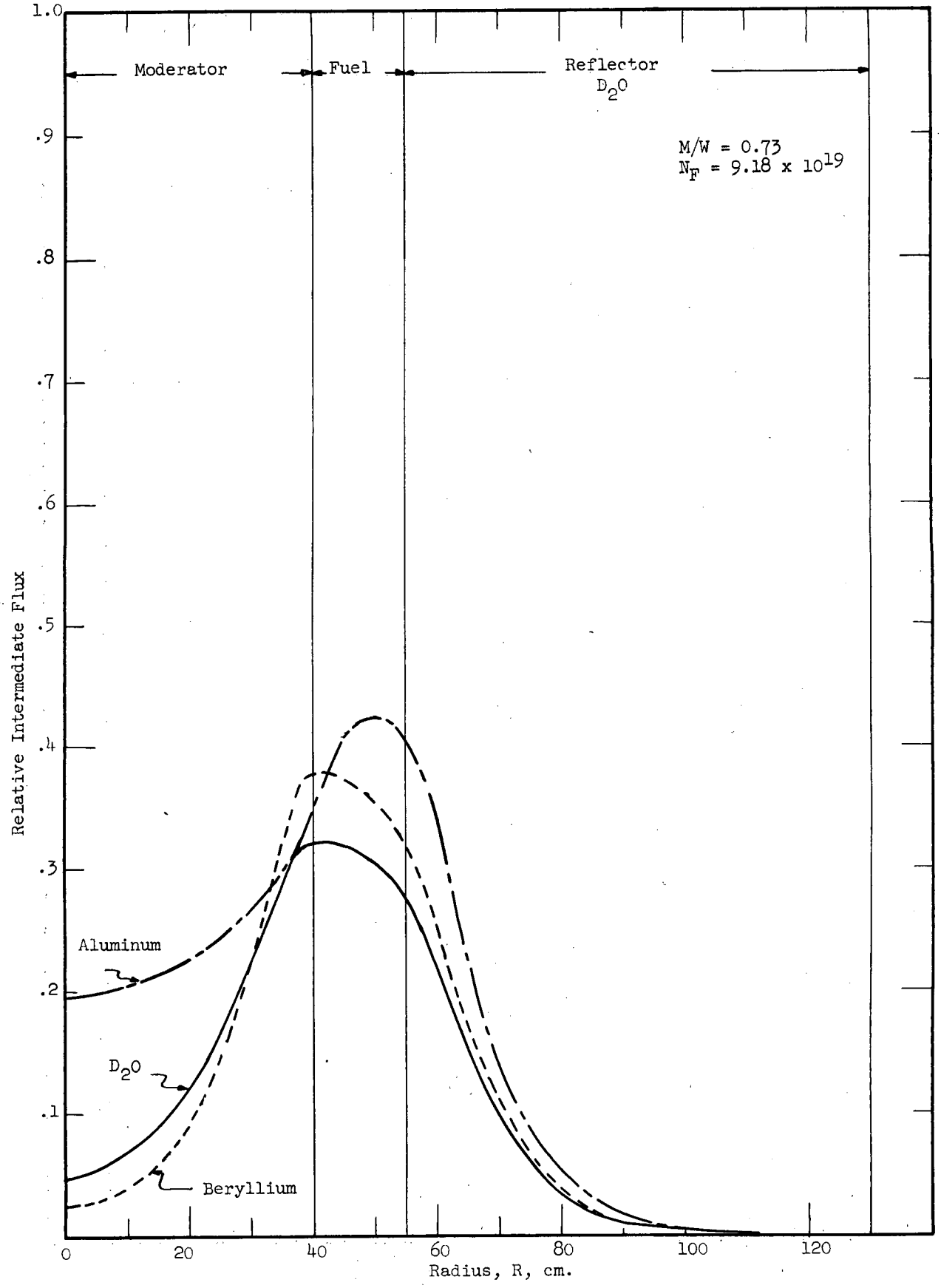

Fig. 17 CONSTANT POWER INTERMEDIATE FLUX DISTRIBUTION FOR D_2O, Al, AND Be IN CENTER REGION

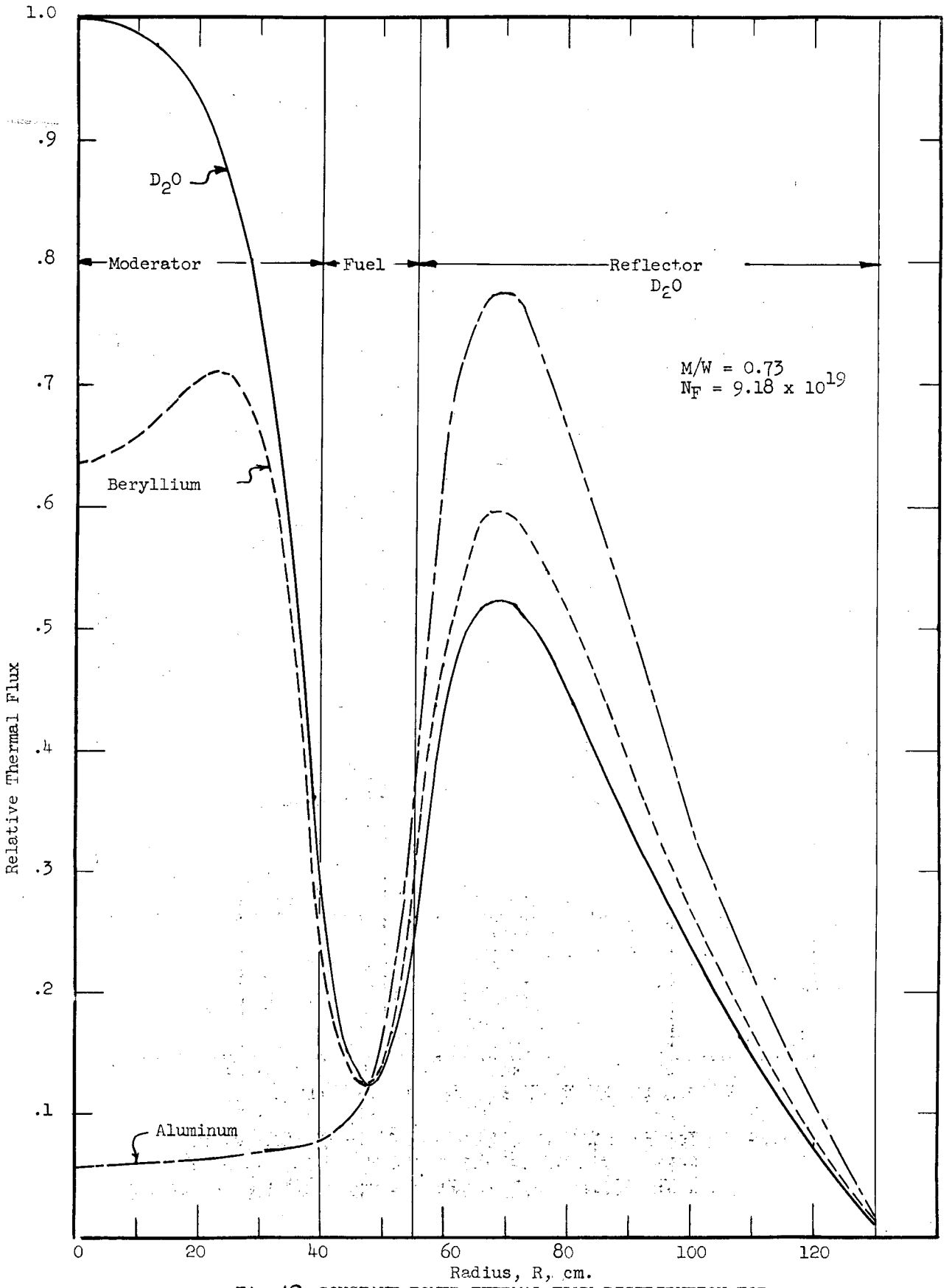

Fig. 18 CONSTANT POWER THERMAL FLUX DISTRIBUTION FOR D_2O, Al, AND Be IN CENTER REGION

ORNL-LR-Dwg.-22467
UNCLASSIFIED

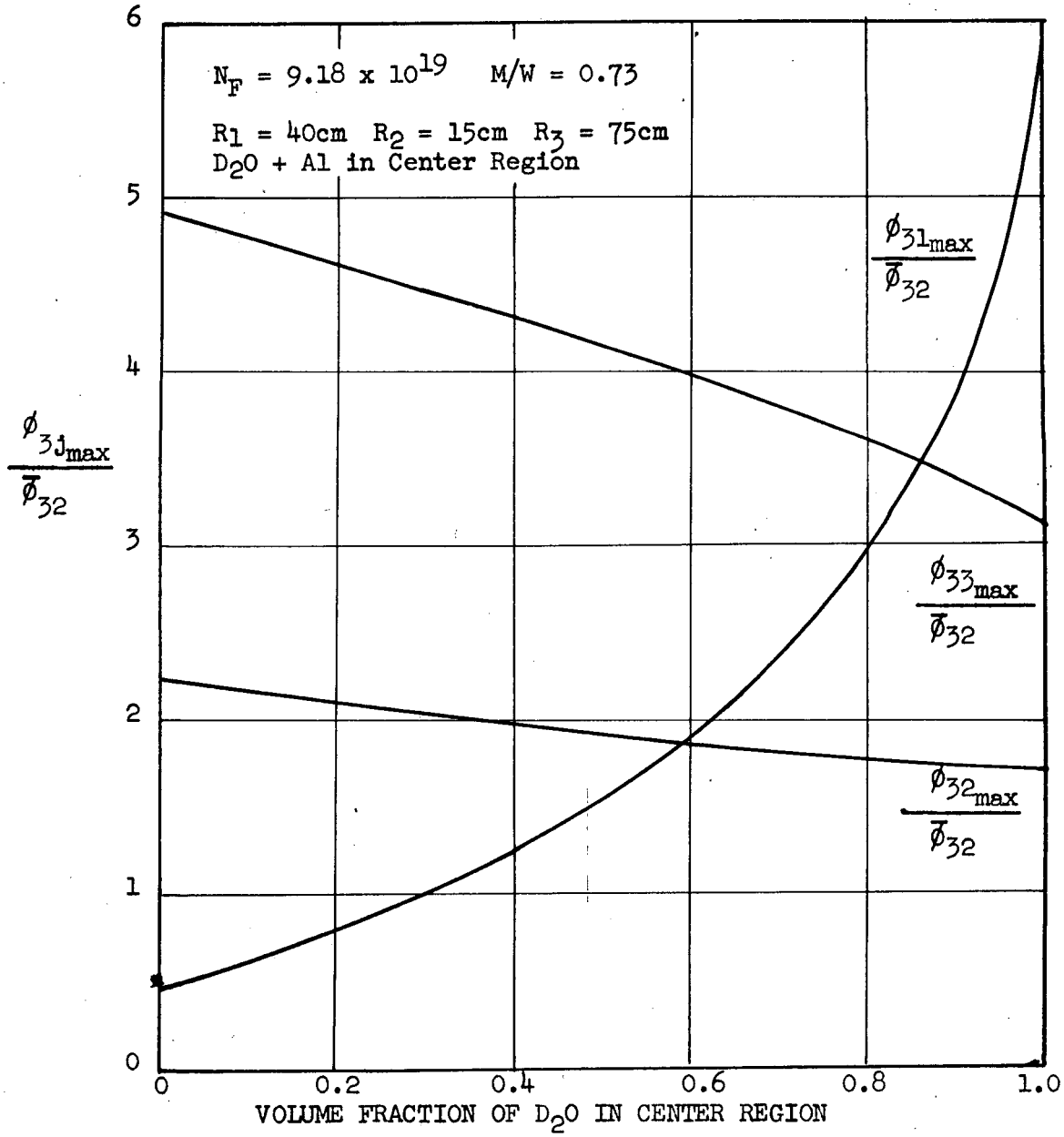

Fig.19 RATIOS OF MAXIMUM THERMAL FLUX IN CENTER REGION, IN FUEL ANNULUS, AND IN REFLECTOR TO AVERAGE THERMAL FLUX IN FUEL, VS. VOLUME FRACTION OF D_2O IN CENTER

ORNL-LR-Dwg.-22468
UNCLASSIFIED

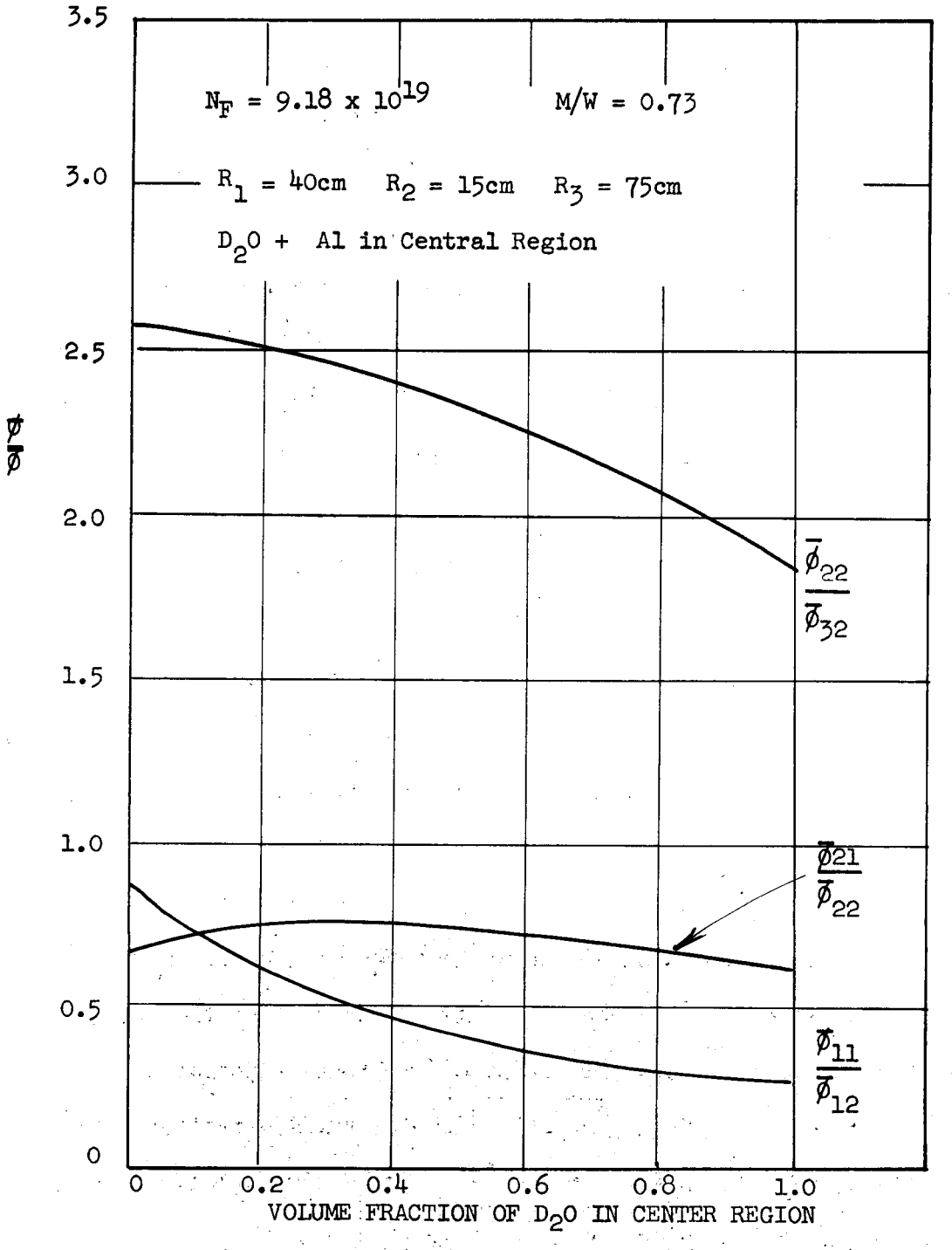

Fig. 20 AVERAGE INTERMEDIATE AND FAST FLUXES IN CENTER REGION TO AVERAGE INTERMEDIATE AND FAST FLUXES IN FUEL; AVERAGE INTERMEDIATE FLUX IN FUEL TO AVERAGE THERMAL FLUX IN FUEL VS. VOLUME FRACTION OF D_2O IN CENTER

in the fuel for varying volume fractions of D_2O and Al in the center region. Addition of aluminum to the center region decreases the multiplication constant as shown in Figure 15.

It is possible that the flux distribution in the central region could be improved with a region of aluminum or beryllium between the fuel region and the heavy water. A region of aluminum would provide a zone of high fast flux in which experiments could be placed. This zone would probably not distort the thermal flux peaking appreciably. These are topics for further study as they were not thoroughly investigated in this analysis.

Calculations indicated that the thermal flux peaking increased with decreasing size of the central hole for radii from about 30 to 50 cm. Figure 3 shows this effect. The peaking will decrease for smaller center region diameters, if the region diameter is less than the slowing down length of fast neutrons in heavy water, because less of the fast leakage out of the fuel region will be converted to thermal neutrons before re-entering the fuel annulus. Figure 4 shows that for a fixed fuel concentration in the fuel region and a fixed fuel region thickness the multiplication constant increases to some maximum value with increasing size of the center region. This indicates that the increase in fuel mass with increasing center region size more than compensates for the increase in leakage out the ends of the center region until a critical size is reached. Increasing the radius further causes k to decrease because the fuel annulus is approaching a flat slab.

Reflector Region: Heavy water was chosen for the reflector region for the same reasons that it was chosen for the central region. As expected and as shown in Figure 2 the thermal flux does not peak up as high in the reflector region as it does in the central region.

In order to reduce the heavy water inventory it appeared desirable to replace a portion of the heavy water reflector with a less expensive material such as carbon. Calculations were made with the 3G3R Code in which the central region was considered to be the fuel, the intermediate region D_2O and the outer region carbon. Figures 21 and 22 show the relationship between percent reactivity and various combinations of D_2O and carbon. Figures 23, 24, and 25 show the relationship between various flux ratios and different reflector combinations. It is concluded that an optimum combination of D_2O and carbon thickness exists that will result in considerable D_2O savings and adequate thermal flux peaking.

As previously shown for the central region the addition of a heavy water cooled aluminum reflector next to the fuel region would appear to be a desirable feature to add to this reactor since experiments in which a high fast flux is required could be placed in this region. Provided the aluminum is not too thick the thermal flux in the reflector region will not be appreciably distorted.

Reactor Control

In an attempt to design a feasible control system for the HFRR, the temperature coefficient of reactivity, xenon instability, and fuel burnup as a function of time were investigated. They appeared to be factors which might limit the maximum neutron flux of the reactor by imposing unreasonable demands on the control system. Solutions to some of the problems were tenatively solved by a rather unique shim and safety system.

Control Elements: The control system will include safety, shim, and regulating elements. In order to leave the upper surface of the reactor free for insertion of experiments it is advisable that all control elements be driven from beneath the core.

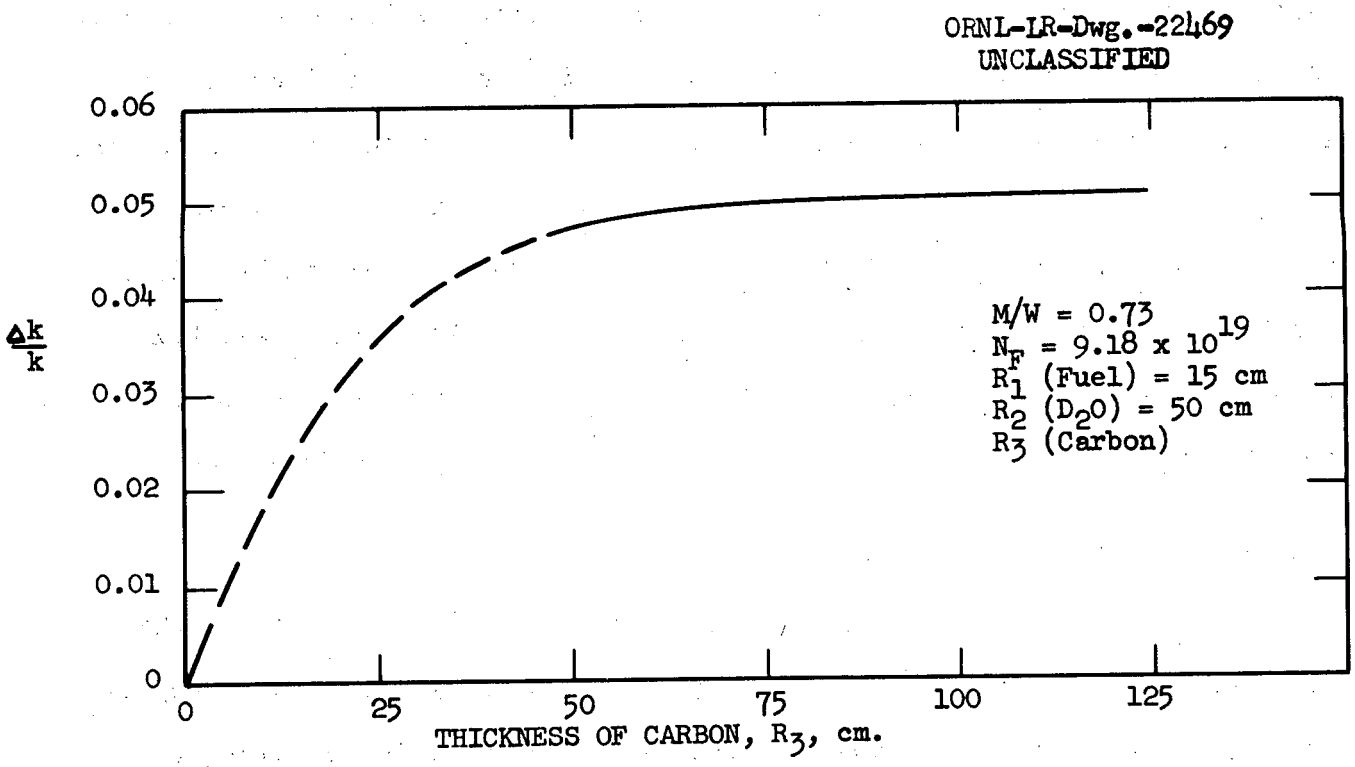

Fig. 21 REACTIVITY ADDED VS. THICKNESS OF CARBON ADDED FOR CONSTANT D_2O REFLECTOR THICKNESS OF 50 CM.

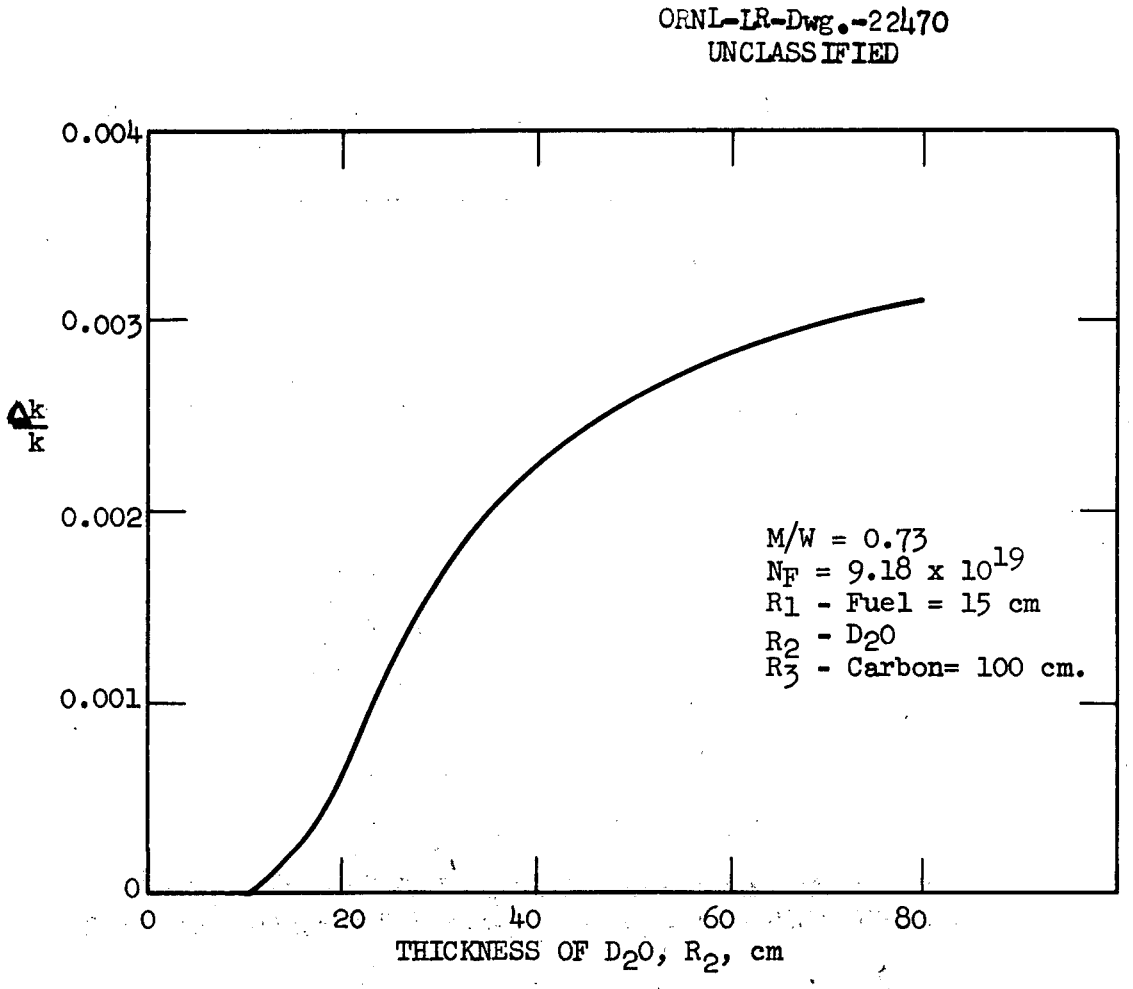

Fig. 22 REACTIVITY ADDED BY INCREASING THE THICKNESS OF D_2O FOR CONSTANT CARBON THICKNESS OF 100 CM.

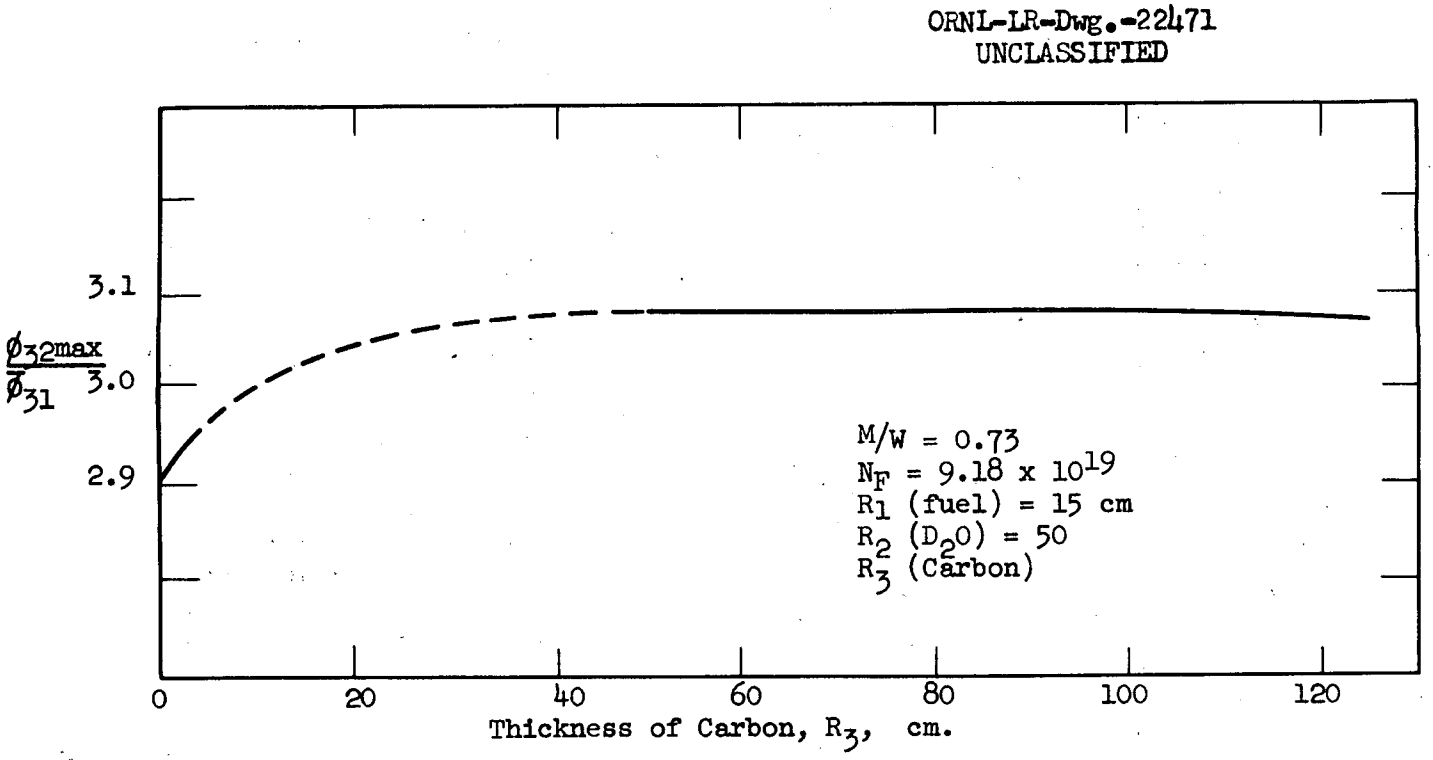

Fig. 23 RATIO OF MAXIMUM THERMAL FLUX IN D_2O TO AVERAGE THERMAL FLUX IN FUEL VS. THICKNESS OF CARBON REFLECTOR FOR CONSTANT D_2O THICKNESS OF 50 CM.

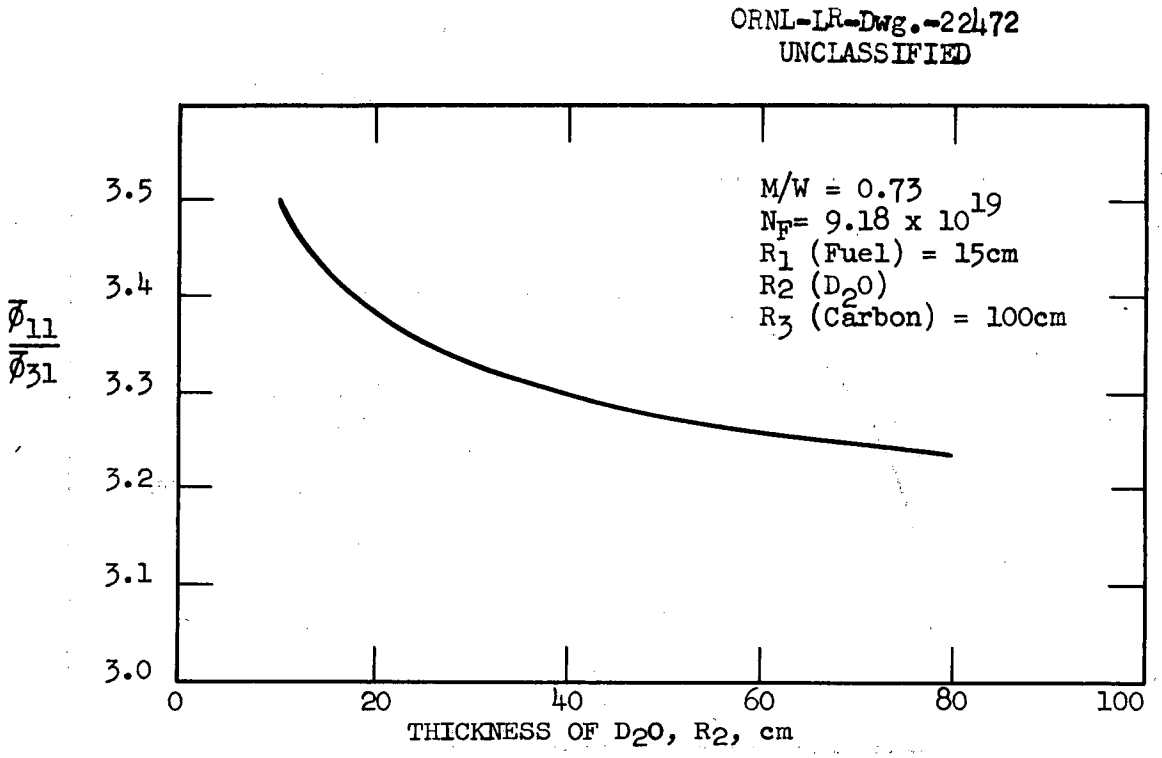

Fig.24 RATIO OF AVERAGE FAST FLUX IN FUEL TO AVERAGE THERMAL FLUX IN FUEL, VS. THICKNESS OF D_2O FOR CONSTANT CARBON THICKNESS OF 100CM.

ORNL-LR-Dwg.-22473
UNCLASSIFIED

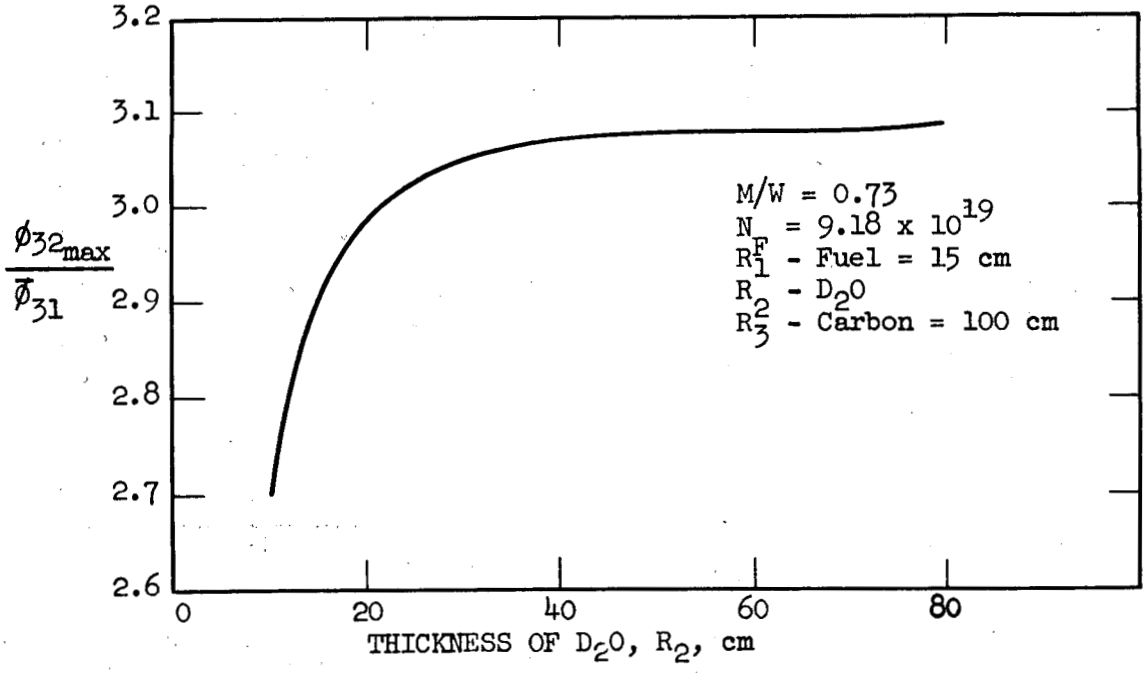

Fig.25 RATIO OF MAXIMUM THERMAL FLUX IN D_2O TO AVERAGE THERMAL FLUX IN THE FUEL VS. THICKNESS OF D_2O, FOR A CONSTANT CARBON THICKNESS OF 100cm.

Safety Elements: The safety elements will consist of concentric cylinders of stainless steel or aluminum clad cadmium located adjacent to the inside and outside surfaces of the fuel annulus. To reduce the possibility of losing all safety action in the event of jamming of the cylindrical shells or failure of the drive mechanism each cylinder will be divided vertically into several segments, each segment having an independent drive mechanism. To determine the effect of absorbing shells such as those suggested, ORACLE calculations were made for boron-stainless steel cylindrical shells. They indicated that for a one quarter inch thick outside shell or for an eighth inch thick inside shell and ten percent boron by volume in boron-stainless steel, sufficient negative reactivity is introduced by either the inside or the outside shell alone to achieve complete shutdown. Specifically, driving the inner group of safety elements into the reactor causes the multiplication constant to change from 1.42 to 0.787. Inserting only the outer group of segments causes the multiplication constant to change from 1.42 to 0.774. The effect of the shells on the flux distributions is shown in Figures 26 and 27.

Several important factors were considered when designing the safety system for the HFRR. In a reactor of this type the reactivity introduced by an experiment may be quite appreciable, and many times a single experiment may be almost critical by itself. Hence, it is very desirable for an experimental reactor to have a control system which is capable of handling large variations in reactivity. The control systems of the Materials Testing Reactor and the Engineering Test Reactor, which are perhaps the best examples of experimental reactors, cannot handle extremely large variations in k, and thus, reactivity measuring facilities had to be constructed to evaluate the worth of an experiment. As previously

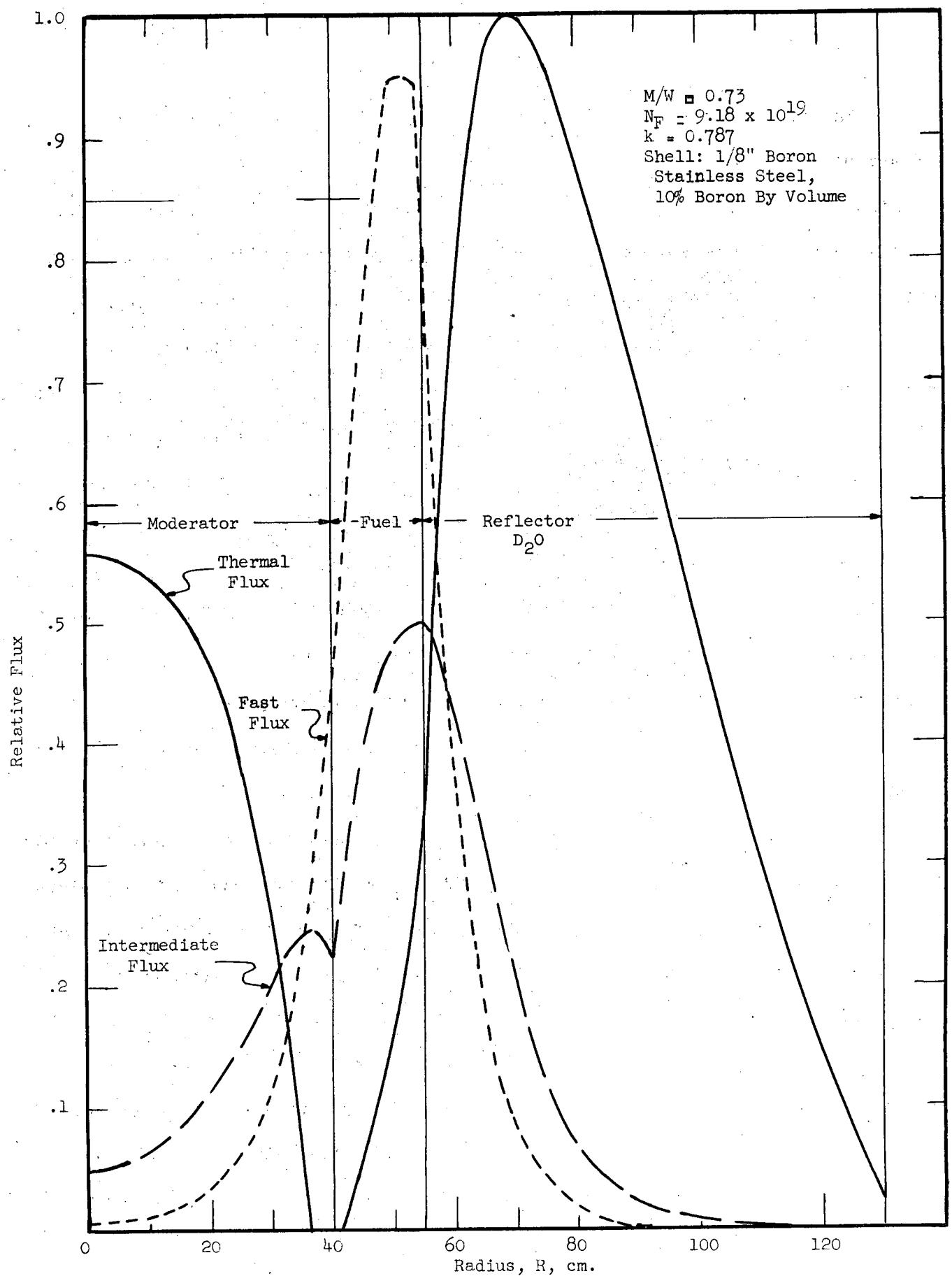

Fig. 26 SPATIAL FAST, INTERMEDIATE AND THERMAL FLUX DISTRIBUTIONS WITH 1/8" BORON STAINLESS STEEL SHELL AT INNER ANNULUS SURFACE

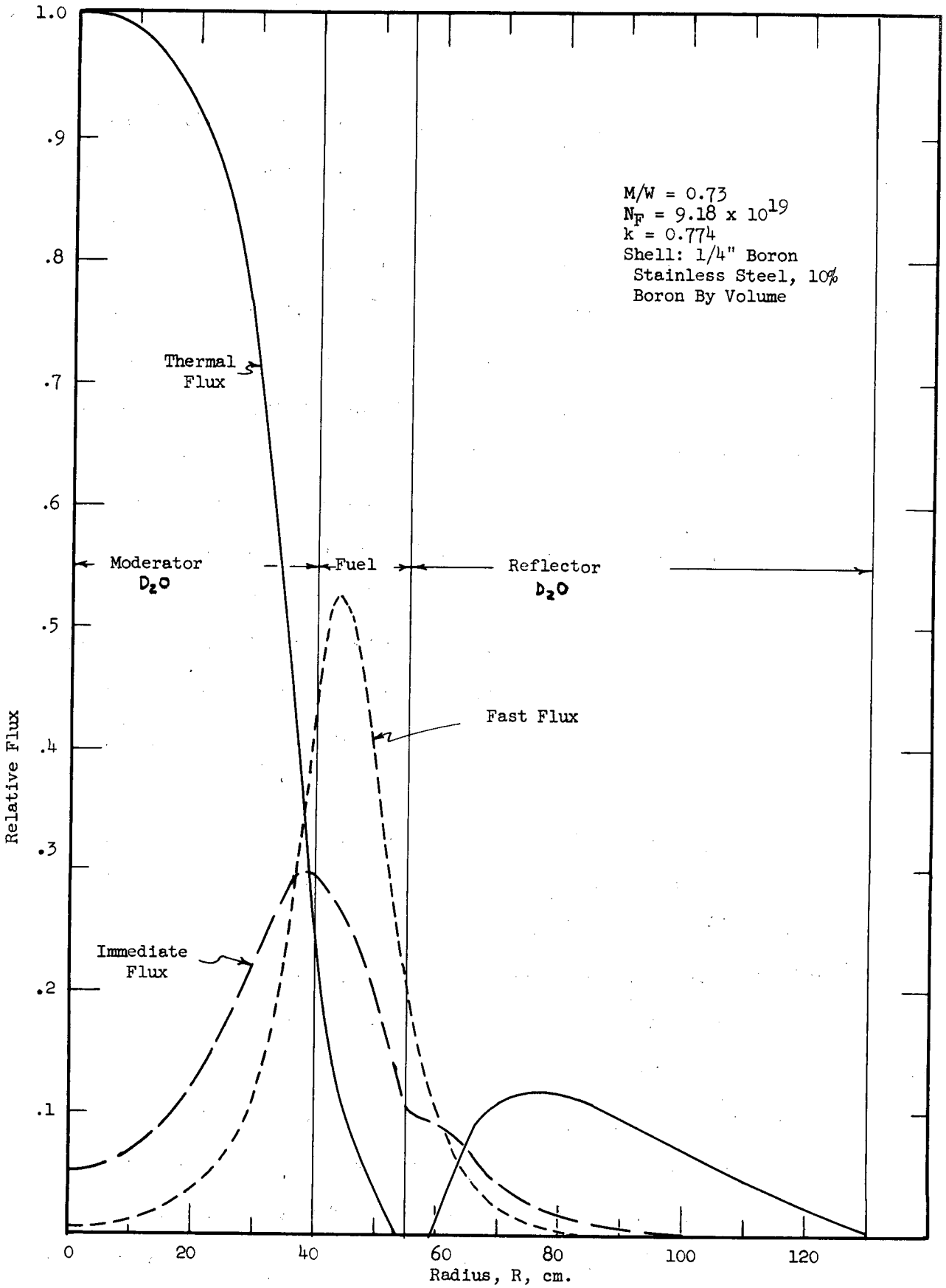

Fig. 27 SPATIAL FAST, INTERMEDIATE, AND THERMAL FLUX DISTRIBUTIONS WITH 1/4" BORON SHELL AT OUTER ANNULUS SURFACE

shown, each of the absorbing shells between the fuel annulus and the heavy water in the HFRR is capable of handling 60 per cent or more excess reactivity because of the large control surface exposed to neutrons. Thus, the HFRR control is quite versatile. The worth of an experiment can be determined by inserting an experiment with the shells fully lowered, followed by slow withdrawal of the shells.

Another factor which was considered was the safety of the reactor in case an experiment should fail. For the purposes of illustration, an experiment containing a concentrated aqueous solution of enriched uranyl sulfate was assumed to be located in the center of the HFRR. If the container for this experiment should fail, the uranyl sulfate would be rapidly dispersed throughout the inner D_2O-filled region of the reactor. Because of the flux depression in the experiment, the uranyl sulfate would be much more effective, when dispersed throughout the D_2O and would introduce a rapid increase in reactivity. Thus a safety system which can handle large reactivity changes is very desirable, if not necessary, for a reactor of this type.

Regulating Rods: Four regulating rod locations will be in the fuel annulus and will be equally spaced around the reactor. The rods will be stainless steel clad cylinders of cadmium and will be approximately one-and-one-quarter inches in diameter and worth approximately one-half per cent reactivity each. One rod in either of the four positions will be used to regulate the power level of the reactor, when the safety shells are withdrawn.

Shim Elements: Most of the excess reactivity will be controlled by the shim elements. Three types of elements were considered; solid rods, tubes containing a fluidized bed of boron-steel pellets, and tubes containing a solution of poison. Stainless steel tubes containing a circulating solution of aqueous boric acid solution were chosen for the shim control of this reactor.

Solid elements were eliminated because of distortion of the vertical flux shape and the resultant uneven fuel burnup. Also, solid shim rods would possibly require frequent replacement because of a high burnup rate.

A fluidized bed of boron-stainless steel pellets in water would allow the reactor to be controlled simply by varying the water flow rate through the bed. The system would be designed so that if water flow ceased, all pellets would drop into the core, decreasing the reactivity. However, to attain a threefold change in the number of pellets in the reactor core, the containing tubes would have to be three times the height of the core. This constitutes a mechanical design problem above the core where it is desired to introduce the experiments and fuel elements. A possible advantage of the fluidized bed is that it might contribute to a negative temperature coefficient of reactivity because of the decrease in water density with temperature and the resulting compression of the boron pellet bed. A possible disadvantage is that small, rapid fluctuations in the density of the bed during steady state operation might introduce fluctuations in the reactivity of the reactor.

The system chosen for shim control of the HFRR consisted of an aqueous boric acid solution contained in vertical stainless steel tubes. In order to remove heat from the solution and to provide means for varying the boron concentration the solution is continuously circulated through an external system. A boric acid solution was chosen because of its low cost, non-corrosive nature, and solubility in water. The solubility of boric acid in light water as a function of temperature is shown in Figure 28. For the cases considered in this report the solubility is more than sufficient to maintain in solution the necessary amount of boron for shim control and burnable poison. The incorporation of burnable poison in the shim tubes is discussed later.

ORNL-LR-Dwg.-22476
UNCLASSIFIED

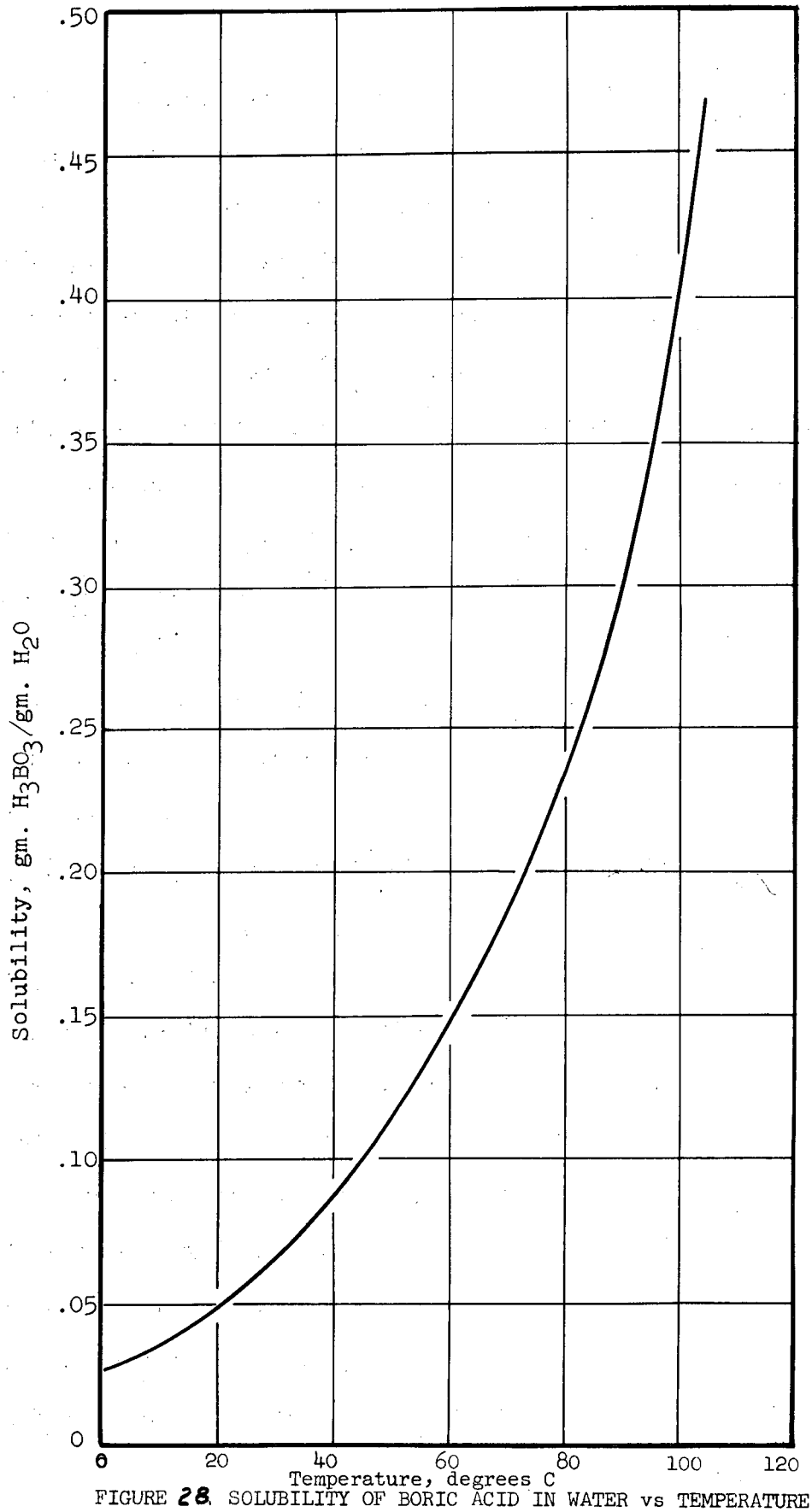

FIGURE 28. SOLUBILITY OF BORIC ACID IN WATER vs TEMPERATURE

One advantage of this type system is that the concentration of the boric acid is uniform along the length of its containing tubes in the core, preventing axial distortion of the flux. Another advantage is the comparatively simple means by which heat may be removed from the shim system. Since it is removed externally it may be possible to obtain fine control of the reactor by varying the flow rate and therefore the temperature and density of the solution.

A disadvantage in having the poison in liquid form lies in the possibility of losing the poison in an accident, requiring that a safety system be devised capable of shutting down the reactor upon the sudden loss of poison.

A typical assembly as shown in Figure 1 might consist of three-and-one-half-inch diameter fuel elements, boric acid tubes one-and-one-quarter inches in diameter being located in the center of the fuel annulus between adjacent fuel elements where there is a slight peaking of the thermal flux due to the absence of fuel. With this size tube, fuel element, and a typical central region radius of 40 cm, there is space in the annulus for twenty-five shim tubes. Four of these locations will contain the regulating rods so that twenty-one will be used for shim control with the boric acid solution.

The neutron capture cross section of the boron in the solution was taken as 755 barns per atom at a neutron velocity of 2200 meters per second[5]. This high cross section is caused principally by the small amount of the boron-10 isotope in natural boron. Boron-10 has a neutron absorption cross section of 4010 barns per atom, the remainder of the natural boron, boron-11, having a negligible absorption cross section. Therefore, most of the neutrons will be captured by the boron-10, according to the following reaction[6]:

$$ {}_5B^{10} + {}_0n^1 \xrightarrow{7\%} {}_2He^4 + {}_3Li^7 + 2.792 \text{ Mev of energy} $$
$$ \xrightarrow{93\%} {}_2He^4 + {}_3Li^{7*} + 2.314 \text{ Mev of energy} $$

The excited state of lithium decays as follows:

$$ {}_3Li^{7*} \longrightarrow {}_3Li^7 + .478 \text{ Mev gamma ray} $$

The lithium which is formed will combine with boric acid to produce lithium borate. Lithium borate is insoluble in water so that some means, such as a settling tank, will have to be provided for removing the precipitate.

In order to determine the worth of the tubes containing boric acid solution, disadvantage factors were obtained from ORACLE calculations using the 3G3R Code. The solution calculated contained 0.20 grams of boric acid per gram of water which is about the maximum concentration that can be attained at room temperature. Later calculations indicated that this concentration was higher than that required for control of the HFRR. The results of the calculations are shown in Figures 29 and 30 as a function of the size of the control rod and the thickness of the fuel section.

Burnup: The high thermal flux (approximately 10^{15} n/cm^2-sec) found in the annular fuel region, and operation at constant power with the attendant increase in flux with time result in rapid fuel depletion. Because of this high burnup rate the use of a burnable poison is desirable to simplify the control system and increase the fuel cycle. ORACLE calculations were made to determine reactor operation, considering burnup.

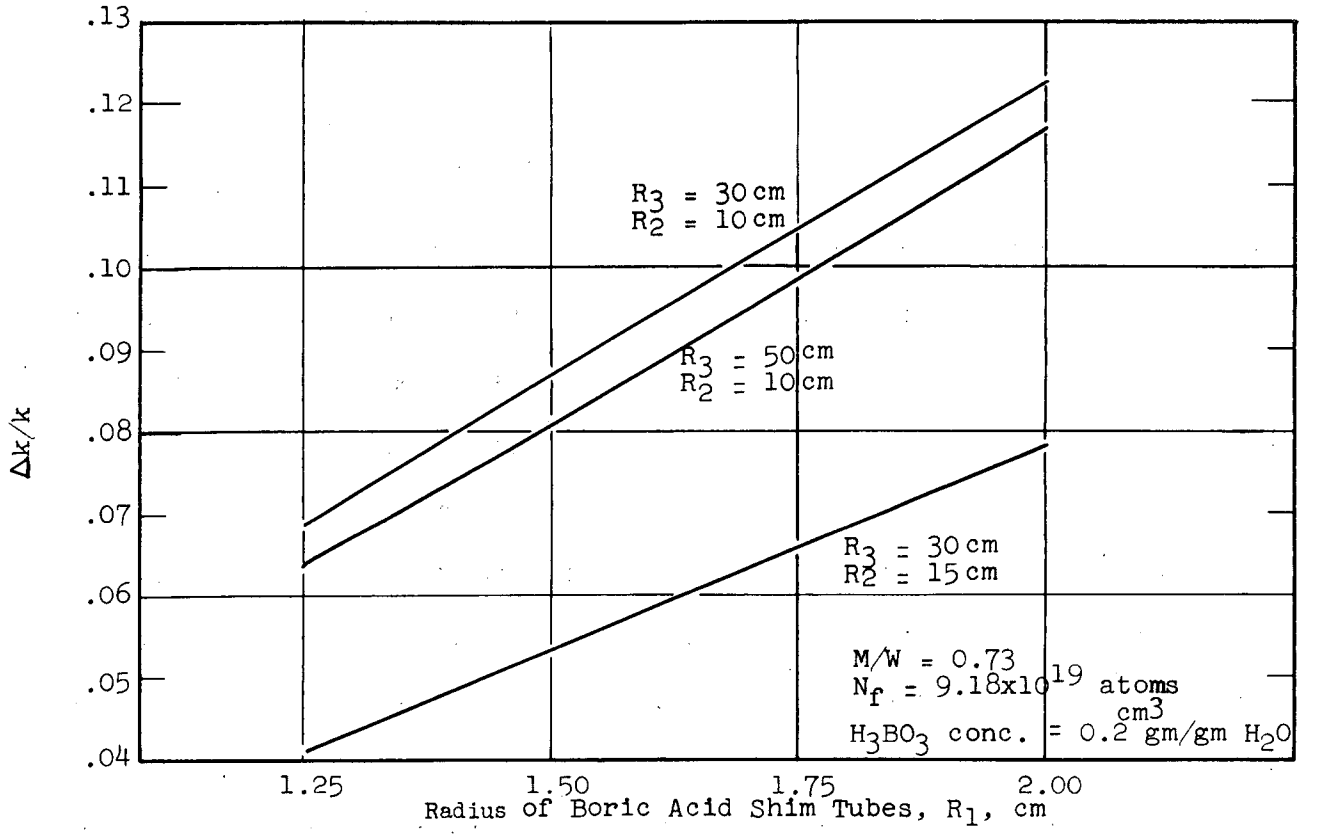

FIGURE 29 REACTIVITY vs RADIUS OF BORIC ACID SHIM TUBE FOR VARIOUS THICKNESSES OF FUEL (R_2) AND REFLECTOR (R_3)

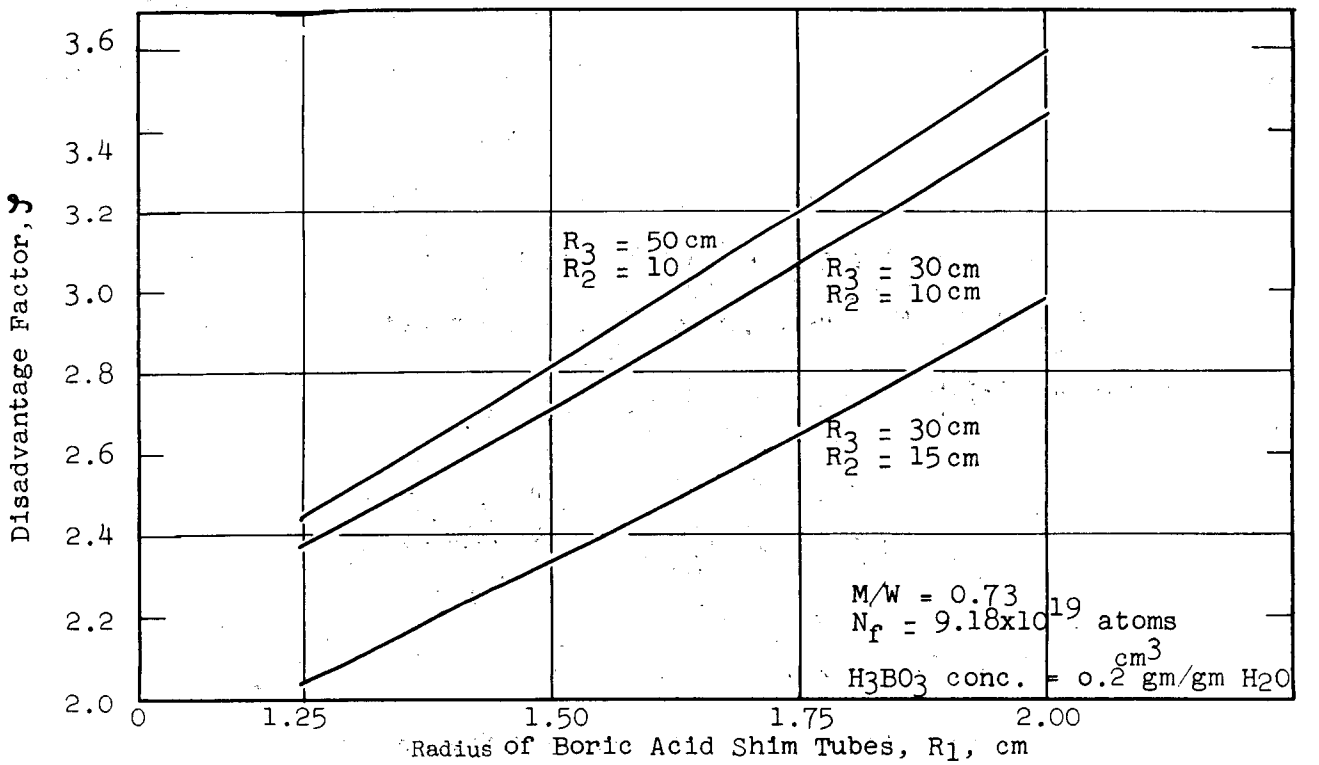

FIGURE 30. DISADVANTAGE FACTOR vs RADIUS OF BORIC ACID SHIM TUBE FOR VARIOUS THICKNESSES OF FUEL (R_2) AND REFLECTOR (R_3)

The burnable poison could be added to the fuel alloy or cladding, during fuel element fabrication. However, use of a boric acid solution for the burnable poison appears to be advantageous. To incorporate this scheme into the reactor, the concentration of the boric acid solution in the shim tubes is increased.

Once a fuel element incorporating boron in the fuel alloy or cladding has been fabricated, there is no control over boron concentration. The liquid system proposed has the advantage of allowing boron concentration to be changed at will during reactor operation. As will be shown ORACLE calculations indicate this may be necessary, if a high fuel burnup and long refueling cycle are to be achieved.

Calculations were made using the ORACLE to determine changes in multiplication factor, k, and in flux shape with time. The following parameters were considered: Fuel concentration, N_f; Boron concentration, N_B; Xenon concentration, N_{Xe}; Samarium concentration, N_{Sm}; and the concentration of other fission products, N_{FP}. Figure 31 indicates the variation of these concentrations with time for a typical case. The burnup calculations were made at a power density, P_o, of 1500 watts/cc, and at initial fuel concentrations, N_{Fo}, of 9.18 and 12 x 10^{19} atoms/cc. From P_o and N_{Fo} the variation of fuel concentration with time was determined using the expression

$$N_F(t) = N_{Fo} - \frac{\sigma_a^F \, P_o \, wt}{\sigma_f^F} \qquad (1)$$

where w = fissions/watt-second and

σ_a^F and σ_f^F are the microscopic absorption and fission cross sections of the fuel.

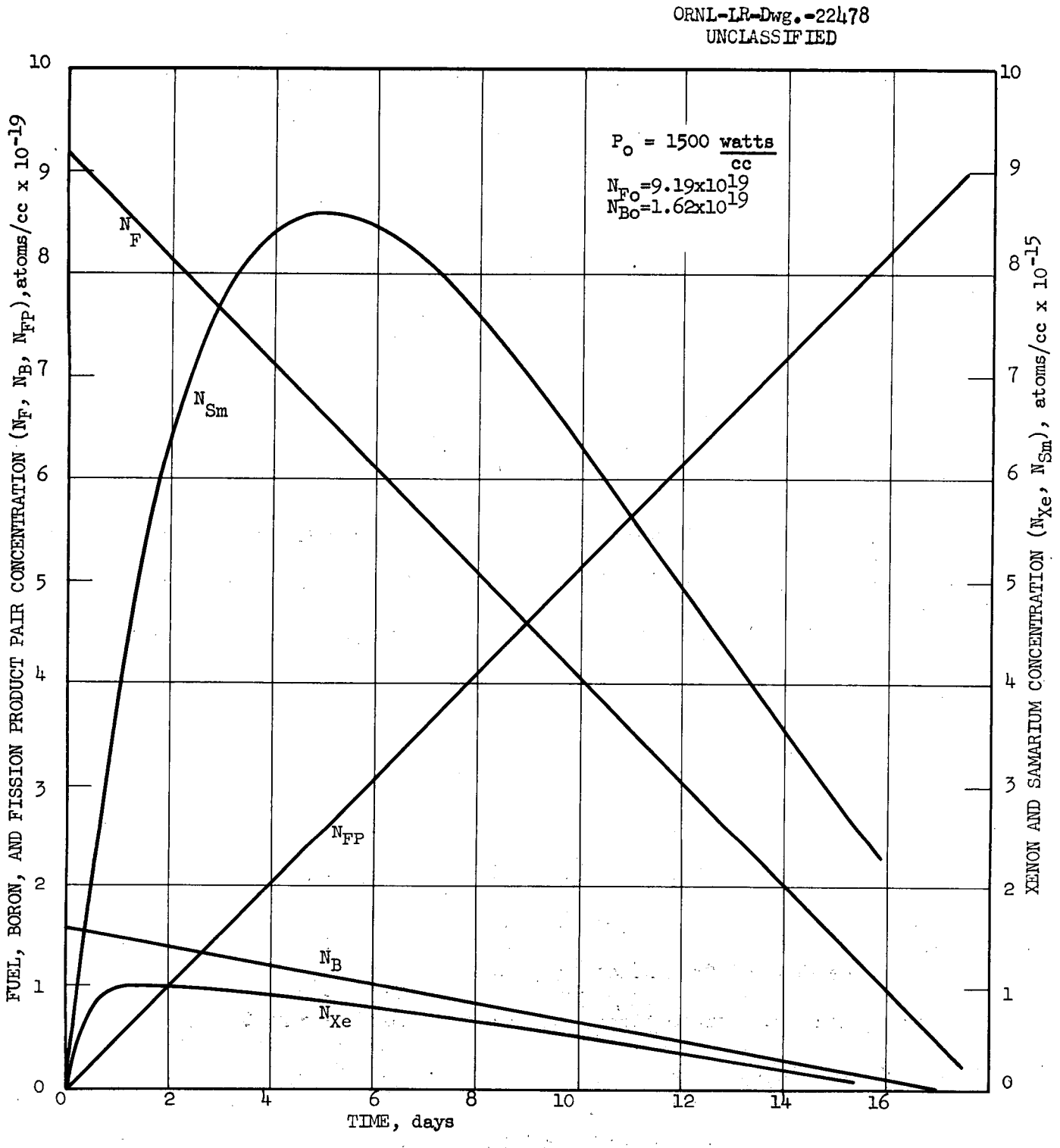

Fig. 31 CONCENTRATION OF FUEL, BORON, XENON, SAMARIUM, AND OTHER FISSION PRODUCTS VS. TIME AFTER STARTUP, FOR CONSTANT POWER OPERATION

These cross sections were calculated taking into consideration both thermal and epithermal fissions in the following manner:

$$\sigma_f^F = \sigma_{f_3} + \frac{\overline{\phi}_2}{\overline{\phi}_3} \sigma_{f_2} \tag{2}$$

$$\sigma_a^F = \sigma_{a_3} + \frac{\overline{\phi}_2}{\overline{\phi}_3} \sigma_{a_2} \tag{3}$$

where the ratio $\overline{\phi}_2/\overline{\phi}_3$ is determined by the ORACLE and was assumed to be independent of boron concentration. Equation (1) can then be solved by iterative methods.

Once $N_F(t)$ is determined the instantaneous average thermal flux may be determined from

$$\phi(t) = \frac{\omega P_o}{N_F(t)\, \sigma_f^F} \tag{4}$$

where σ_f^F is determined from Equation (2).

Assuming startup with no fission products initially present, $N_{Xe}(t)$ and $N_{Sm}(t)$ may be found from:

$$N_{Xe}(t) = \frac{\mu_{Xe}\, \Sigma_F\, \phi}{\lambda_{Xe}^*} \left[1 - e^{-\lambda_{Xe}^* t} \right] \tag{5}$$

$$+ \mu_I\, \Sigma_F\, \phi \left[\frac{1 - e^{-\lambda_{Xe}^* t}}{\lambda_{Xe}^*} - \frac{\left(e^{-\lambda_I t} - e^{-\lambda_{Xe}^* t}\right)}{\lambda_{Xe}^* - \lambda_I} \right]$$

and

$$N_{Sm}(t) = \mu_{Pm} \Sigma_F \phi \left[\frac{1 - e^{-\sigma_a^{Sm} \phi t}}{\sigma_a^{Sm} \phi} - \frac{(e^{-\lambda_{Pm} t} - e^{-\sigma_a^{Sm} \phi t})}{\sigma_a^{Sm} \phi - \lambda_{Pm}} \right] \quad (6)$$

Fission product pair concentration is found from

$$N_{FP} = \frac{\sigma_f^F}{\sigma_a^F} (N_{Fo} - N_F) \quad . \quad (7)$$

The equation for boron concentration for constant power operation is

$$N_B(t) = N_{Bo} \exp \left[- \frac{\sigma_a^B}{\sigma_a^F} \ln(1 - \phi \sigma_a^F t) \right] \quad . \quad (8)$$

The above relations were used to determine the amount of fuel, boron, and other poisons present at any given time after startup. These concentrations were programmed for the Three Group-Three Region ORACLE Code and the final calculations yielded the multiplication factor, k , and graphs of fast, epithermal, and thermal flux vs radial distance from the center of the reactor. Plotted in Figure 32 is the variation of k with time in days after startup for initial fuel concentrations of 9.18 and 12 x 10^{19} and initial boron concentrations of 3.76, 2.16 and 1.62 x 10^{19} atoms/cc.

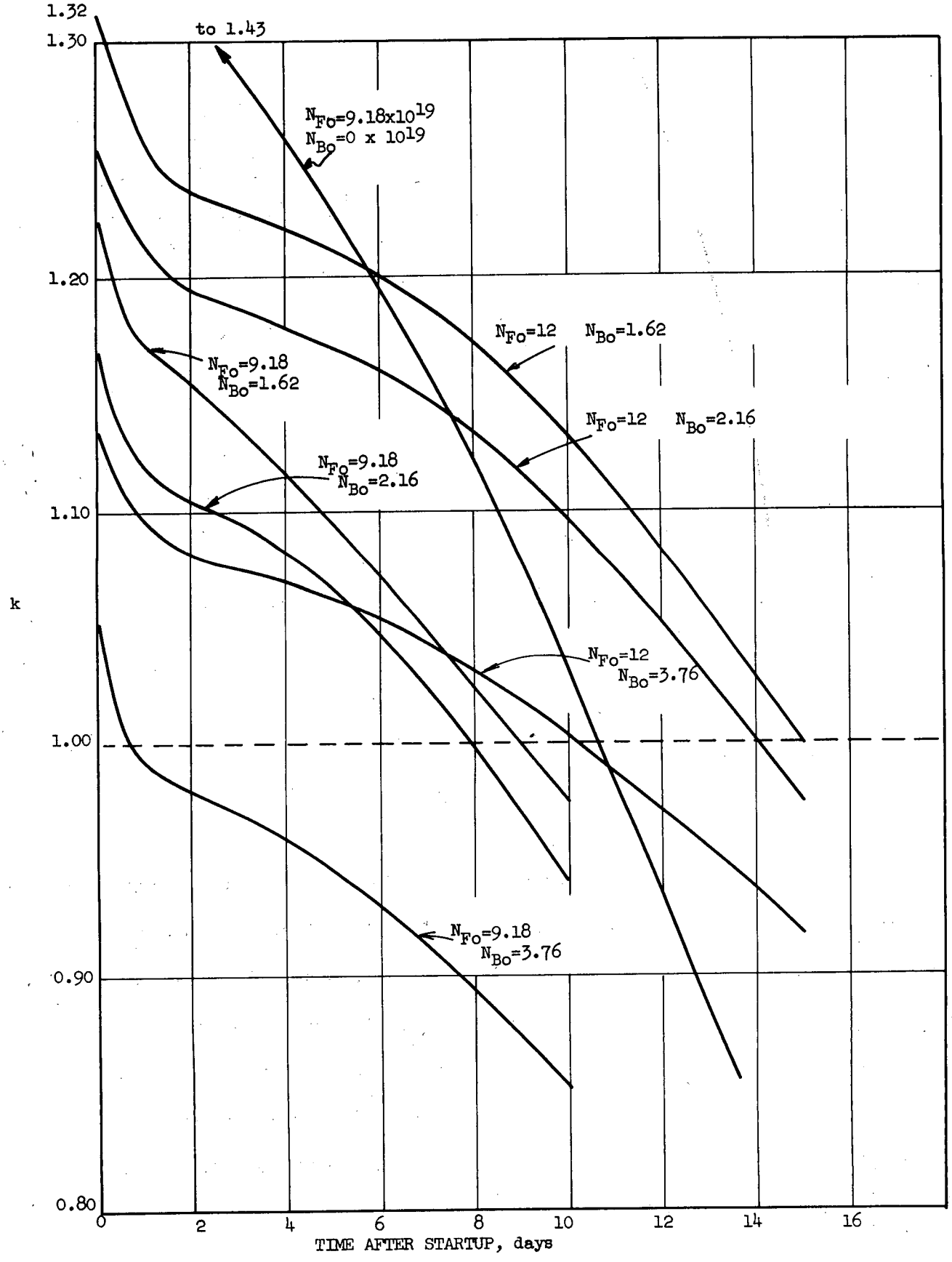

Fig. 32 MULTIPLICATION FACTOR VS. TIME FOR VARIOUS INITIAL CONCENTRATIONS OF FUEL AND BORON

The sharp drop in the curve of k vs time in the first one to two days after startup is caused by buildup of xenon and samarium. The variation in k at time zero illustrates the decrease in k as initial boron concentration is increased. A high concentration of boron should be present initially to minimize the amount of excess reactivity which must be compensated for by the control elements. However, once the reactor has been operating for some time, resulting in fuel depletion and fission product buildup, the boron concentration must be decreased to reduce the total poison present in the system and to enable the reactor to approach maximum burnup. The limiting case is the addition of no burnable poison, in which instance reactor operating lifetime is a maximum.

As an illustration assume an initial fuel concentration of 9.18×10^{19} atoms/cc and an initial boron concentration of 2.16×10^{19}. Figure 32 indicates that the boron reduces k at time zero from 1.43 to 1.17, which is within controllable limits. Assuming the boron concentration is decreased by burnout only, the reactor would go subcritical, for the conditions considered, after operating for 7.9 days with a fuel burnup of 44.0%. If on the other hand a portion of the boron were removed from the reactor at a sufficient rate, reactor operation could approach the limiting case of 10.6 days with a fuel burnup of 59.2%.

The graph of k vs time illustrates that satisfactory reactor control in conjunction with high burnup and a long fuel cycle can be achieved by providing a high initial concentration of boron and then decreasing the concentration during reactor operation. This then indicates the definite advantage of having the burnable poison in a form in which its concentration in the reactor can be varied.

Temperature Coefficient of Reactivity: It appeared that possibly a change in temperature in the reactor would decrease the density of the boric acid solution in the shim tubes, resulting in a positive contribution to the temperature coefficient of reactivity. This was investigated using the 3G3R ORACLE Code. The concentration of the boric acid was assumed to be 0.070 grams of boric acid per gram of water. The multiplication constant as a function of temperature is shown in Figure 33. In these calculations it was assumed that the temperature of the boric acid increased instantaneously with the temperature of the fuel. Also, since details of the cooling system were not definite, various D_2O temperatures outside the fuel annulus were assumed to correspond to the instantaneous fuel temperature. For the purpose of comparison, the variation of the multiplication constant with temperature for the clean reactor with no boron is plotted in Figure 34. For this calculation it was assumed that the temperature rise occurred in the fuel region only. Reference to Figure 33 indicates that for zero temperature change in the central and reflector regions of the reactor the temperature coefficient is positive. The slope of these curves are the temperature coefficients and are plotted in Figure 35. The temperature coefficient does not become negative until 60 per cent of the fuel temperature change occurs instantaneously in the central and reflector regions.

Careful analysis of the proposed reactor configuration shown in Figure 1 indicates that the curves showing positive temperature coefficients are quite pessimistic. The boric acid solution is well insulated from the fuel region of the reactor. Therefore, gamma and neutron heating are essentially the only factors which will affect the temperature of the boric acid solution instantaneously, after an increase in reactivity. The heavy water which cools the fuel elements circulates

ORNL-LR-Dwg.-22480
UNCLASSIFIED

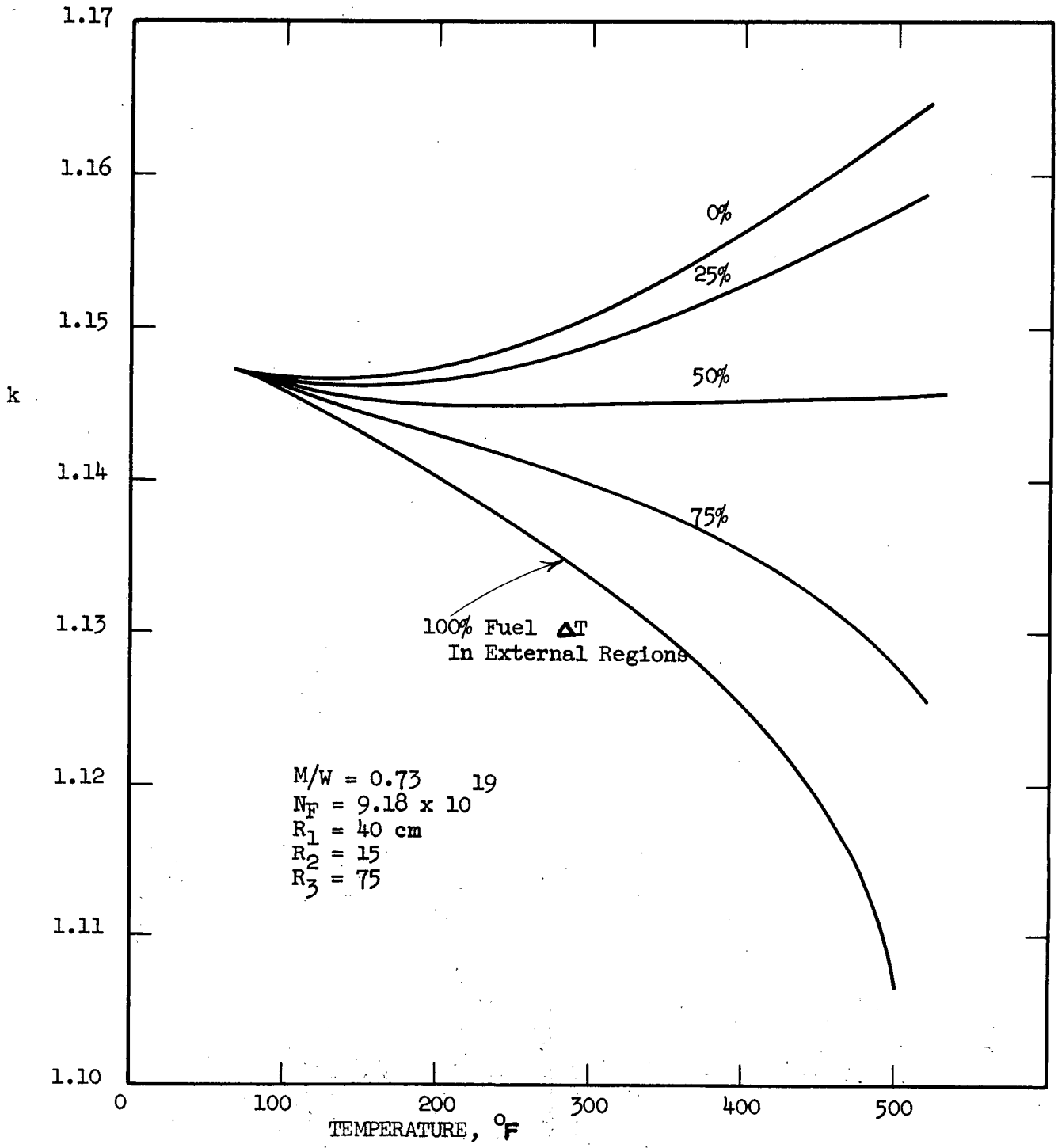

Fig. 33 MULTIPLICATION CONSTANT VS. TEMPERATURE FOR VARIOUS INCREMENTS OF TEMPERATURE CHANGE IN EXTERNAL D_2O REGIONS, ASSUMING INSTANTANEOUS TEMPERATURE RISE IN THE BORIC ACID SOLUTION

ORNL-LR-Dwg.-22481
UNCLASSIFIED

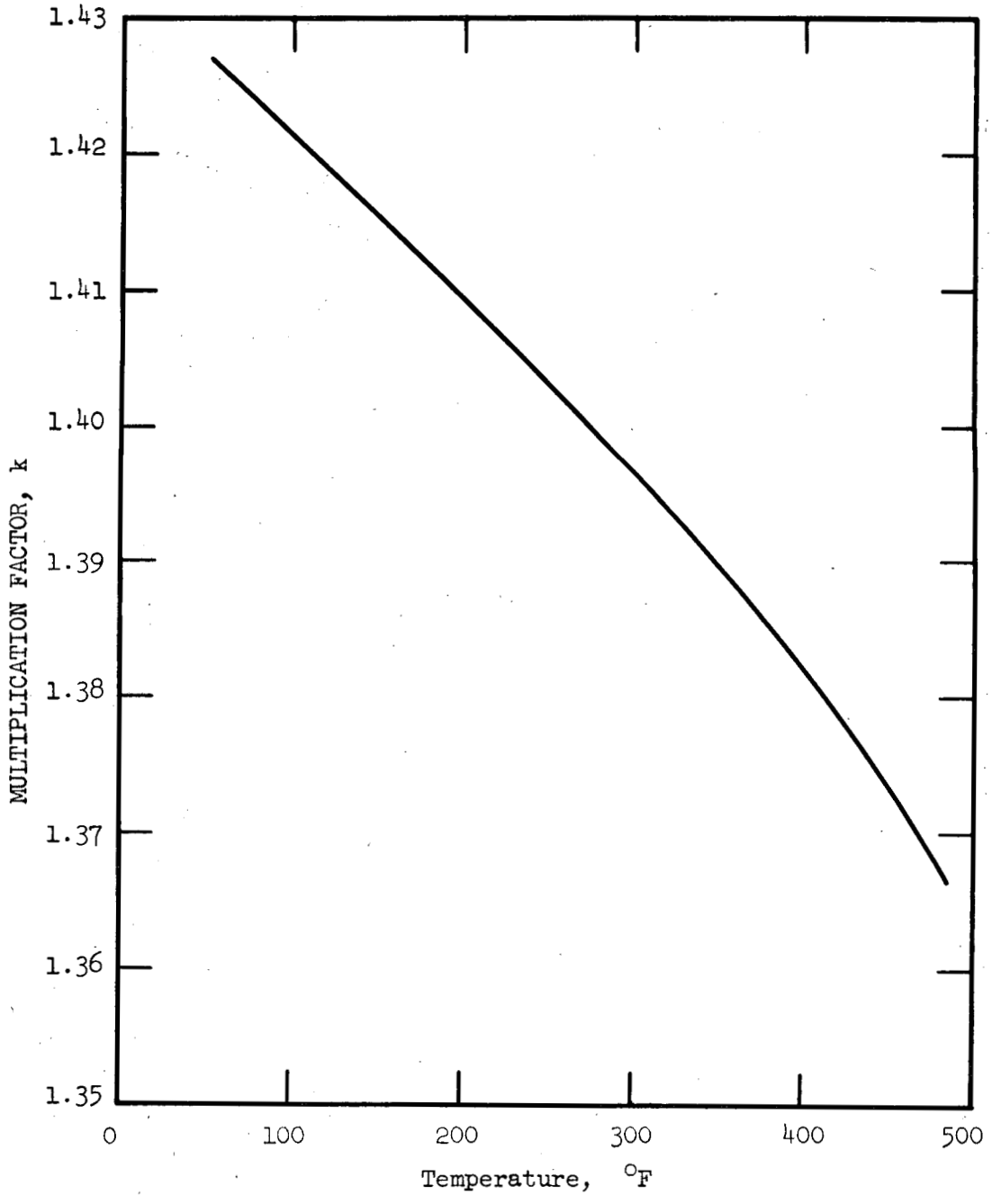

Fig. 34 MULTIPLICATION FACTOR Vs. TEMPERATURE FOR CLEAN REACTOR WITH NO BORON

ORNL-LR-Dwg.-22482
UNCLASSIFIED

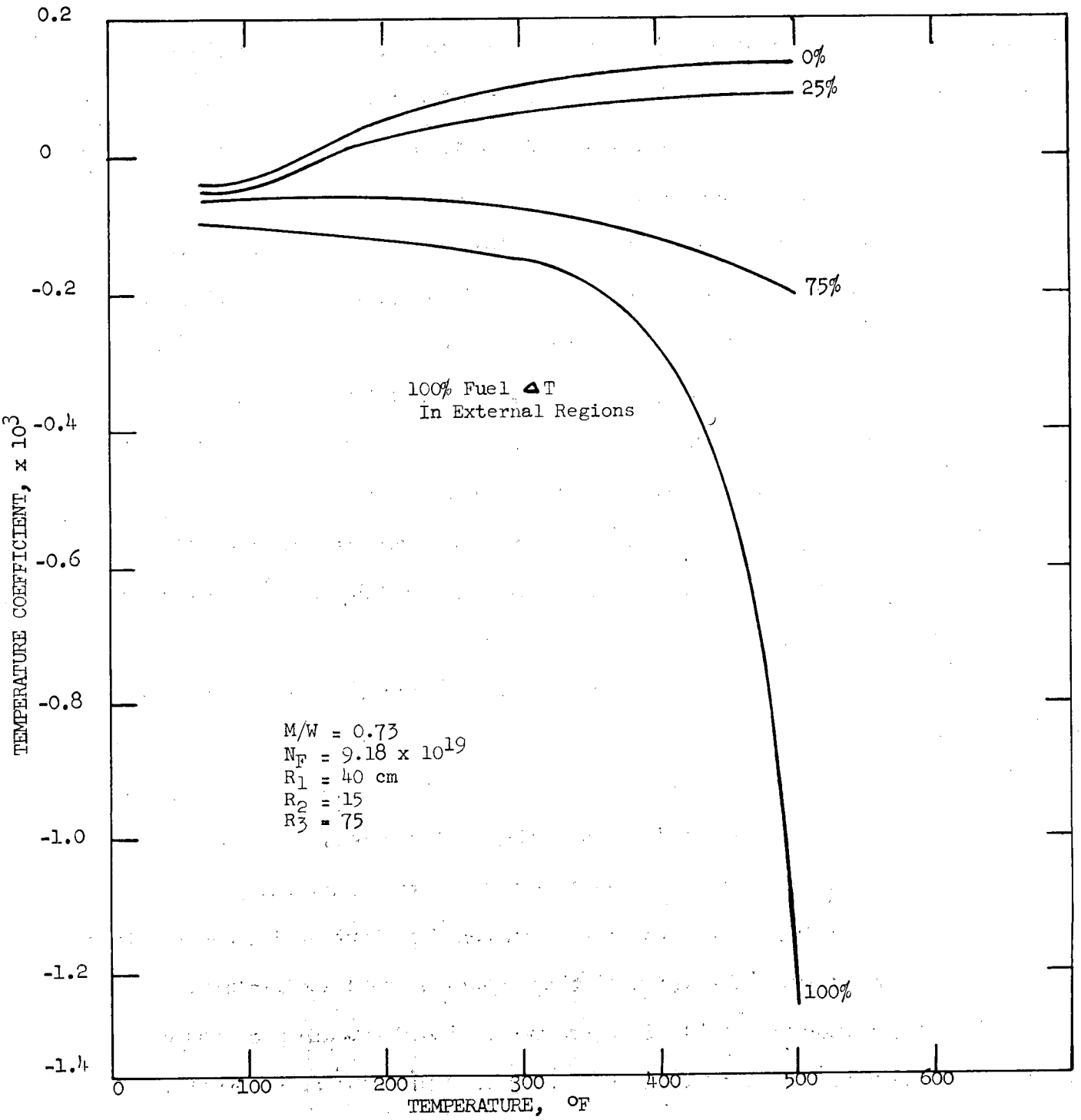

FIG. 35 TEMPERATURE COEFFICIENT OF REACTIVITY VS. FUEL TEMPERATURE, FOR VARIOUS EXTERNAL REGION TEMPERATURE RISES AS EXPRESSED AS PERCENTAGE OF FUEL TEMPERATURE RISE.

out the top of the elements and then down through the central and reflector regions. Thus, after an increase in fuel coolant temperature, the end reflector temperature will increase rapidly and the temperatures of the central and reflector regions will increase more slowly.

It appears that by maintaining a high flow rate of the boric acid in the one and one-quarter inch tubes the temperature of the boric acid could be kept essentially independent of the temperature in the fuel elements. For this reason plus the fact that the temperature of the external regions will rise fairly rapidly after a temperature rise in the fuel, the boric acid shim system is not expected to produce a positive temperature coefficient.

In conclusion, it appears that the problems regarding the temperature coefficient of reactivity of the present design of the HFRR can be overcome by proper mechanical design.

Xenon Instability: Xenon-135 has a large capture cross section and a high concentration in thermal neutron reactors. Hence, any perturbation which disturbs the concentration or distribution of xenon-135 would cause a fluctuation in the neutron flux. The effect is unstabilizing since, when the rate of xenon burnout is increased by an increase in the neutron flux, the poisoning effect of xenon is decreased and hence the neutron flux further increases. This effect is similar to that of a positive temperature or void coefficient.

This phenomenon is exhibited in two ways. The first and most common way is known as the xenon power instability. This is manifested as an overall exponential rise or drop in the neutron flux and power level. The period on which the neutron flux drifts has been calculated by K. O. Donelian and J. R. Menke[26,27], for various values of neutron flux and prompt neutron lifetime.

Using their formulae and the values of the prompt neutron lifetime and neutron flux for the HFRR, the period is calculated to be about 28 seconds. This period would be increased by a negative temperature coefficient. However, the 28 second period is long enough to be controlled by a conventional servomechanism.

The second way in which this instability can occur is in a constant power flux oscillation. This is exhibited in large thermal reactors with low neutron leakage as a rise in neutron flux in one part of the reactor and a corresponding drop in neutron flux in another part such that the reactor power remains constant. If the control system maintains the total power generated in the reactor constant, this oscillation could go unnoticed. As the name indicates, however, the increase in neutron flux in one part of the reactor does not continue without limit but reaches a maximum and begins to decrease. The neutron flux decreases until it passes through a minimum as far below the equilibrium value as the maximum was above it. Neutron flux in the other part of the reactor oscillates in opposite phase so that constant power is maintained. The oscillation continues until some compensating action is taken. The period of this oscillation is long, 12 to 14 hours, and the oscillation is therefore controllable.

A. G. Ward[28] has investigated this phenomenon theoretically and has derived an expression which can be used to determine whether or not a reactor will oscillate. His criterion has been applied to the HFRR and has indicated that the reactor will not oscillate. Detailed calculations on both types of instabilities are presented in Appendix X.

Effect of Experiments

To determine the actual neutron flux which is available in each experiment it is necessary to evaluate the flux depression caused by the experiment. Several

studies were made to determine the maximum perturbation which could be expected. The 3G3R ORACLE Code was used and the center region was made the experiment; the intermediate region, heavy water; and the outer region, fuel. A reflector savings was added to the fuel region to approximate the actual conditions which would exist in the reactor.

Figure 36 is a plot of the thermal neutron flux in the core, using various experiments for the central region. It should be pointed out that the experiments extend over the full length of the core and that with the exception of the fuel element, they are solid, containing no voids for D_2O coolant. Therefore, the perturbations indicated are greater than would exist in a practical experiment. The fuel element contains approximately MTR concentrations of enriched uranium. Only one size experiment was investigated for this project.

One of the important uses of a high flux research reactor is for testing nuclear reactor fuels. For the testing of an enriched solid fuel element it is difficult to make use of a higher thermal neutron flux than that for which the fuel element was designed because of heat removal problems and rapid burnup. The enrichment must be reduced or an experimental specimen must be prepared in such a form that heat removal is not difficult. Thus, a very high thermal neutron flux can be better utilized for studies of fertile materials and fuel elements of low enrichment. In the design proposed for the HFRR such experiments would probably be placed in the high flux central region and highly enriched experiments would be placed in the outer reflector.

Most fluid fuel reactors have been proposed to operate at thermal neutron fluxes far in excess of that presently available in solid fuel systems. Hence, the high flux available in the center of the HFRR would be useful for studies

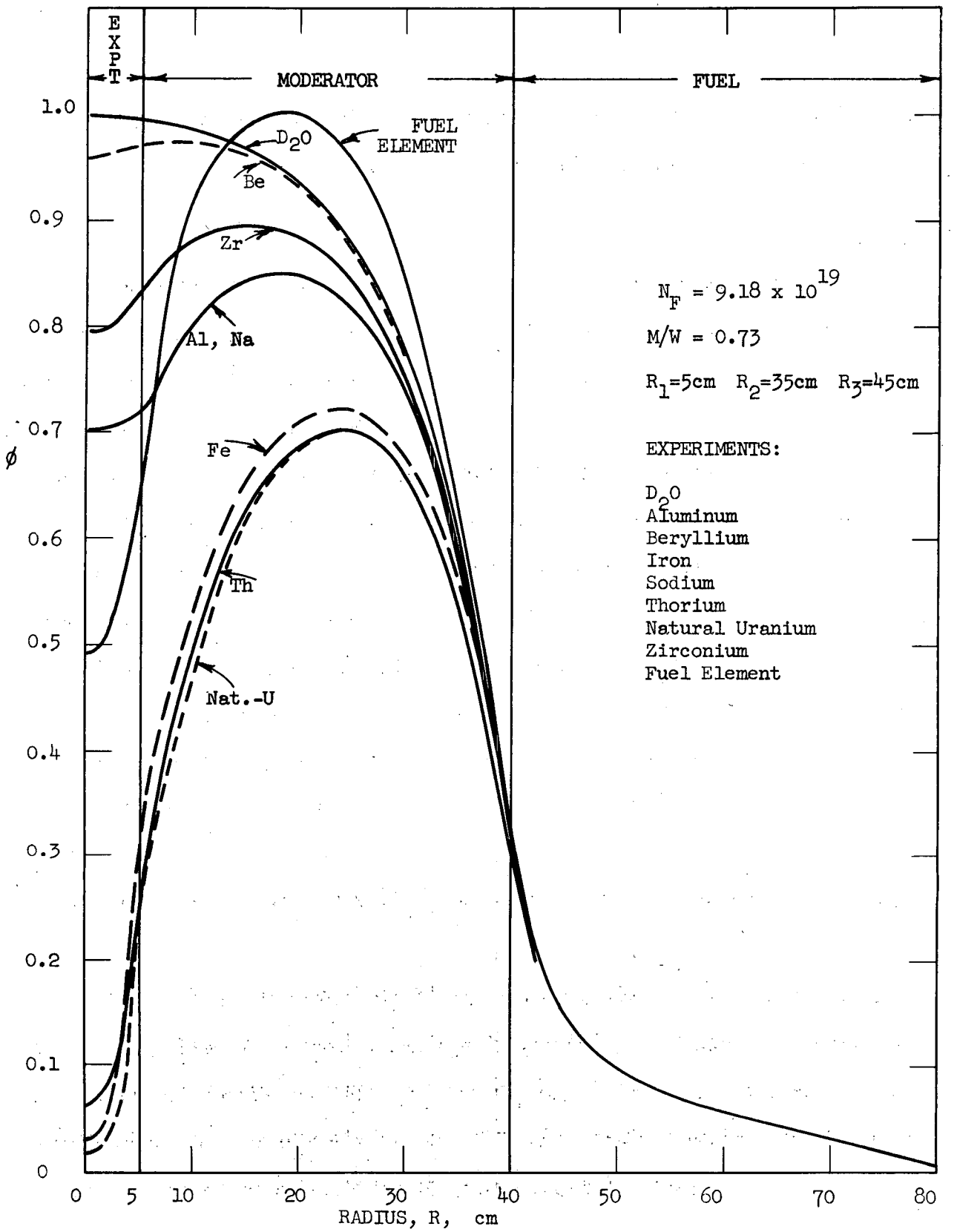

Fig. 36 THERMAL FLUX SPATIAL DISTRIBUTION WITH VARIOUS EXPERIMENTS IN CENTER OF MODERATOR

of fluid fuel reactor systems. An investigation was not completed on the flux perturbations caused by various fluid reactor fuels.

Topics for Future Study

Future study appears to be warranted on several topics pertaining to the physics aspects of the design of the HFRR. It would be desirable to use a multi-group reactor code which would calculate the neutron energy spectrum for the HFRR configuration and possibly increase the accuracy of the flux distributions.

The possibility of providing a region to test experiments in a high fast flux by placing an aluminum or carbon reflector next to the outside of the fuel annulus should be investigated further. The flux characteristics in a void in the central region of the reactor should be investigated as a possible means for obtaining a high fast flux. The analysis of a void placed in the reactor is difficult because diffusion theory does not apply within the void.

The actual flux perturbations to be expected from practical experiments should be determined. The effects of burnup on the flux distribution should be evaluated more carefully, using a multi-dimensional reactor code. The effect of the regulating rods and the shim tubes on the flux distributions should be analyzed.

The practical fuel annulus, consisting of an inhomogeneous array of fuel elements, should be analyzed in detail. Possible methods of decreasing the ratio of the maximum to average thermal flux in the fuel annulus without decreasing the peaking should be studied further. The time lag of the temperature change should be calculated for all regions of the reactor and an accurate temperature coefficient determined.

An optimum outside reflector should be selected on the basis of experimental facilities and cost. The optimum hydrogen content in the D_2O should be determined from the standpoint of effect on reactor parameters and cost.

It is felt that further consideration of the above topics is necessary to complete a thorough feasibility study on the HFRR.

REACTOR ENGINEERING

Heat Transfer

Fuel Elements: To obtain the desired nuclear characteristics this reactor must operate at extremely high power density. Therefore, one of the limiting factors in the design of a high flux reactor is the rate at which heat can be removed. Since the purpose of this study was not to arrive at a final design, but rather to study the limiting characteristics, a parameter study was undertaken and the results presented in the form of graphs which enable one to select certain pertinent information used for determination of the limiting power density of the reactor. These curves, of course, do not take into consideration mechanical design features which in themselves are limitations.

In deriving the equations it was assumed that the thermal and intermediate neutron fluxes, and therefore the heat flux, have cosine axial distributions, going to zero at the extrapolated boundary in the end reflectors independently of the radial distribution. The assumption is based on a theoretical solution to the flux distribution in a one-dimensional, side-reflected, cylindrical core, using reflector savings on the ends.

The necessary equations in the order in which they were used to make the parameter study are as follows:

$$\frac{T_o - T_i}{2} = \frac{4 q_o \tilde{H} \operatorname{Sin} \frac{\pi H}{2\tilde{H}}}{\rho V C_p \epsilon} \qquad (1)$$

$$h = .0115 \frac{K}{\epsilon} \left(\frac{2 \epsilon V_p}{\mu}\right)^{.8} (N_p)^{.4} \qquad (2)$$

$$z_{max} = \frac{2\tilde{H}}{\pi} \text{Tan}^{-1} \frac{4\tilde{H}h}{\pi \rho V C_p \epsilon} \quad (3)$$

$$T_{s_{max}} - T_i = q'_o \left\{ \frac{1}{h} \text{Cos} \frac{\pi z(\text{Max})}{2\tilde{H}} + \frac{4\tilde{H}}{\pi \rho C_p V \epsilon} \left[\text{Sin} \frac{\pi z(\text{Max})}{2\tilde{H}} + \sin \frac{\pi H}{2\tilde{H}} \right] \right\} \quad (4)$$

Assuming values of ρ and C_p for the coolant, equation (1) is used to determine the average bulk mean temperature of the coolant. Thus, the average properties of the coolant can be determined. Equation (2) is taken from McAdams.[8] Equation (3) determines at what point along the length of a given fuel plate the maximum surface temperature occurs. In some cases this temperature is calculated to exist within the end reflector. In such a case the actual maximum surface temperature exists at the end of the fuel plate. Equation (4) gives the maximum surface temperature in the axial direction on a surface having heat flux, q'_o. The derivations of these equations are found in Appendix III.

It should be noted that T_i for all calculations was taken as 100°F. Small variations in the coolant inlet temperature will not affect the results appreciably until the average bulk mean temperature reaches about 200°F. Use of the curves beyond this temperature gives a conservative answer, however. In all calculations the length of the core was fixed at 3.00 feet and the reflector savings at 0.66 feet.

Figures 37, 38, 39, and 40 represent the results of the parameter study. One method of using the curves begins with the determination of a maximum power

ORNL-LR-Dwg.-22483
UNCLASSIFIED

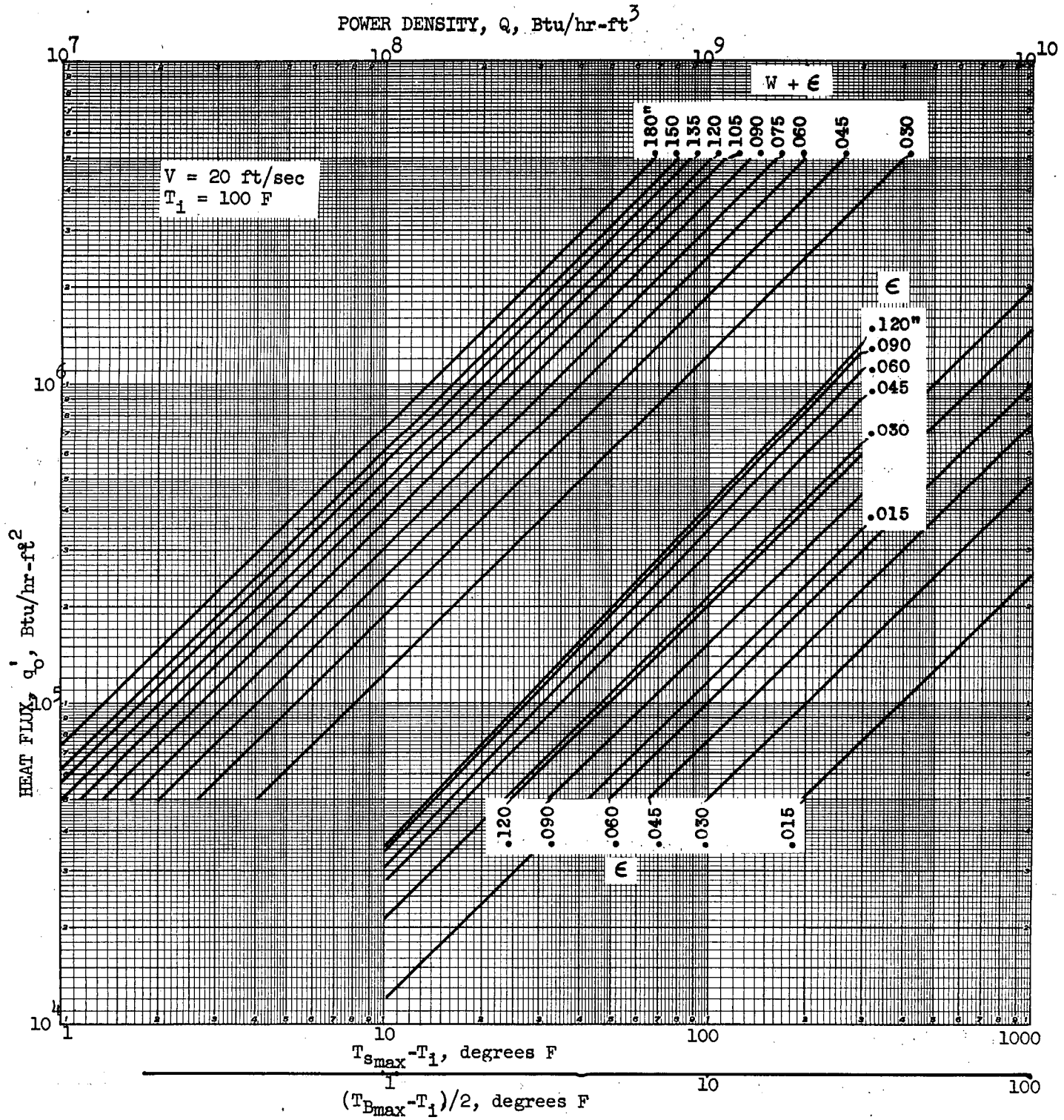

FIGURE 37 MAXIMUM RELATIVE SURFACE TEMPERATURE AND BULK MEAN WATER TEMPERATURE AS A FUNCTION OF HEAT FLUX, COOLANT GAP, AND FUEL THICKNESS. V = 20 FPS

ORNL-LR-Dwg.-22484
UNCLASSIFIED

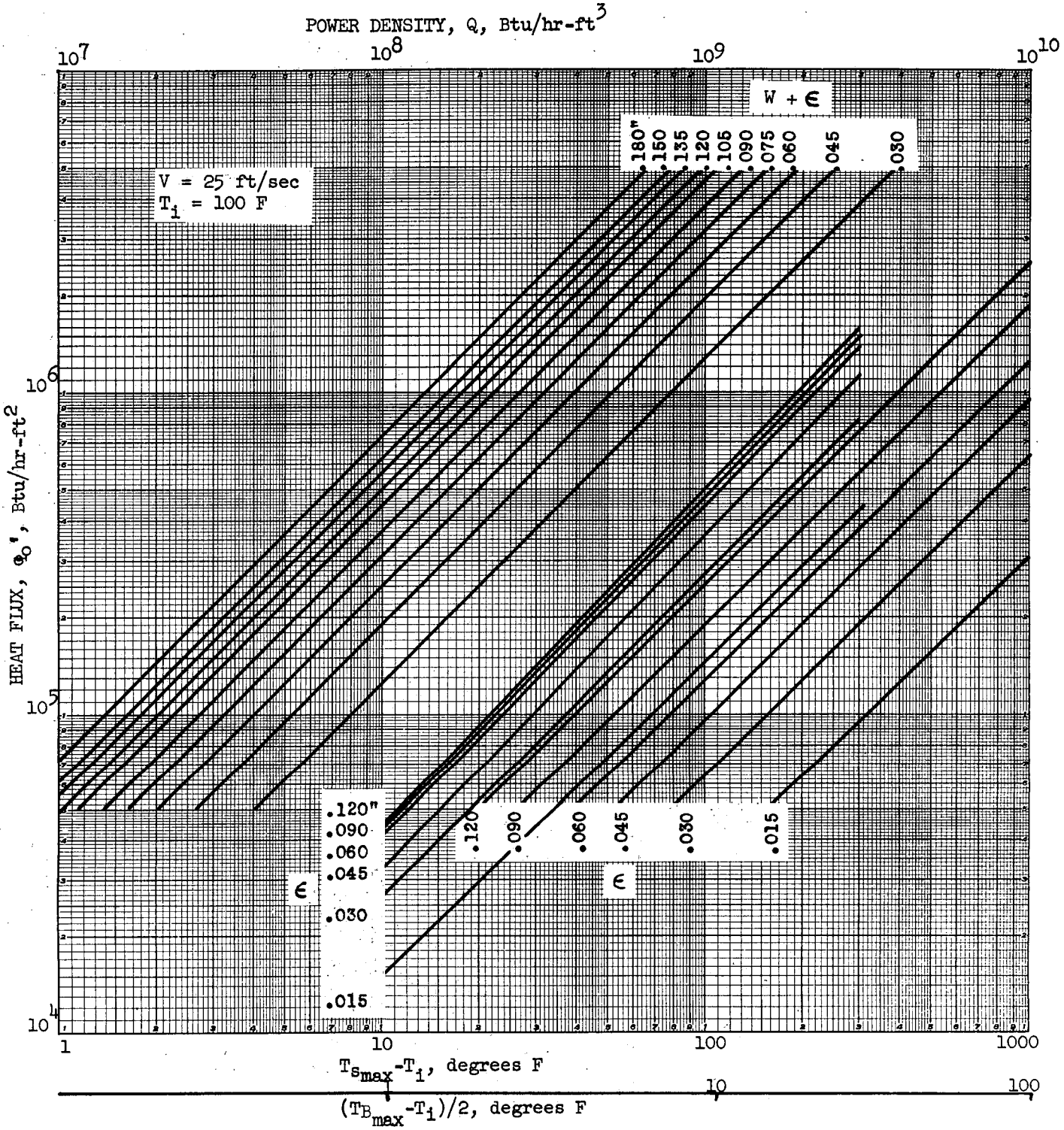

Fig. 38 MAXIMUM RELATIVE SURFACE TEMPERATURE AND BULK MEAN WATER TEMPERATURE AS A FUNCTION OF HEAT FLUX, COOLANT GAP, AND FUEL THICKNESS V = 25 FPS

ORNL-LR-Dwg.-22485
UNCLASSIFIED

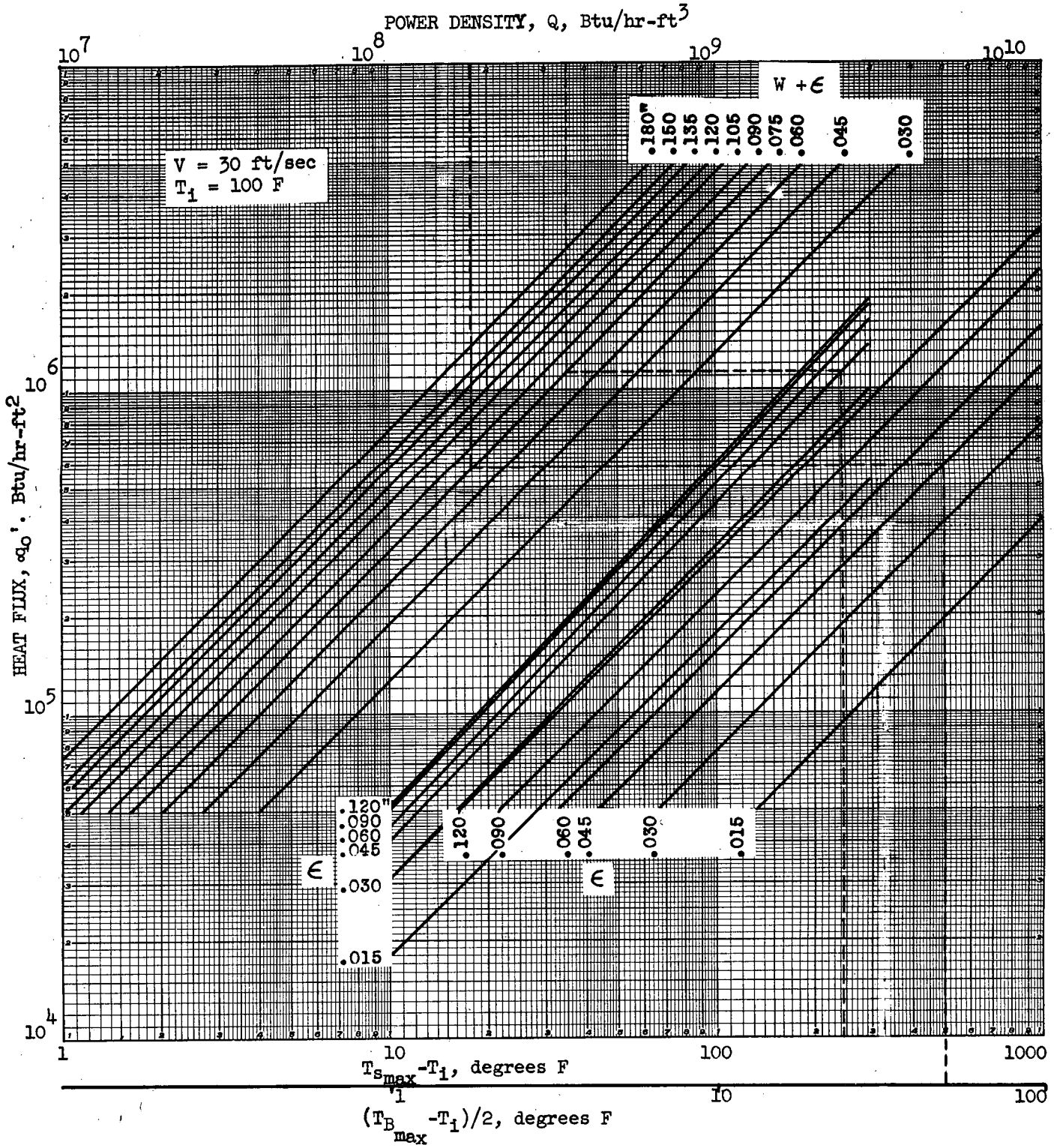

Fig. 39 MAXIMUM RELATIVE SURFACE TEMPERATURE AND BULK MEAN WATER TEMPERATURE AS A FUNCTION OF HEAT FLUX, COOLANT GAP, AND FUEL THICKNESS. V = 30 FPS

ORNL-LR-Dwg.-22486
UNCLASSIFIED

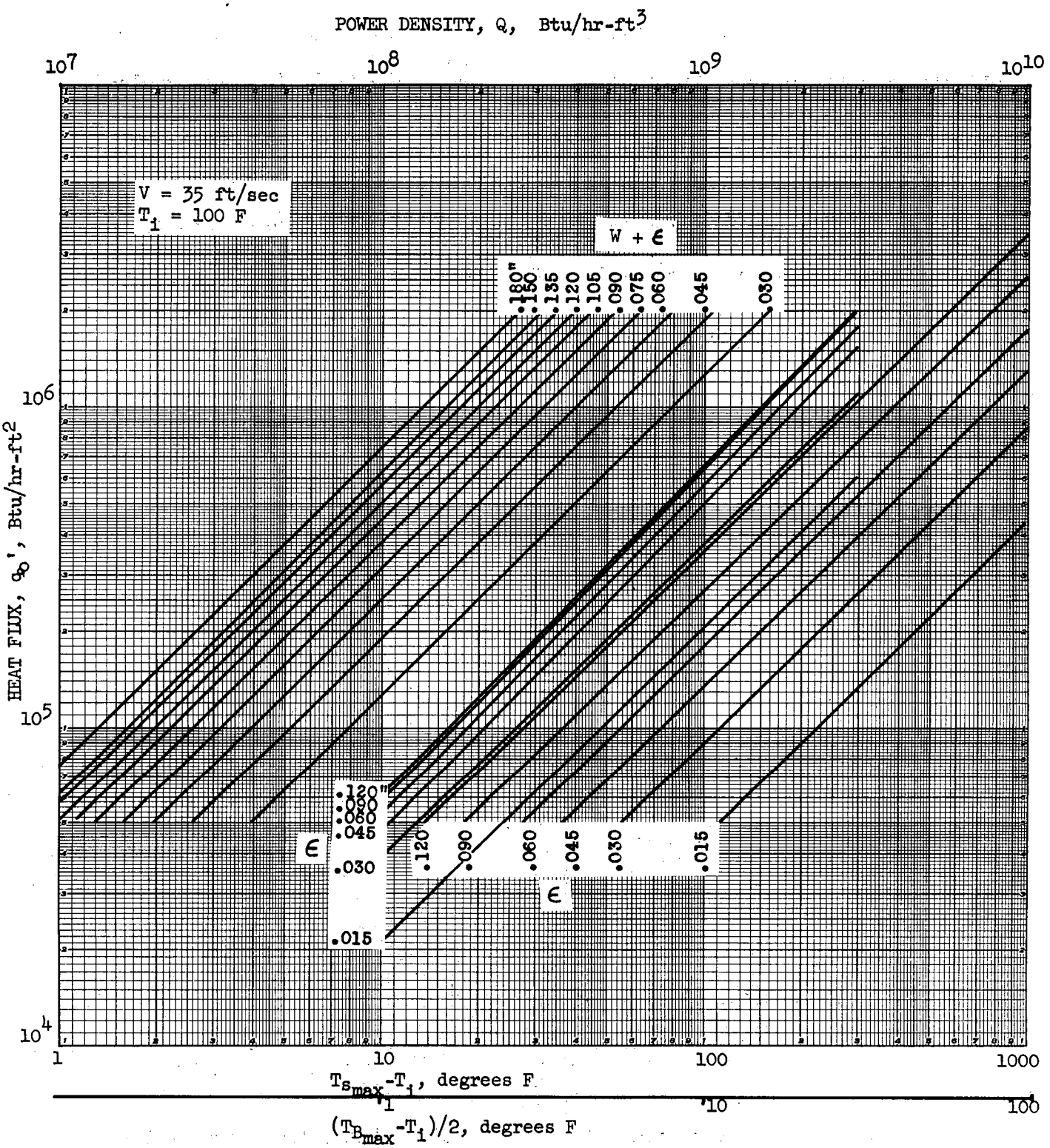

Fig. 40 MAXIMUM RELATIVE SURFACE TEMPERATURE AND BULK MEAN WATER TEMPERATURE AS A FUNCTION OF HEAT FLUX, COOLANT GAP, AND FUEL THICKNESS. V = 35 FPS

density from nuclear characteristics. If an upper limit has been set on the operating pressure of the system, the dimensions of the fuel plate and coolant channel can be determined as indicated on the graphs.

In order to determine the location and temperature of the hot spot in the core it is necessary to know the ratio of maximum to average power density in the core. By assuming a radial flux shape similar to ORACLE flux plots, the following relationship was derived:

$$\frac{q'_{avg}}{q'_{o(max)}} = \left[1 - \frac{2}{\pi}\left(\frac{X-1}{X}\right)\right]\left[\frac{2\tilde{H}}{\pi H}\sin\frac{\pi H}{2\tilde{H}}\right] \tag{5}$$

where

$$\frac{q'_{o(avg)}}{q'_{o(max)}} = \left[1 - \frac{2}{\pi}\left(\frac{X-1}{X}\right)\right] \tag{6}$$

and

$$\frac{q'_{(avg)(axial)}}{q'_{o}} = \left[\frac{2\tilde{H}}{\pi H}\sin\frac{\pi H}{2\tilde{H}}\right] . \tag{7}$$

Derivations of the equations appear in Appendix III. Using the aforementioned values for H and $\tilde{H}$, equation (7) gives a value of 1/1.23. The value of X

depends on several parameters and may be obtained from ORACLE data. However, a more accurate method is to determine $q'_{o(max)}/q'_{o(avg)}$ directly from Figure 8 and then to calculate $q'_{o(max)}/q'_{avg}$ as indicated above. This ratio is of considerable importance in selecting the thickness of the fuel annulus and the concentration of the fuel. It is seen in Figure 5 that the ratio increases as the thickness of the annulus increases for a given fuel concentration. There is also an increase in the ratio, when the fuel concentration is increased. If all other variables are held constant, it is desirable to minimize the ratio of maximum to average power density, in effect maximizing the average allowable power density in the core. As was explained in the section on nuclear physics, it is desirable to obtain as high an average power density as possible.

A hot channel factor to take into consideration variations in the coolant flow area and prediction of special flux distribution was assumed to be unity for the following reasons: Because of the axial flux shape and the cylindrical geometry of the fuel element the hotspot is actually just a point on the outer surface of the element. Even if boiling did occur at a localized spot, it would not be too serious since it could not cause blockage of flow through a channel since as explained elsewhere, there are no single isolated channels. Rotation of the fuel element does not effect heat removal. Another important reason is that when selecting the ratio $q'_{o(max)}/q'_{o(avg)}$ from Figure 8 it is assumed that the fuel is homogeneously distributed in the fuel annulus and that the fuel concentration is the same as in a fuel cylinder. As explained in greater detail in the nuclear physics section, this results in a value of $q'_{o(max)}/q'_{o(avg)}$ greater than in the actual case.

When using the curves in Figures 37, 38, 39, and 40 it must be remembered that for any particular solution all values read from the curves pertain to a

particular vertical line through the fuel element. If, for example, it is desired to determine the maximum surface temperature in a fuel element for a given specified average power density, it is necessary to use the maximum power density in the fuel element as determined above. To find the average coolant discharge temperature it is necessary to use $Q_{(avg)} \times q'_o/q'_{(avg)(axial)}$ as the power density. See Appendix I for a sample calculation.

For a high power density reactor, it is necessary to develop as much heat transfer surface area per gram of fuel as possible. This is accomplished by increasing the surface area to volume ratio.

Several basic types of fuel elements were studied, giving consideration to the practicability of fabrication and to mechanical design features as well as to heat transfer. The type selected is basically a curved plate fuel element. For this type element the relationship between heat flux and power density is as follows:

$$q'_o = Q \frac{(W + \epsilon)}{2} \quad . \tag{8}$$

Therefore, for a given power density the sum of the thickness of the fuel plate and coolant channel must be small enough to give a reasonable heat flux. Since it has not yet been demonstrated that heat removal by film boiling is unquestionably satisfactory, the maximum heat flux to be considered should be approximately 10^6 Btu/hr/ft^3. A further restriction on equation (8) is the metal to water ratio needed to give desired nuclear characteristics. This ratio generally is between 0.5 and 1.0. Thus, for a desired maximum power density

of 3×10^8 Btu/hr/ft^3, $W + \epsilon = 0.08$ inches. Therefore, $W = 0.027$ to 0.04 inches and $\epsilon = 0.053$ to 0.04 inches. These comparatively small dimensions are typical of those required for any type fuel element considered. It was felt that a satisfactory fuel element could be more readily developed using curved plates.

A more detailed discussion of the design of the fuel element is found elsewhere in the report.

Fuel Element Housing: The heat generated by neutrons and photons in the aluminum fuel element housings can be removed from the inside by the fuel element coolant and from the outside by the D_2O that acts as reflector and moderator. Calculations indicate that within practical limits of power for this reactor that there should be no real problem in removing enough heat from the housings to prevent boiling.

Cooling System

The cooling system of this reactor utilizes heavy water as a cooling medium and involves all of the heavy water used in the moderator, fuel, and reflector regions. Coolant is pumped into the fuel element tubes from the bottom, removes heat from the elements, and is orificed to atmospheric pressure at the top of the tubes and allowed to flow into the moderator and reflector regions at a mean temperature somewhat below the saturation temperature corresponding to atmospheric pressure. Pressurization of individual fuel elements is obtained by the pump head and the pressure drop across the orifice at the outlet end of each fuel element housing. Additional cooling of the aluminum fuel element housing may be provided by forced circulation between the fuel region and baffles placed in the reflector and moderator regions as shown in the schematic diagram of the reactor. Low pressure coolant in quantity approximately equal to the fuel

coolant flow is supplied to the moderator and reflector regions to prevent the temperature in these regions from approaching the fuel coolant outlet temperature and to provide the removal of the heat generated in the moderator and reflector.

Coolant is withdrawn from the reactor only from the moderator and reflector regions, is then cooled in heat exchangers, and is returned to the reactor through high pressure and low pressure pumping systems.

Determination of the coolant supply pressure required for a given set of reactor conditions is accomplished through the use of data presented on the heat transfer and pressure drop graphs, Figures 37, 38, 39, 40, and 41. For a given fuel plate thickness, coolant gap width, and maximum power density, the heat transfer graphs give the maximum fuel surface temperature which will be reached. The minimum coolant pressure required is then taken to be the saturation pressure at a temperature above this maximum surface temperature by the amount of the safety factor considered necessary to guarantee the prevention of local boiling in the fuel region. To this must be added the pressure drop occurring in the fuel region, which may be evaluated using the pressure drop graph, data for which were obtained from the equations below.

$$\Delta P_s = \frac{0.092\, H \rho V^2}{g_c \epsilon N_R^{0.2}} \tag{9}$$

$$\Delta P_I + \Delta P_E = \frac{\rho V^2}{2g_c} \left[K_1 + \left(1 - \frac{\epsilon}{W + \epsilon} \right)^2 \right] \tag{10}$$

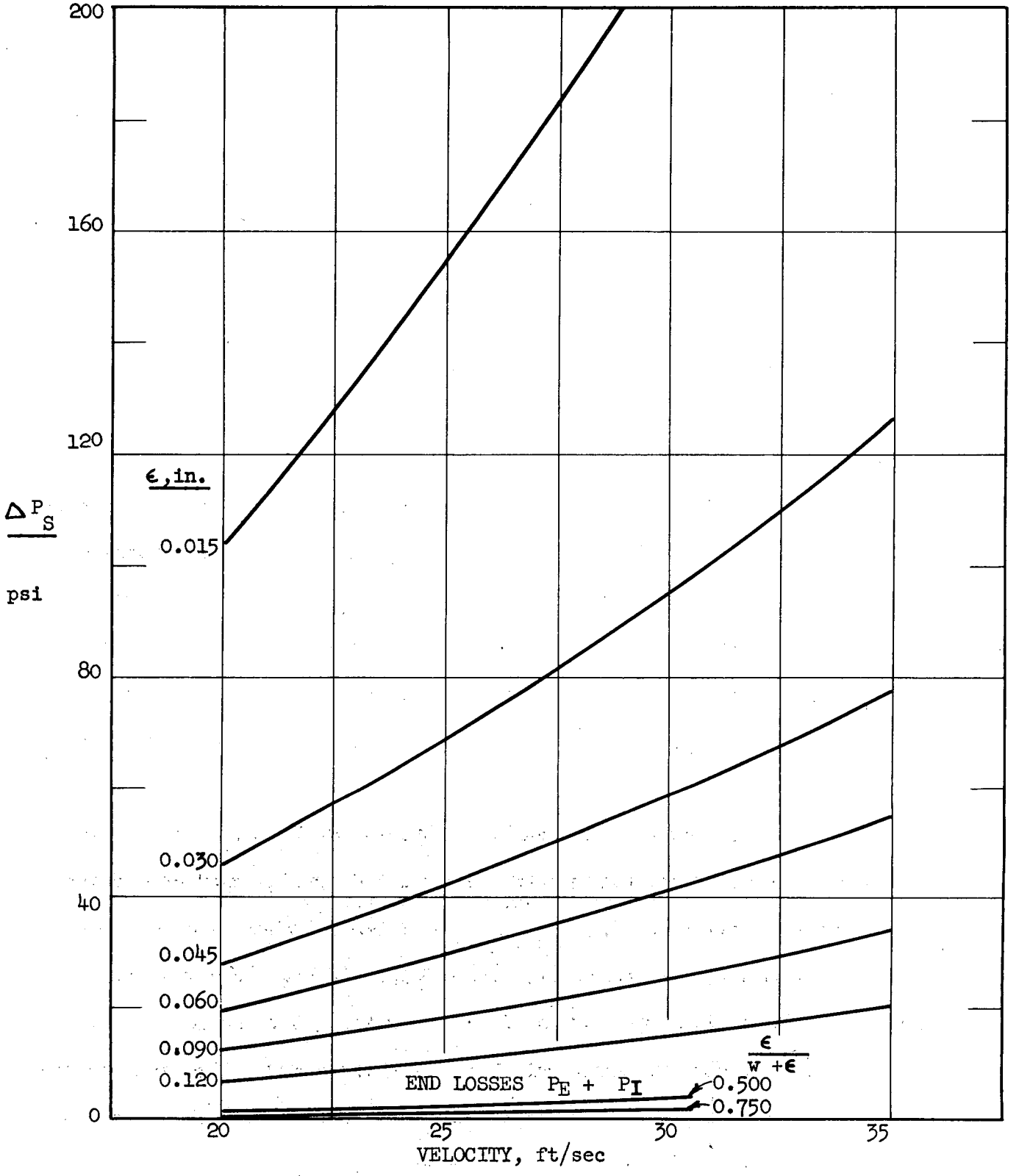

Fig. 41 STRAIGHT CHANNEL AND END LOSS PRESSURE DROP VS. VELOCITY IN CHANNEL

where

$$K_1 = 0.4 \left(1.25 - \frac{\epsilon}{W + \epsilon}\right) \text{ for } \frac{\epsilon}{W + \epsilon} < 0.715$$

$$K_1 = 0.75 \left(1 - \frac{\epsilon}{W + \epsilon}\right) \text{ for } \frac{\epsilon}{W + \epsilon} > 0.715 \quad .$$

The result of this calculation is the required coolant supply pressure. The bulk mean coolant temperature at outlet from the fuel region must then be determined from the heat transfer curves, and must be below the saturation temperature corresponding to atmospheric pressure, to which the coolant is orificed upon leaving the fuel region. The preceding calculation may be performed for various coolant velocities in the fuel region by the use of the appropriate heat transfer graphs.

The flow rate of high pressure coolant required may be easily calculated, when the required velocity and fuel plate thickness and spacing have been determined.

As an example, for a fuel plate thickness of 0.030 inches, a coolant gap of 0.045 inches, and a maximum power density of 3.5×10^8 Btu per hour-cubic foot, a maximum fuel surface temperature of 350°F is indicated, using the heat transfer graph plotted for a velocity of thirty feet per second. Adding a safety factor of fifty degrees to this value, a minimum coolant pressure of 262 pounds per square inch absolute is obtained. From the pressure drop graph it is

determined that 62 pounds per square inch must be added to this value to account for pressure drop in the fuel element, giving a supply pressure of 324 pounds per square inch absolute, or an overall pressure drop of 309 pounds per square inch. From Figure 39, using the average power density of 1.5×10^8 Btu/hr/ft^3, the bulk mean water temperature at the fuel region outlet is determined to be 200°F, which is below the saturation temperature corresponding to atmospheric pressure. Using the chosen values of fuel region velocity, coolant gap, and fuel plate thickness for three-inch diameter fuel elements, the high pressure coolant flow rate is calculated to be 27,470 gallons per minute. At the pressure calculated, this corresponds to a high pressure pumping horsepower of 4950 as determined from Figure 42.

Design of the Fuel Element

It is suggested elsewhere in this report that a plate type fuel element be used. The mechanical stability of a plate can be improved by curving the plate. The smaller the radius of curvature the more stable the plate will be. This would indicate that concentric cylinders should be used, the maximum radius being held to a minimum. If the entire fuel annulus were made of large concentric cylinders, the radius of curvature would effectively be infinite and, therefore, satisfactory stability could not be obtained. Furthermore, when replacing burned fuel elements, such a design would require that the entire annulus be changed as one unit. Because of the comparatively short fuel cycle in a high flux reactor, fuel replacement and fuel element fabrication should be as simple and quick as possible. To satisfy these requirements it is suggested that the fuel annulus be made up of a number of cylindrical fuel elements as shown in Figure 1.

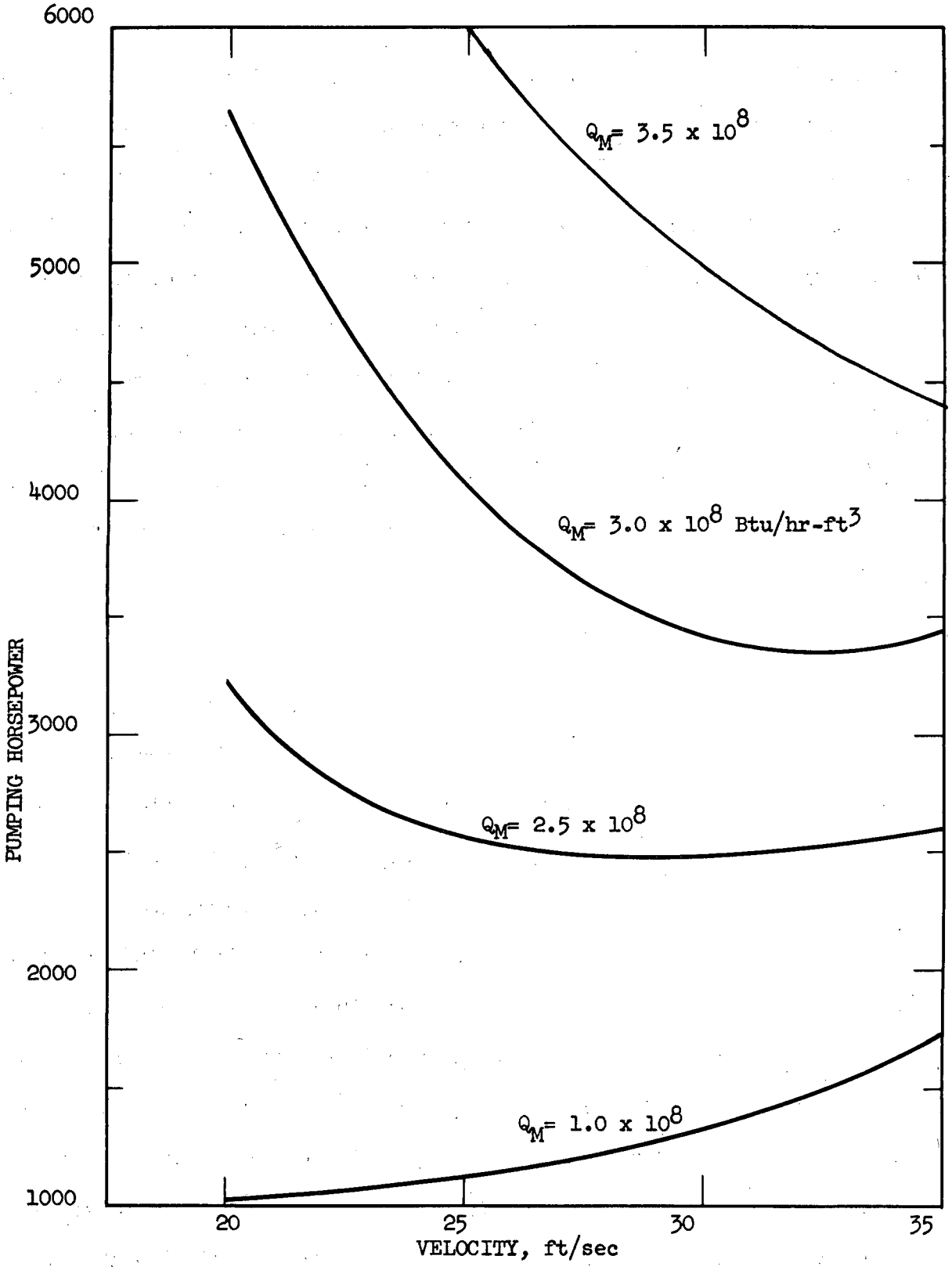

Fig. 42 PUMPING POWER VS. VELOCITY FOR MAXIMUM SURFACE TEMPERATURE 50°F BELOW SATURATION TEMPERATURE CORRESPONDING TO OUTLET PRESSURE

There are several reasons for suggesting a cylindrical fuel element in preferance to the MTR type. As is indicated on the neutron flux plots, there is a considerable thermal flux gradient near the edges of the annulus. This means that during the operation of the reactor the fuel annulus will effectively become narrower because of non-uniform fuel burnup. The advantages and disadvantages of such a situation are discussed in the "Nuclear Physics" section. To obtain uniform burnup in the radial direction the possibility of rotating the fuel elements was considered. Such a design would require a cylindrical fuel element design for more effective space utilization.

A second reason for the selection of a cylindrical element is the need for locating the control rods and shim tubes in the fuel region. Figure 1 indicates the solution to this problem by the use of cylindrical fuel elements.

A third reason for using cylindrical geometry is the necessity of pressurizing the fuel element housing. To minimize the amount of material for mechanical strength in the housing it is necessary that the housing have a cylindrical geometry.

A fourth reason for selecting a cylindrical fuel element is that such an element may have desirable fabrication and performance characteristics. The method of fabrication suggested is that of rolling a plate three feet in width by whatever length is necessary into a spiral, allowing sufficient space between each successive turn for a coolant channel. An adequate number of aluminum spacers would be inserted into the coolant channel to insure sufficient stability of the unit. The spacers would be intermittent along the length of the element so that through the entire length of the element there would be no isolated coolant channels. This is a very desirable feature since it makes it almost

impossible to plug any portion of the element without plugging the entire coolant flow area at one end. Since the desired nuclear characteristics of the reactor demand a very small coolant channel thickness, plugging of the element becomes a more serious problem and a possible limitation to the maximum power density obtainable in the fuel element.

This particular type of fuel element was discussed with Mr. J. E. Cunningham[9] to determine the practicability of fabrication. It was concluded that a 0.030 inch aluminum fuel plate three feet in width and about ten feet long could very likely be rolled and fabricated into the spiral shape. The aluminum spacers quite possibly could be spot welded to the aluminum cladding. This would be done while the plate was flat. Spring back would be eliminated by spot welding the non-fuel-bearing ends of the plate to the opposite sides of the spacers as the plate is rolled into a spiral.

Rotation of the fuel elements provides some mechanical problems. Perhaps the most obvious is the design of a suitable bearing since the force on the element due to pressure drop and fluid friction would be considerable. A tentative solution to this problem is to use a simple pivot or conical bearing and hydrostatic lubrication. The bearing would be located outside the orifice in the low pressure system as shown in Figure 1. High pressure lubricant (water) would be supplied to the bearing through a calibrated tube coming from the high pressure side of the orifice.

Rotation of the element could be accomplished by means of the tangential velocity of the coolant escaping from the partially open end of the spiral or by installing the spacers at an angle, taking advantage of the normal component of the straight through coolant flow.

Fuel Element Assembly

A compact unit consisting of two fuel elements and an aluminum fuel element housing can be assembled and disassembled outside of the reactor. In the reactor the complete units are plugged into the plenum chamber in the bottom of the reactor tank, forming the fuel annulus.

Heat Production

Heat production in the following locations was investigated.

I. Moderator and reflector.

II. Boron tubes.

III. Aluminum fuel element housings.

The methods of investigating the various sources of heat generation are as follows:

1. Gamma heating - This was calculated by means of the Hurwitz straight ahead scattering approximation[10]. One assumes that although the photons suffer energy degradation they are scattered either through such small angles that the deviations from the line of flight are ignored or through such large angles that the resulting low energy photons are absorbed near the point of scattering. An integral energy equation derived in Appendix IV is expressed as

$$G = \frac{S \bar{E} \bar{\mu}_e}{2 \mu_t} \left[E_2(\bar{\mu}_e X) - E_2(\bar{\mu}_t b + \bar{\mu}_e x) \right] \quad \ldots \qquad (1)$$

2. Elastic Collisions - The elastic collision heating rate is

$$G_{ne} = \int_{E_o}^{\infty} \delta_{ne} E_n \Sigma_{ne} (E_n) \phi_n (E_n) dE_n \ldots \quad (2)$$

3. Neutron Capture - Heat generation due to capture of fast neutrons is

$$G_{nc} = \int_{E_o}^{\infty} \delta_{nc} E_n \Sigma_{nc} (E_n) \phi_n dE_n \ldots \quad (3)$$

Another equation derived in Appendix V yields the following expression for capture gamma heating.

$$G(b) = N_\gamma \Sigma_a \phi_1 \mu_e EI(b, E) \ldots \quad (4)$$

where

$$I = 1/2 \left[b + \frac{t}{\pi} P(\cos \frac{\pi b}{t} - 1) \right] me^{-\mu t b}$$

$$+ 1/2 \left[b + \frac{t}{\pi} P(\cos \frac{\pi b}{t} - 1) \right] \int_{\mu_t R = \mu_t b}^{\mu_t R = \infty} e^{-(\mu_t R)} \frac{d(\mu_t R)}{(\mu_t R)}$$

$$+ 1/2 \left[(t-b) - \frac{t}{\pi} P(\cos \frac{\pi b}{t} + 1) \right] me^{-\mu_t (t-b)}$$

$$+ 1/2 \left[(t-b) - \frac{t}{\pi} P\left(\cos \frac{\pi b}{t} + 1\right)\right] \int_{\mu_t R = (t-b)\mu_t}^{\mu_t R = \infty} e^{-\mu_t R} \frac{d(\mu_t R)}{(\mu_t R)}$$

I. Moderator and Reflector.

Heat production is due mainly to three sources.

a. Prompt gammas.

b. Elastic collisions.

c. Neutron capture.

(a) Prompt gammas. Power density per Mw for various distances into the moderator appears in Figure 43. Such a plot will determine the local cooling rates. The total heat in watts is $Q = 5.72 \times 10^2 P(Mw)$. The calculation in Appendix VI considers the cylindrical fuel annulus to be an infinite slab.

(b) Elastic collisions. Total heat in watts is $Q = 3.4 \times 10^4 P(Mw)$. If one further assumes $\phi_n = \phi_{12M} e^{-\Sigma_f r}$ the power density in the moderator is described by Figure 44 for various ratios of $\frac{\phi_{12M}}{\phi_{12}}$ and $\frac{\phi_{12}}{\phi_{32}}$ and computed in Appendix VI.

(c) Neutron capture. The contribution of neutron capture is small compared to the heat released by neutron elastic scattering and a simple calculation yields $37P(Mw)$ watts.

The total heat in watts developed in the moderator is largely due to elastic collisions and is equal to about $3.4 \times 10^4 P(Mw)$.

One may also consider the heating in the reflector to be the same as the moderator because it was assumed that the cylinder was a slab. If this is the

ORNL-LR-Dwg.-22489
UNCLASSIFIED

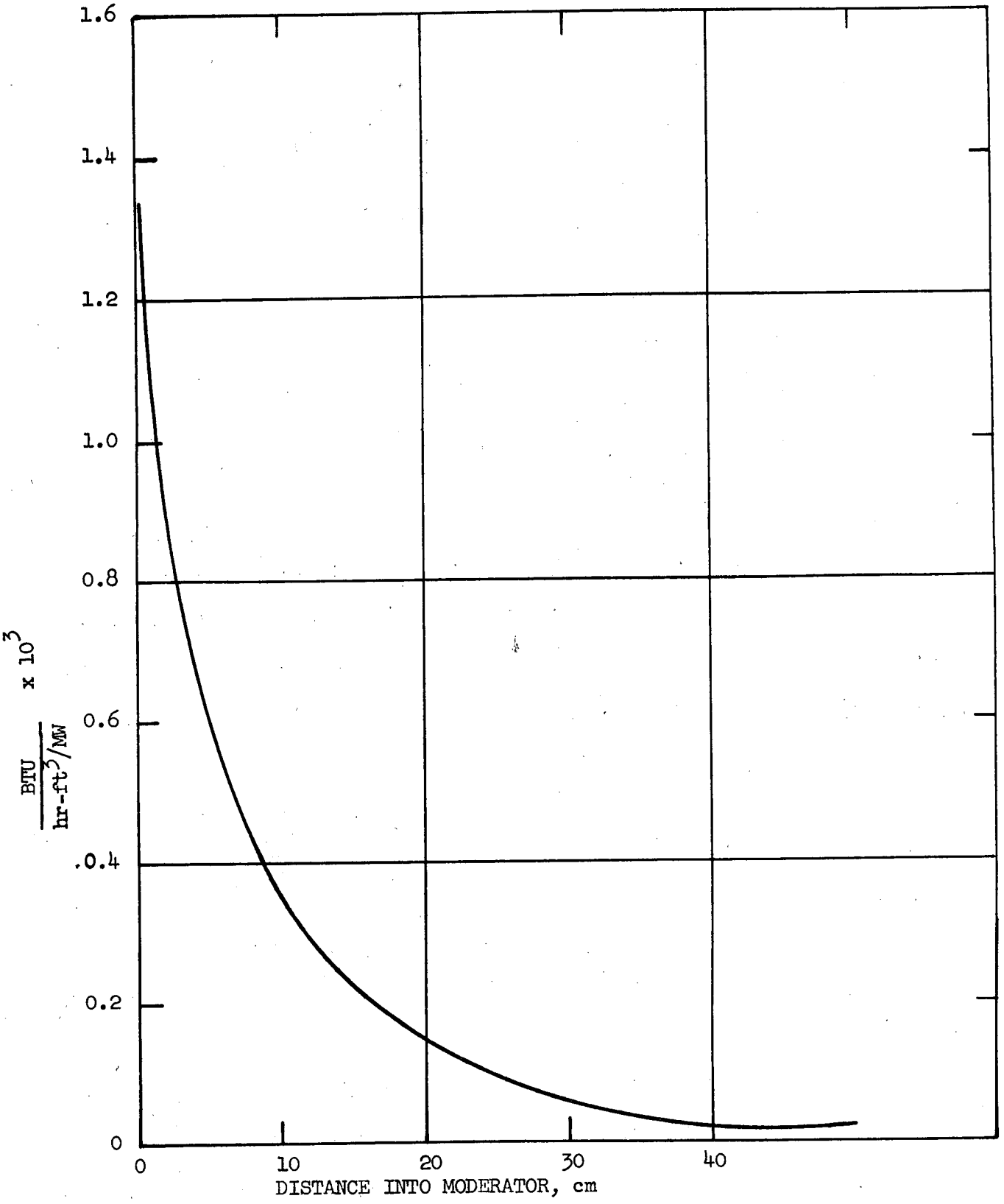

Fig. 43 PRIMARY GAMMA HEAT PRODUCTION IN D_2O VS. DISTANCE INTO MODERATOR

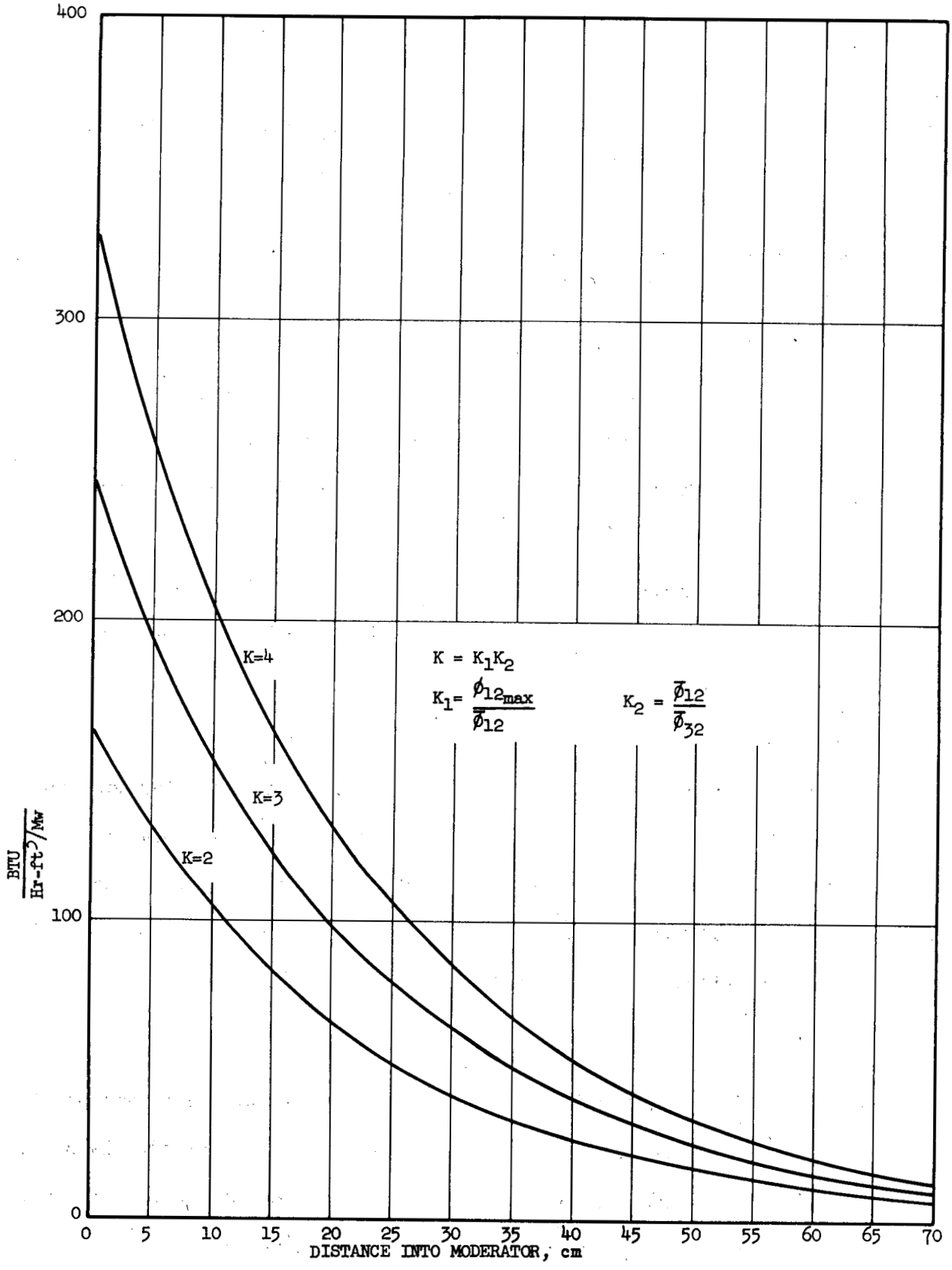

Fig. 44 HEAT PRODUCTION DUE TO ELASTIC COLLISIONS IN D_2O VS. DISTANCE INTO MODERATOR FOR VARIOUS K's

case then the heat produced for a 300 Mw reactor is $2(300)(3.4 \times 10^{4}) = 20.4$ Mw or 6.8% of the total power.

II. Heat Production in Boron Tubes.

Heating is due to three sources:

(a) Boron capture α particles. All of the kinetic energy associated with the 2.314 Mev α particles and Li^{7}, arising from neutron capture in the boron, is captured in the tube. Power density is 1.39×10^{-3} Btu/hr-ft^3/Mw.

(b) Boron capture gammas. In this case the 0.48 Mev gammas contribute 2.88×10^{-4} Btu/hr-ft^3/Mw.

(c) Elastic collision. The calculation is based on an average flux of 3.3×10^{15} n/cm^2-sec in the tube and yields 5.38×10^{-5} Btu/hr-ft^3/Mw. Calculations appear in Appendix VII.

III. Aluminum Housing.

Heat production was calculated for prompt fission gammas using equation (1) and yielded 8.46×10^{3} Btu/hr-ft^3/Mw. Likewise capture gamma heating is 1.31×10^{3} Btu/hr-ft^3/Mw for a flux of 1.58×10^{15}. Elastic collision heat generation is 2.36×10^{2} Btu/hr-ft^3/Mw resulting in a total of 1×10^{4} Btu/hr-ft^3/Mw. The method of calculation is illustrated in Appendix VIII.

Shielding

The purpose for investigating the shielding problem was to determine if a high column of water above the reactor, such as is present in the MTR, is necessary. If the column were required, the D_2O inventory would be considerably increased. Also, since it is necessary to maintain the D_2O as clean as possible it does not seem practical for personnel to work directly over a column of D_2O exposed to

the atmosphere. A solution to the problem then would be to use remote handling of the experiments and fuel in an inert atmosphere above the core. With the concrete plugs in place while the reactor is running the dose directly above the reactor would be permissible. With the plug removed during operation or one day after shutdown the dose would be excessive. However, in an emergency the void left by removal of the concrete plug could be filled with D_2O, and one day after shutdown a person could work directly over the reactor.

Radiations considered in shielding calculations for the top of the reactor were prompt fission gammas, secondary gammas, and neutrons. Two methods of calculation were employed.

1. Linear buildup factor.
2. NDA buildup factors.

The shield design consists of three materials, D_2O, steel, and concrete. One of the main considerations was to limit the amount of D_2O employed, the height of which was fixed at 200 cm. Since the fuel elements and connections are somewhat over 100 cm long, the 200 cm allowed sufficient space to mechanically remove the fuel while immersed in the coolant. Using various thicknesses of steel, which also acts as a thermal shield, the dose in rad/hr-Mw is plotted as a function of concrete thickness in Figure 45. Calculations are in Appendix IX. The horizontal lines represent the maximum permissible dose of .3 rad/wk at the specified power level for both gammas and neutrons. A typical shield may be composed of 200 cm D_2O, 10 cm steel plus 295 cm of concrete.

Figure 46, plotted from data in Appendix IX, was computed using NDA build-up factors. For the same conditions as above the required thickness of concrete

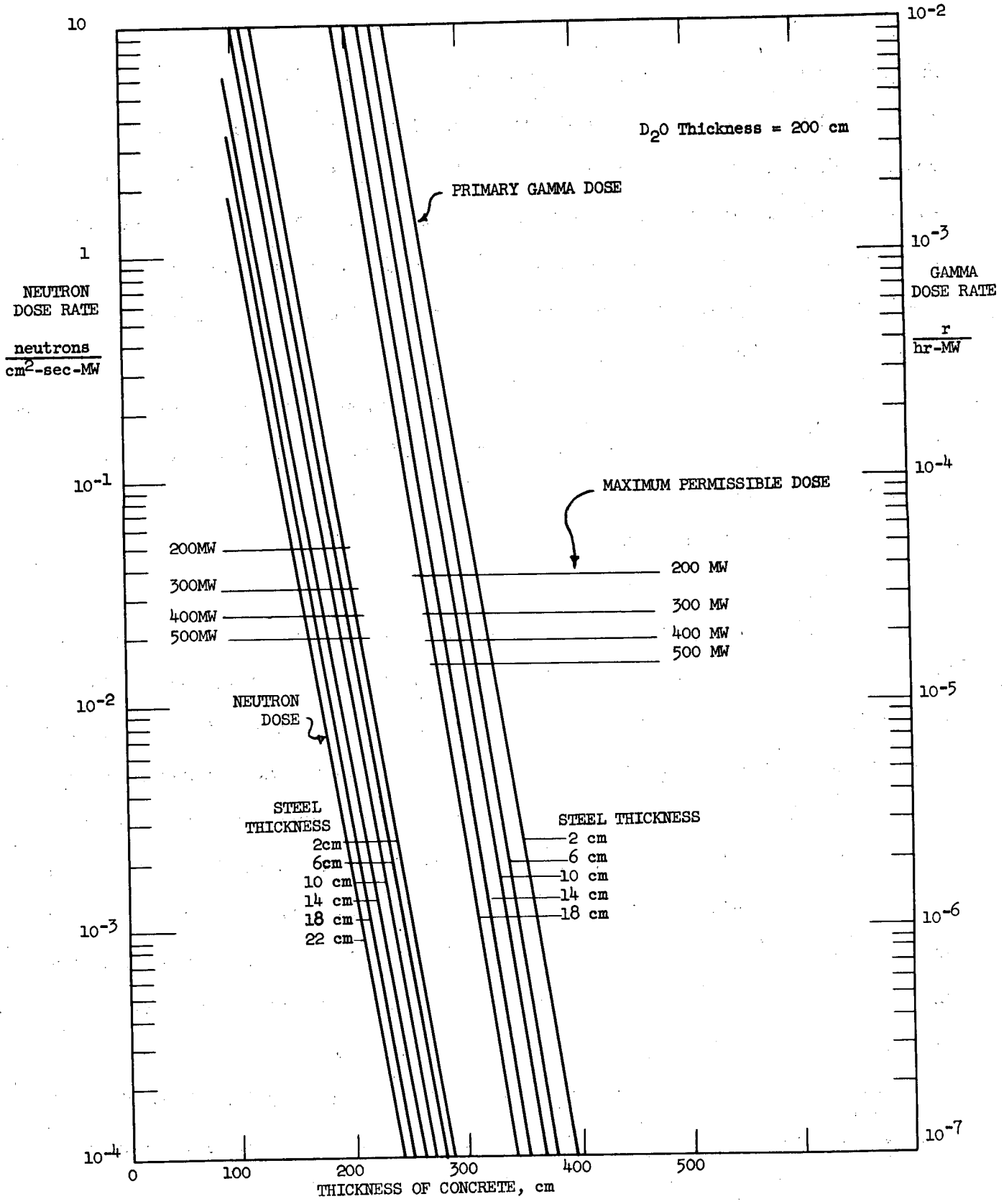

Fig. 45 GAMMA AND NEUTRON DOSE VS. THICKNESS OF CONCRETE FOR VARIOUS STEEL THICKNESSES AND POWER LEVELS

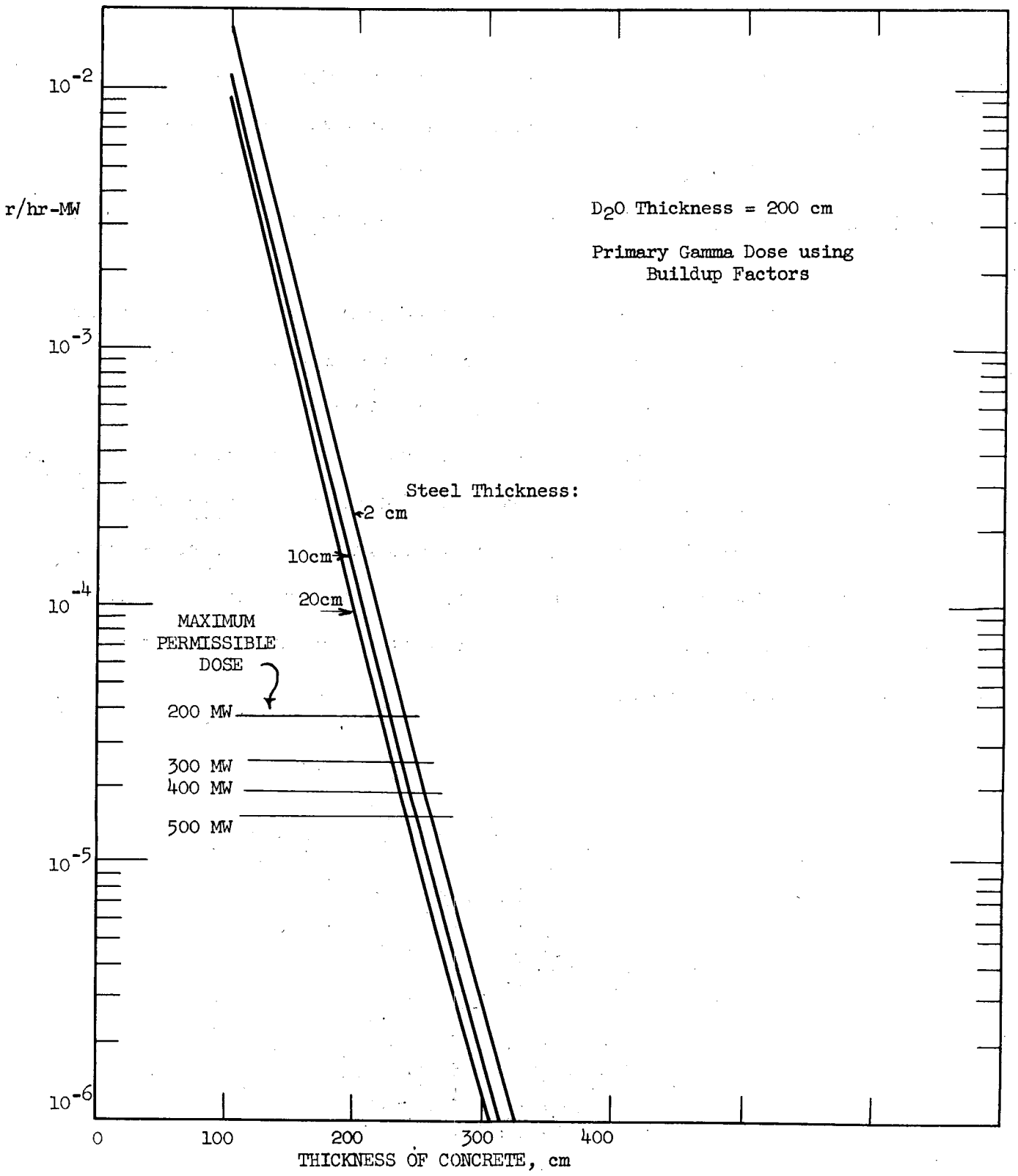

Fig. 46 PRIMARY GAMMA DOSE VS. CONCRETE THICKNESS FOR VARIOUS STEEL PLATES

is 235 cm. An analysis of the calculations show that the first method assumed a source of fission product gammas plus capture and decay gammas of 20 Mev/fission, while the second method assumed 7.5 prompt gammas per fission. If the first method considered only a 7.5 Mev/fission source the dose curve (Figure 47) would be shifted by a factor of $7.5/20 \sim .35$.

The limiting factor in determining the thickness of concrete is the prompt gamma radiations since more concrete is required for the prompt gammas than any other source. The addition of more steel is probably impractical.

After Shutdown: It may be necessary to remove the top concrete shield for maintenance after a shutdown of 1 day. Doses are plotted in Figure 47 as a function of distance above D_2O surface for various heights of D_2O after reactor operation of 100 and 1000 hrs. As an illustration, the tank may be fitted with 400 cm of D_2O so that a person working 40 cm above this surface would receive the usual maximum permissible gamma dose.

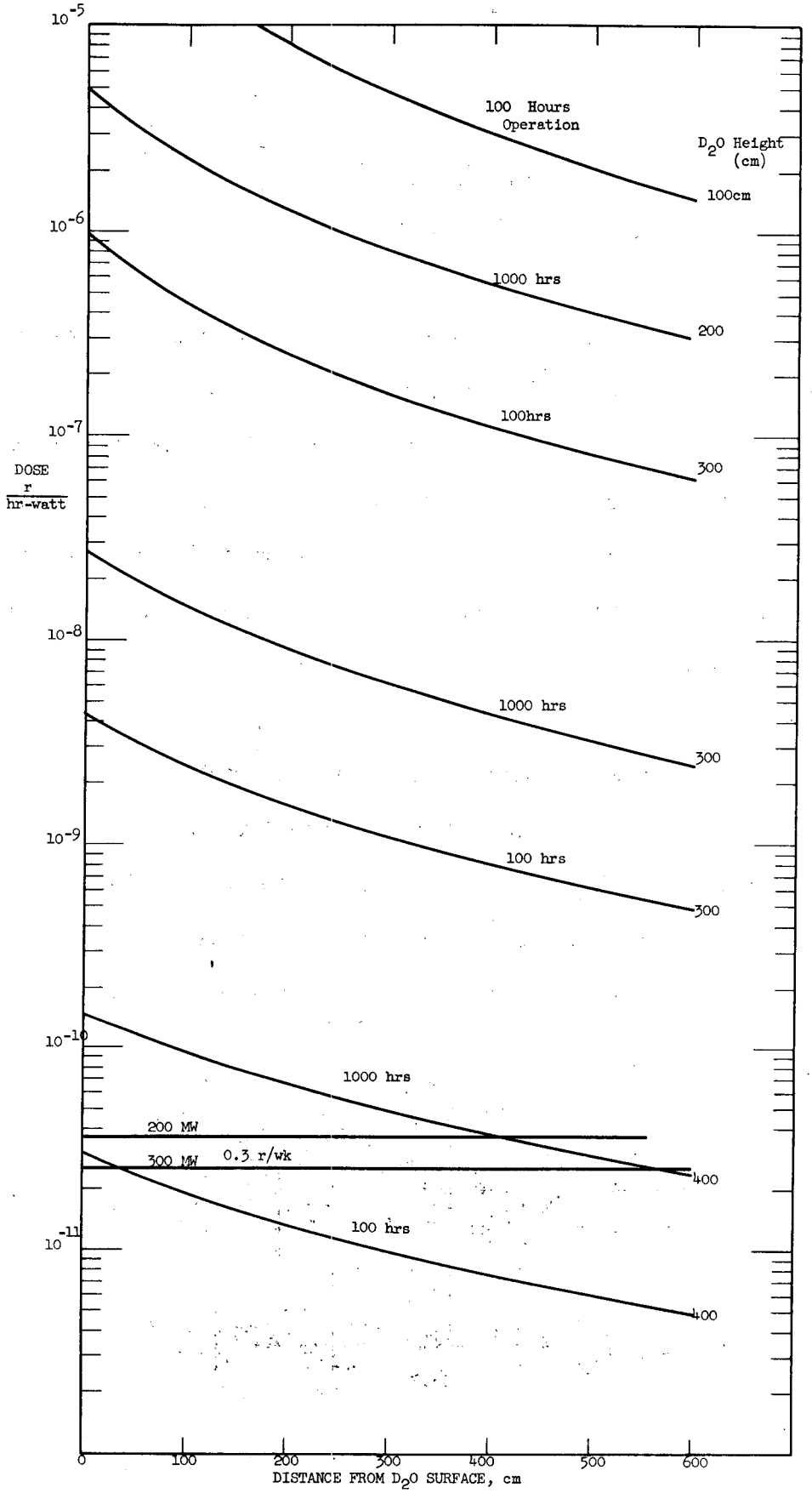

Fig. 47 DOSE FROM FISSION PRODUCT GAMMAS AFTER ONE DAY SHUTDOWN VS. DISTANCE FROM D_2O SURFACE, FOR VARIOUS D_2O HEIGHTS AND HOURS OF OPERATION

APPENDIX I

TYPICAL HFRR

Values for the typical HFRR were calculated, assuming an average power density in the fuel elements of 1500 watts/cm^3.

Flux ratios needed in the calculations were taken from flux plots for a homogeneous annulus, having a fuel concentration equal to 1.3×10^{20} atoms/cm^3 and an annulus thickness equal to 15 cm. It is assumed that the decrease in peaking due to the actual fuel element geometry will be offset by the increased peaking due to the greater actual annulus thickness.

Flux ratios:

Maximum thermal in moderator/average thermal in fuel	7.85
Maximum thermal in fuel/average thermal in fuel	1.95
Maximum thermal in reflector/average thermal in fuel	4.01
Average fast in fuel/average thermal in fuel	3.86
Average intermediate in fuel/average thermal in fuel	2.39

Fluxes:

$$\frac{P}{V} = \frac{\bar{\phi}_{32}}{3.35 \times 10^{10}} \left[\frac{\bar{\phi}_{22}}{\bar{\phi}_{32}} \Sigma_{f_2} + \Sigma_{f_3} \right]$$

$$1500 = \bar{\phi}_{32} \left[\frac{2.39 \times .00697 + .0655}{3.35 \times 10^{10}} \right]$$

or

$$\bar{\phi}_{32} = 6.12 \times 10^{14} \text{n/cm}^2 \text{ sec}$$

$$\phi_{31(max)} = 7.85 \times 6.12 \times 10^{14} = 4.81 \times 10^{15} \text{ n/cm}^2 \text{ sec}$$

$$\phi_{33(max)} = 4.01 \times 6.12 \times 10^{14} = 2.45 \times 10^{15} \text{ n/cm}^2 \text{ sec}$$

$$\bar{\phi}_{12} = 3.86 \times 6.12 \times 10^{14} = 2.36 \times 10^{15} \text{ n/cm}^2 \text{ sec}$$

$$\phi_{22} = 2.39 \times 6.12 \times 10^{14} = 1.46 \times 10^{15} \text{ n/cm}^2 \text{ sec} .$$

Maximum power density:

$$\frac{q'_{ave}}{q'_{o(max)}} = \frac{1}{1.23 \times 1.95} = \frac{1}{2.40}$$

$$Q_{(max)} = 2.40 \times 1500 \frac{\text{watts}}{\text{cm}^3} \times 9.66 \times 10^4 \frac{\text{Btu/hr ft}^3}{\text{watts/cm}^3}$$

$$= 3.48 \times 10^8 \text{ Btu/hr ft}^3 .$$

Using this value of maximum power density with Figure 39, the maximum surface temperature is found to be 345°F by the method indicated graphically on the figure. To find the coolant discharge temperature from the elements the following value of power density is used:

$$Q_{(avg)} \times \frac{q'_o}{q'_{(avg)(axial)}}$$

$$= 1500 \text{ watts/cm}^3 \times \frac{9.66 \times 10^4 \text{ Btu/hr/ft}^3}{\text{watts/cm}^3} \times 1.23$$

$$= 1.78 \times 10^8 \text{ Btu/hr ft}^3 .$$

As indicated in Figure 39 the increase in water temperature through the elements is 100°F, making the discharge temperature 200°F. In Figure 1 it is seen that the 200°F water mixes with the reflector regions. It is desired to maintain the reflector regions at about 150°F by introducing additional coolant to these regions. The flow rates are determined as follows:

Flow through elements, w_e = velocity, v x area, A

$$= 30 \text{ ft/sec} \times \pi(1.75)^2 \frac{\text{in}^2 \times \text{ft}^2}{144 \text{ in}^2} \times \frac{1}{1 + .667} \times \frac{7.48 \text{ gal}}{\text{ft}^3}$$

$$\times \frac{60 \text{ sec}}{\text{min}} \times 50 \text{ elements} = 27{,}000 \text{ gpm} .$$

Additional flow, w_R, through the reflector regions is obtained by making a heat balance, assuming thirteen percent of the total heat is transferred to these regions.

Heat into coolant = heat carried out by coolant

$$C_p\, w_e\, \Delta t_e + 13\% \times \text{total heat} = (w_R + w_e)\, C_p\, \Delta t_R$$

$$\frac{1 \text{ Btu}}{\#\ ^\circ F} \times 27{,}000 \text{ gal/min} \times \frac{ft^3}{7.48 \text{ gal}} \times 62 \text{ lb/ft}^3 \times 100^\circ F + 0.13 \times 425$$

$$\times\ 10^6 \text{ watts} \times 3.413 \text{ Btu/watt hr} \times \text{hr/60 min.}$$

$$= 1 \text{ Btu/lb } ^\circ F\ (w_R + 27{,}000 \text{ gal/min}) \times ft^3/7.48 \text{ gal} \times 62 \text{ lb/ft}^3 \times 50^\circ F$$

$$w_R = 27{,}000 + 7{,}600 = 34{,}600 \text{ gpm}$$

Total flow = $w_R + w_e$ = 27,000 + 34,6000

= 61,600 gpm .

APPENDIX II

GROUP CONSTANT PREPARATION AND METHODS OF CALCULATION

Heavy water, beryllium, and carbon moderated systems were calculated using three-group theory. Light water moderated systems were calculated using two-group theory.

The three-group constants were determined by averaging 30 group "Eyewash" cross sections. The Eyewash cross sections are not the best presently available data. However, they were readily available and therefore were used because of time limitations on this summer study. Integrated fluxes versus lethargy were obtained from previous UNIVAC calculations with the "Eyewash Code"[2]. These calculations were for heavy water moderated spherical reactors. Since the system studied had a cylindrical fuel annulus the flux weighting functions did not correspond exactly to those which should have been used. The weighting functions were matched as closely as possible to the uranium concentration of the system studied. The weighting functions which were used are listed in Table 1.

The "Eyewash Code" assumed that in the intermediate range the flux is of the form

$$\phi(u) = \frac{q(u)}{\Sigma_t(u)} \quad .$$

This is not exactly true for heavy water but was assumed to be an adequate approximation.

The average fission cross sections, absorption cross sections, diffusion coefficients, and transfer cross sections are the group constants which must be

determined by averaging cross sections over lethargy.

TABLE 1

THIRTY GROUP INTEGRATED FLUXES (WEIGHTING FUNCTIONS)[a]

Designation Nu-235 Radius, ft.	Group	Lethargy Width	WFB 6.9×10^{-5} 2.5	WF3 2.9×10^{-5} 3	WF2 1.5×10^{-5} 3.5	WF1 $.75\times10^{-5}$ 4.5	F_i[b]
Weighting Functions Scaled by 10^{-5}	1	.5	.7686	.7837	.5051	0	.01050
	2	.5	4.147	4.155	4.016	4.016	.07215
	3	.5	10.60	11.07	10.95	10.99	.2268
	4	.5	17.27	17.90	18.03	18.52	.4461
	5	.5	21.76	22.54	22.99	23.95	.6537
	6	1.5	77.06	80.06	82.60	85.07	.8552
	7	3.0	157.6	168.2	176.5	184.0	.9825
	8	3.0	142.9	156.9	168.6	179.5	1.000
	9	1.4	60.94	68.64	75.06	81.11	1.000
	10	1.2	49.07	56.47	62.52	68.30	1.000
	11	.8	30.95	36.39	40.78	44.95	1.000
	12	.4	14.91	17.81	20.13	22.30	1.000
	13	.8	28.63	34.77	39.63	44.17	1.000
	14	1.2	40.70	52.16	62.13	69.82	1.000
	15	.4	13.03	16.58	19.48	22.03	1.000
	16	.4	12.55	16.29	19.43	22.06	1.000
	17	.4	11.99	15.68	18.73	21.36	1.000
	18	.4	11.33	14.90	17.74	20.34	1.000
	19	.2	5.352	7.155	8.571	9.873	1.000
	20	.2	5.095	6.905	8.331	9.627	1.000
	21	.2	4.837	6.646	8.064	9.345	1.000
	22	.2	4.649	6.469	7.892	9.177	1.000
	23	.2	4.558	6.294	7.727	9.009	1.000
	24	.2	4.211	6.021	7.430	8.699	1.000
	25	.2	3.945	5.722	7.096	8.338	1.000
	26	.2	3.731	5.502	6.867	8.102	1.000
	27	.2	3.508	5.262	6.610	7.830	1.000
	28	.2	3.280	5.040	6.400	7.540	1.000
	29	.2	3.040	4.800	6.140	7.240	1.000
	30	.2	2.800	4.740	5.880	7.000	1.000

[a] Obtained from UNIVAC Calculations on D_2O moderated spherical reactors[(3)].

[b] Fraction of neutrons born above the group based on Watt's fission spectrum.

The energy separating groups one and two was chosen to be 10 Kev because this is approximately the bottom of the fission spectrum. This corresponds to the bottom of group 7 in the "Eyewash Code". The average absorption cross sections were calculated from

$$\Sigma_{a_1} = \frac{\int_{10\ \text{Mev}}^{10\ \text{Kev}} \Sigma_a^T \phi\, du}{\int_{10\ \text{Mev}}^{10\ \text{Kev}} \phi\, du} = \frac{\sum_{n=1}^{7} \Sigma_a^T \overline{\phi}\, \Delta u}{\sum_{n=1}^{7} \overline{\phi}\, \Delta u} \qquad (1)$$

and

$$\Sigma_{a_2} = \frac{\sum_{n=8}^{n_{th}} \Sigma_a^T \overline{\phi}\, \Delta u}{\sum_{n=8}^{n_{th}} \overline{\phi}\, \Delta u} \qquad (2)$$

where

$$\Sigma_a^T = \Sigma_{a_x} + \Sigma_{a_y} + \Sigma_{a_z} + \cdots$$

Subscripts 1 and 2 indicate the first and second groups in the three-group approach and x, y, and z correspond to different elements. Similarly the

average fission cross sections were determined from

$$\nu\Sigma_{f_1} = \frac{\sum_{n=1}^{7} \nu\Sigma_f \bar{\phi} \triangle u}{\sum_{n=1}^{7} \bar{\phi} \triangle u} \qquad (3)$$

and

$$\nu\Sigma_{f_2} = \frac{\sum_{n=8}^{n_{th}} \nu\Sigma_f \bar{\phi} \triangle u}{\sum_{n=8}^{n_{th}} \bar{\phi} \triangle u} \qquad (4)$$

In all cases the thermal absorption and fission cross sections were averaged over a Maxwell-Boltzman distribution and thus

$$\bar{\sigma}_{a_{th}} = \frac{\sigma_a (E_{th})}{1.128}$$

and

$$\Sigma_{a_3} = \bar{\Sigma}_{a_x} + \bar{\Sigma}_{a_y} + \bar{\Sigma}_{a_z} + \cdots$$

The "neutron temperature" was assumed to correspond to the temperature of the moderator.

The diffusion coefficients in the upper two groups were determined by averaging in the following manner:

$$D_1 = \frac{\int_{10\ Mev}^{10\ Kev} D\,\phi\,du}{\int_{10\ Mev}^{10\ Kev} \phi\,du} = \frac{\sum_{n=1}^{7} D\,\bar{\phi}\,\Delta u}{\sum_{n=1}^{7} \bar{\phi}\,\Delta u} \qquad (5)$$

and

$$D_2 = \frac{\sum_{n=8}^{n_{th}} D\,\bar{\phi}\,\Delta u}{\sum_{n=8}^{n_{th}} \bar{\phi}\,\Delta u} \qquad (6)$$

where

$$D = \frac{1}{3\,\Sigma_{tr}}$$

and

$$\Sigma_{tr} = \Sigma_{tr_x} + \Sigma_{tr_y} + \Sigma_{tr_z} + \ldots$$

In the thermal group the diffusion coefficient was defined in a manner consistent with the P-1 approximation to the transport equation. Thus

$$D_3 = \frac{1}{3(\Sigma_{tr_3} + \Sigma_{a_3})} \quad . \tag{7}$$

The thermal transport cross sections for light and heavy water are dependent on the chemical binding of the hydrogen and deuterium within the light and heavy water molecules. Thus, the best values of the thermal transport cross sections were assumed to be the values corresponding to an experimentally measured diffusion length, L_3. Using the relation

$$L_3^2 = \frac{D_3}{\Sigma_{a_3}}$$

and the above relation for D_3, the thermal transport cross sections were calculated for light and heavy water. The chemical binding varies with neutron temperature and must be corrected for, when calculating thermal diffusion coefficients at various temperatures. These effects have been calculated by Noderer[11] and Radkowsky[12]. Transport cross sections were calculated from their results and are plotted in Figures 48 and 49. The variation of the transport cross section of aluminum with temperature was obtained from Eyewash data and is plotted in Figure 50.

Perhaps the more difficult or undefinable group parameters which must be calculated are the transfer cross sections for the epithermal groups. For the

ORNL-LR-Dwg.-22494
UNCLASSIFIED

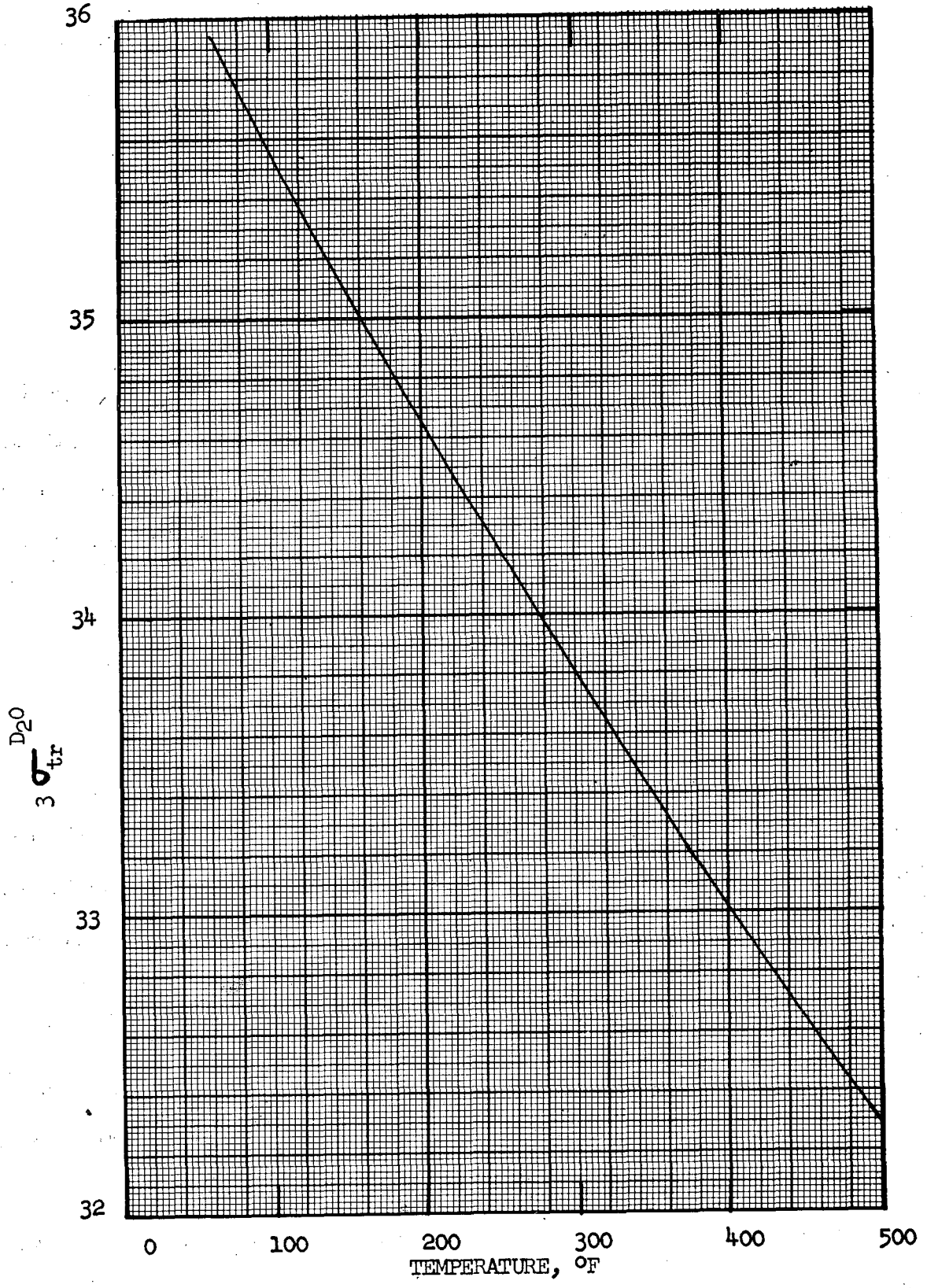

Fig.48 $3\sigma_{tr}^{D_2O}$ VS. TEMPERATURE (ORNL - CF - 54 -4-142)

ORNL-LR-Dwg.-22495
UNCLASSIFIED

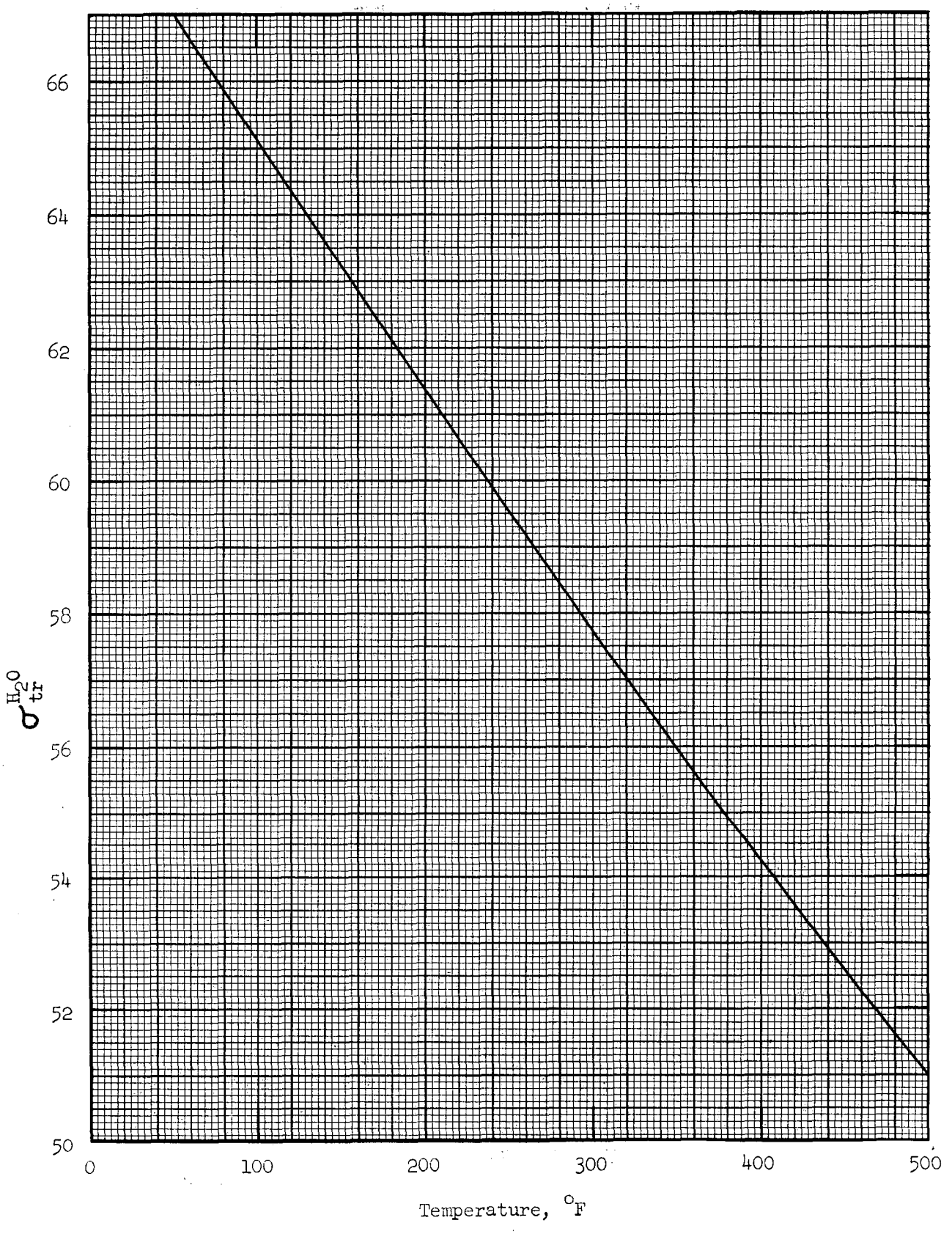

Fig. 49 $\sigma_{tr}^{H_2O}$ Vs. TEMPERATURE (ANL - 4476)

ORNL-LR-Dwg.-22496
UNCLASSIFIED

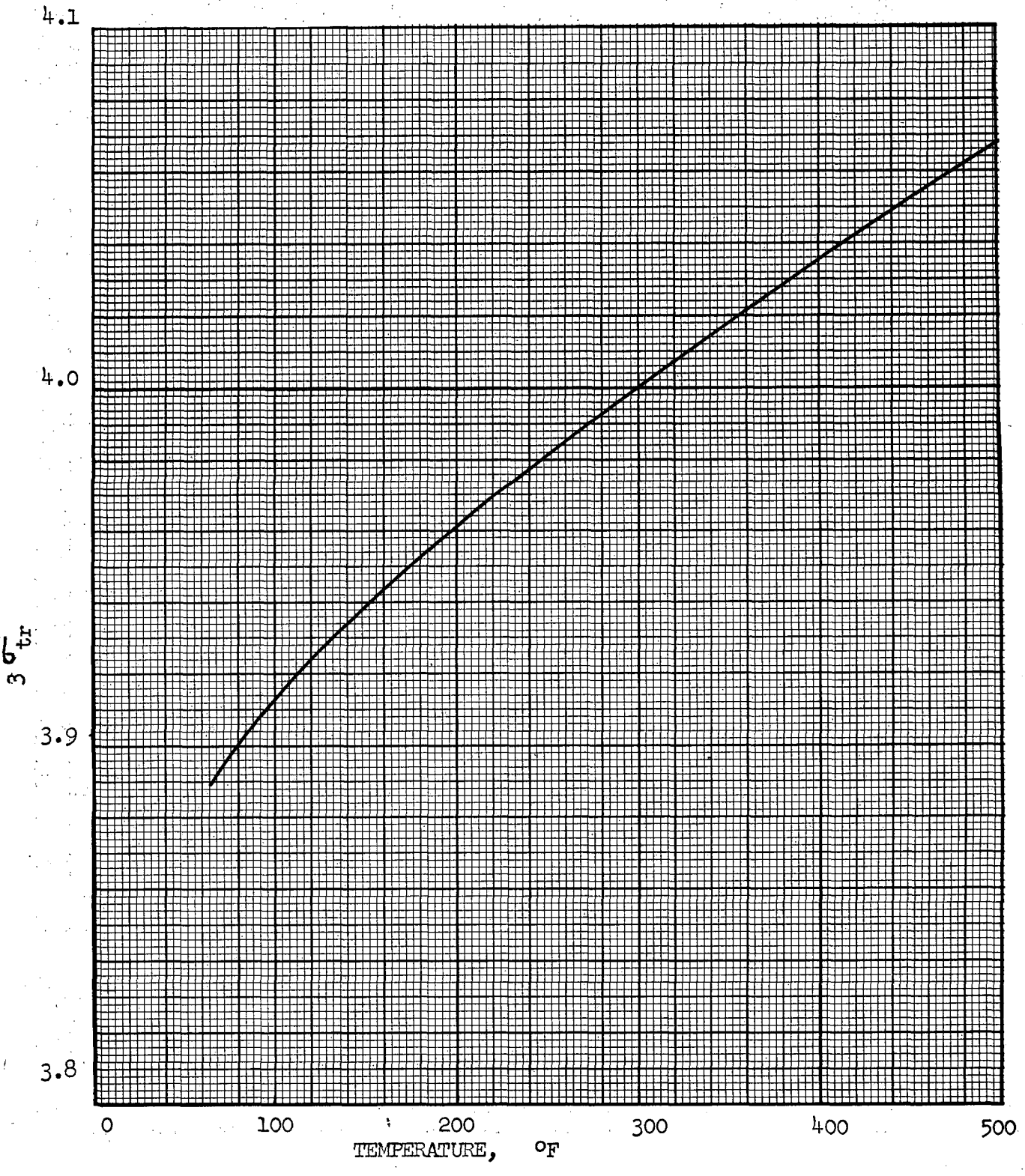

Fig.50 $3\sigma_{tr}^{Al}$ VS. TEMPERATURE (EYEWASH DATA)

purposes of this study the transfer cross sections were calculated from a Fermi age and an average diffusion coefficient. Hence

$$\Sigma_{x_1} = \frac{D_1}{\tau_1} \tag{8}$$

and

$$\Sigma_{x_2} = \frac{D_2}{\tau_2} \quad . \tag{9}$$

The age is defined as

$$\tau = \int \frac{D}{\xi \Sigma_t} \, du = \int \frac{du}{3 \Sigma_{tr} \xi \Sigma_t} \quad .$$

There are a number of ways to calculate the age. One is to integrate to the energy corresponding to the average energy of the U-235 fission spectrum ($\sim$ 2 Mev) and another is to average over the entire fission spectrum and weight each group with a function, F_i, which accounts for the number of neutrons born above each group. The age for heavy water was calculated by both these methods using the Eyewash cross sections. The age determined by averaging to 2 Mev was 120.9 cm^2 and that determined by weighing for the fission spectrum was 117.8 cm^2. The available experimental data indicates that the best age for heavy water is about

120 cm^2 (0.16 percent H_2O). Weighting with the fission spectrum should be a more consistent method of determining ages in mixtures, and this method was used. The values of F_i are listed with the integrated fluxes in Table 1.

The next problem concerned division of the age into two parts so as to obtain three-group constants. It seemed reasonable that the age for groups one and two could be determined by summing over the corresponding Eyewash groups just as was done to evaluate the average macroscopic cross sections and the diffusion coefficients. The assumption of continuous slowing down is good for a carbon moderated system and fair for a beryllium moderated system. Hence, this method was used for calculating systems employing these moderators. Thus, for beryllium or carbon

$$\tau_1 = \sum_{n=1}^{7} \frac{F_i \, \Delta u}{3 \, \Sigma_{tr} \, \xi \, \Sigma_t}$$

and

$$\tau_2 = \sum_{n=8}^{n_{th}} \frac{F_i \, \Delta u}{3 \, \Sigma_{tr} \, \xi \, \Sigma_t} \quad .$$

Because the continuous slowing down approximation does not exactly apply to heavy water moderated systems the above method for calculating three-group ages does not yield the best results. Spinrad and Katsumi Tomaka[13] discuss a method which works well in heavy water, and this was used. It was assumed

that the ratio of the ages of the fast and intermediate groups for a dividing energy of 10 Kev was 48/73. This ratio was assumed to hold for all mixtures containing a large percentage of heavy water. Thus, the ages in heavy water moderated systems were defined as follows:

$$\tau_1 = \frac{48}{121} \sum_{n=1}^{n_{th}} \frac{F_i \Delta u}{3 \Sigma_{tr} \xi \Sigma_t}$$

and

$$\tau_2 = \frac{73}{121} \sum_{n=1}^{n_{th}} \frac{F_i \Delta u}{3 \Sigma_{tr} \xi \Sigma_t} \quad .$$

Then the transfer cross sections are obtained from Equations (1) and (2).

The transfer cross sections defined in this way are possibly more accurately "removal" cross sections which indicate the total removal from a group. Since the absorption and transfer are included explicitly in the three group equations a better definition of the transfer cross section would be

$$\Sigma_x = \frac{D}{\tau} - \Sigma_a \quad .$$

Initially this correction was not made, and thus, in order to keep the calculations consistent for comparison purposes the correction was neglected throughout the study. The correction is small in the first group since the absorption is small. However, the correction could become appreciable in the second group, where resonance absorption may make Σ_a appreciable.

Another way to calculate the transfer cross section is

$$\Sigma_x = \Sigma_n \frac{\xi \Sigma_t}{\Delta u} .$$

Using this method, transfer cross sections were calculated for several cases. These checked reasonably well with transfer cross sections calculated from D/τ.

Possibly another modification which may have given better results would have been to define the epithermal diffusion coefficients in the same manner as the thermal diffusion coefficient was defined (equation 7). Here again, because of time limitations, this modification was not used.

Initially many of the three-group constants were averaged by hand, but later an ORACLE constant preparation routine prepared by W. E. Kinney[14] was used to obtain the epithermal constants. For heavy water moderated systems the results of this routine were modified to correspond to the methods described above.

The previous methods of calculating the age are poor approximations for light water systems. Hence, to obtain the epithermal two-group ages the experimental age in light water (33 cm^2) was corrected for the diluents. Experimental

ages for aluminum water mixtures were used where applicable. These are plotted in Figure 51. Averaged cross sections were used to obtain the other epithermal two-group constants.

Since the 3G3R or 2G3R ORACLE Code was one dimensional, one of the input parameters to the code was an axial buckling. The code made allowance for three bucklings, one for each of the three energy groups. The bucklings for each of the regions had to be equal, and thus, for all cases it was assumed that the end reflectors would be heavy water.

A reflector savings had to be added to arrive at an axial buckling which accounted for the end reflectors. An experimentally determined reflector savings of 26 cm[15], which corresponds to a thick end reflector, was added to the height of the reactor for each of the end reflectors. It was not at all certain that this was the best value. Figure 52 indicates the variation in the multiplication constant with reflector savings.

Several critical experiments[16] were calculated to estimate the accuracy of the three-group calculations for heavy water systems. The calculated multiplication constants were 12 to 15 percent too high indicating the approximate maximum range of error. Part of this difference can be explained by the difference between the actual critical experiment and the one which was calculated. The critical experiment consisted of a cylindrical assembly filled with D_2O. An enriched uranium solution was contained in one inch aluminum tubes. To calculate this assembly the uranium was homogenized over the core and the aluminum was neglected. Since enriched uranium is more effective when homogenized and since the aluminum absorbs some neutrons, the calculated multiplication constant would be expected to be too high. This indicated that the three-group constants were reasonably adequate.

ORNL-LR-Dwg.-22497
UNCLASSIFIED

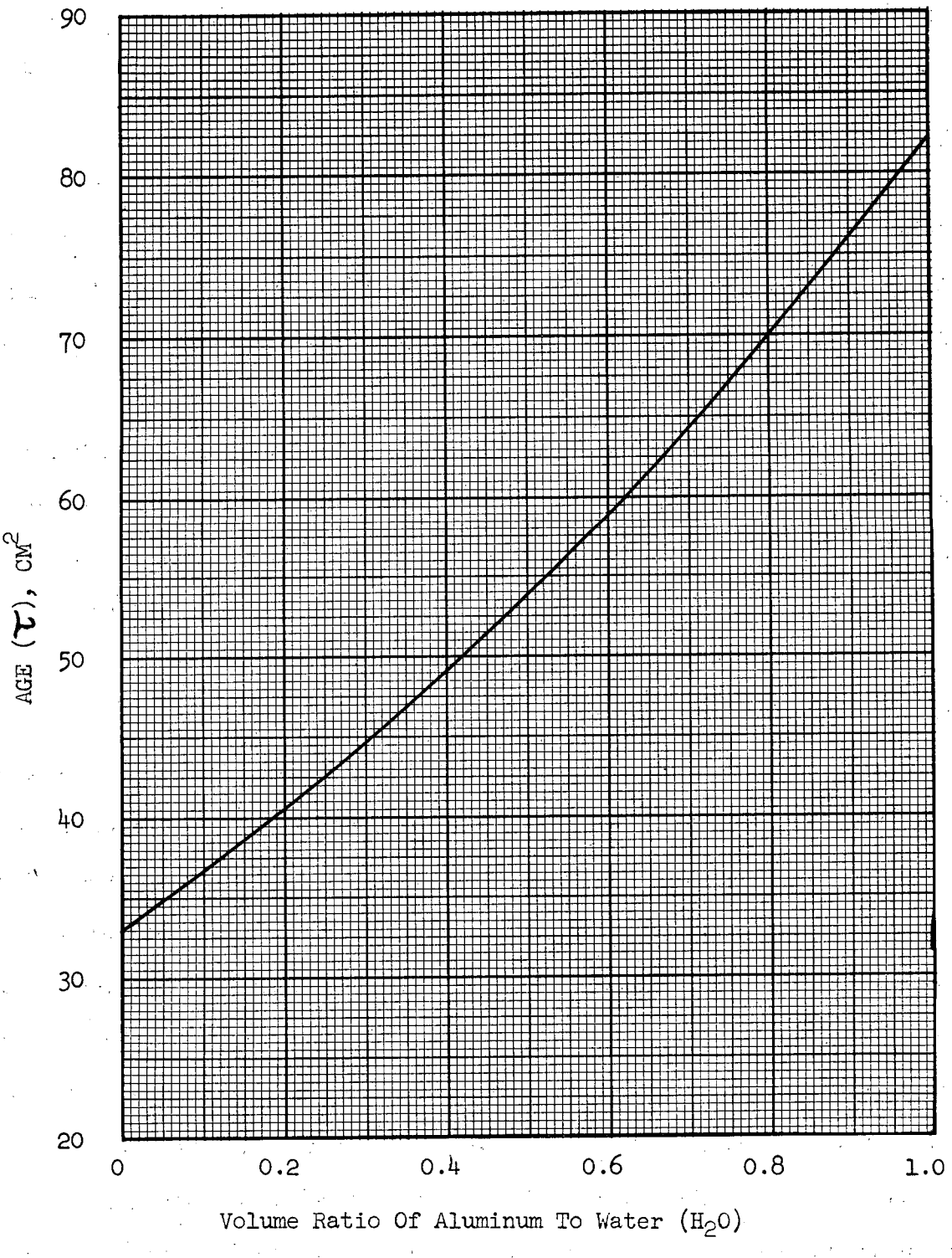

Fig. 51 AGE OF FISSION NEUTRONS IN H_2O - AL. MIXTURES (P/490)

ORNL-LR-Dwg.-22498
UNCLASSIFIED

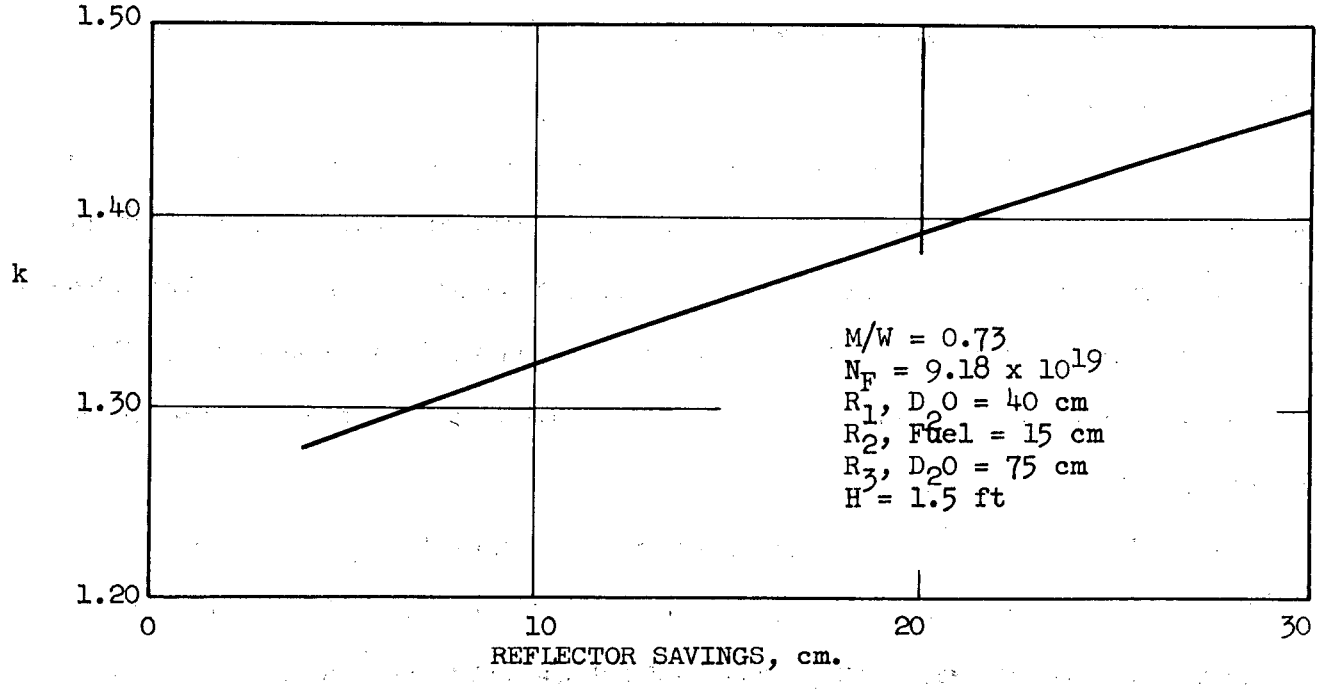

Fig. 52 MULTIPLICATION CONSTANT VS. END REFLECTOR SAVINGS FOR ALL THREE NEUTRON GROUPS

The group constants which were used for some of the calculations are tabulated in Tables 2 through 8. In calculating temperature coefficients all effects were corrected for except the Doppler broadening of the resonances. It was found that sufficient accuracy could not be obtained by reading the thermal, fission and absorption cross section for U-235 off the curves and hence, they were assumed to vary as 1/v. In order to attain sufficient accuracy for temperature coefficient calculations the group constants had to be calculated to at least five place accuracy.

The burnup calculations were made by recalculating the reactor at finite intervals of time to determine the multiplication constant and the flux distributions. The 3G3R code had provision for shells between the regions. The effects of boron stainless steel absorbing shells were calculated using the code. The shell constants were calculated with a shell constant preparation routine which was prepared by W. E. Kinney.

In order to compare the flux distributions resulting from some of the calculations, the cases were normalized to constant power. This was done by setting the average fission rates equal within the core regions of the cases to be compared. Thus for reactors a and b

$$(\Sigma_{f_1} \overline{\phi}_1 + \Sigma_{f_2} \overline{\phi}_2 + \Sigma_{f_3} \overline{\phi}_3)_a = (\Sigma_{f_1} \overline{\phi}_1 + \Sigma_{f_2} \overline{\phi}_2 + \Sigma_{f_3} \overline{\phi}_3)_b \quad .$$

Then ratios of $\overline{\phi}_{3a}/\overline{\phi}_{3b}$, $\overline{\phi}_{2a}/\overline{\phi}_{2b}$, and $\overline{\phi}_{1a}/\overline{\phi}_{1b}$ for constant power were calculated. The fluxes were then normalized to constant power by comparing these ratios of average fluxes with the actual ratios from the flux plots.

In all calculations the heavy water was assumed to contain 0.16 percent H_2O. Indications are that the economical hydrogen content is about 2 percent. The effect of a varying hydrogen content on the reactor parameters was not completely investigated and hence, requires further study.

APPENDIX III

HEAT TRANSFER EQUATIONS

Heat transfer calculations:

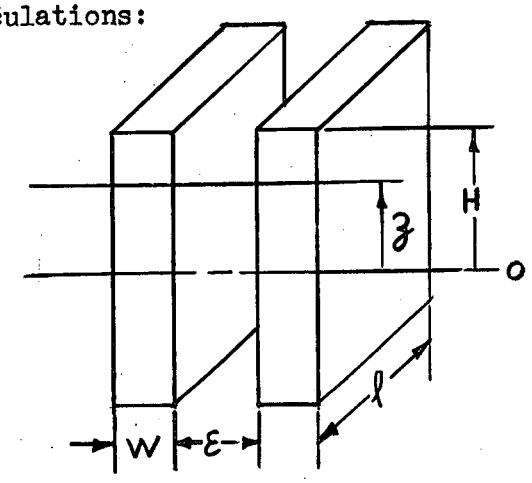

The heat picked up by the coolant between (-H) and z is

$$q(z) = \rho V A_f C_p \left[T_B(z) - T_i \right] \quad . \tag{1}$$

The heat that flows across the coolant film at z is

$$q(z) = h A_s \left[T_s(z) - T_B(z) \right] \quad . \tag{2}$$

Let $q' = q/A_s$, and assume that

$$q' = q'_o \cos \frac{\pi z}{2\tilde{H}} \quad .$$

Making this substitution in equation (1),

$$T_B(z) - T_i = \frac{q'_o}{V A_f C_p} \int_{-H}^{z} \cos \frac{\pi z}{2\tilde{H}} \, d A_s(z) \quad . \tag{3}$$

Solving equations (2) and (3),

$$T_s(z) - T_i = \frac{q'_o}{h} \cos \frac{\pi z}{2\tilde{H}} + \frac{q'_o}{\rho V A_f C_p} \int_{-H}^{z} \cos \frac{\pi z}{2\tilde{H}} \, d A_s(z) \tag{4}$$

$$= q'_o \left\{ \frac{1}{h} \cos \frac{\pi z}{2\tilde{H}} + \frac{4\tilde{H}}{\pi \rho V \epsilon C_p} \left[\sin \frac{\pi z}{2\tilde{H}} + \sin \frac{\pi H}{2\tilde{H}} \right] \right\} ,$$

since

$$\frac{d A_s}{A_f} = \frac{1 dz}{\frac{\epsilon}{2} 1} = \frac{2dz}{\epsilon} \quad .$$

To determine the maximum surface temperature along the length of a plate, equation (4) is differentiated with respect to z and set equal to zero. The location of the maximum temperature is found to be

$$z_{(max)} = \frac{2\tilde{H}}{\pi} \tan^{-1} \frac{4 h \tilde{H}}{\pi \rho V \epsilon C_p} \quad . \tag{5}$$

Substitution of equation (5) into (4) gives the maximum surface temperature.

The properties of the coolant were determined for the average bulk mean temperature, which was calculated using equation (3), integrated from the inlet end to the middle.

$$T_B(o) - T_i = \frac{4\tilde{H} q'_o}{\pi \rho V \epsilon C_p} \sin \frac{\pi H}{2\tilde{H}} \quad . \tag{6}$$

Calculation of maximum to average heat flux in the fuel annulus:

In the axial direction a cosine flux shape was assumed, the flux being zero at $\tilde{H}$. Therefore,

$$q'_{(av_e)(axial)} = \frac{\int_o^H q'_o \cos \frac{\pi z}{2\tilde{H}} dz}{\int_o^H dz} \tag{7}$$

$$= q'_o \frac{2\tilde{H}}{\pi H} \sin \frac{\pi H}{2\tilde{H}} \quad .$$

In the radial direction

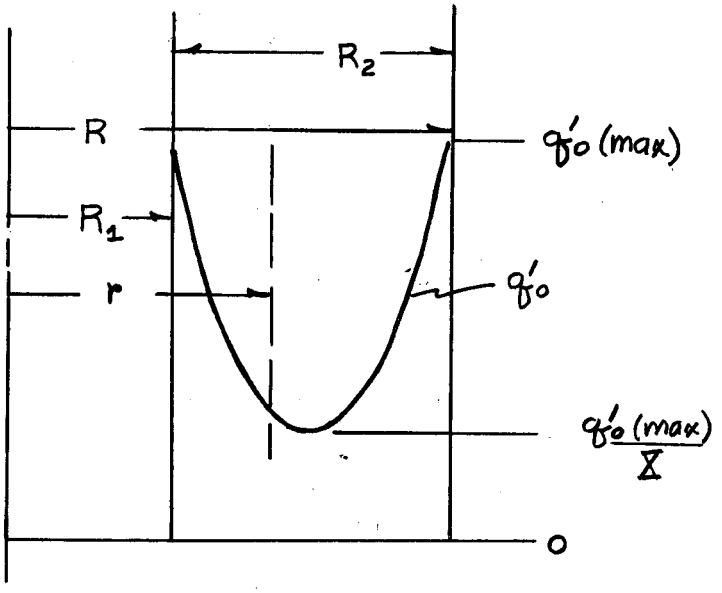

X = ratio of maximum to minimum flux in the fuel annulus.

Assuming the radial flux to have a cosine distribution,

$$q'_o = q'_{o(max)} - \left[q'_{o(max)} - \frac{q'_{o(max)}}{X} \right] \sin \frac{\pi(r - R_1)}{(R - R_1)}$$

$$= q'_{o(max)} \left[1 - \left(\frac{X - 1}{X} \right) \sin \frac{\pi(r - R_1)}{(R - R_1)} \right] . \qquad (8)$$

Substitution of equation (7) and (8) into

$$q'_{ave} = \frac{\int_{R_1}^{R} q'_{(ave)(axial)} \, dV}{\int_{R_1}^{R} dV}$$

leads to

$$\frac{q'_{ave}}{q'_{o(max)}} = \left[\frac{2\tilde{H}}{\pi H} \sin \frac{\pi H}{2\tilde{H}}\right] \left[1 - \frac{2}{\pi} \left(\frac{X - 1}{X}\right)\right] . \qquad (9)$$

From equation (7) the following is obvious:

$$\frac{q'_{(ave)(axial)}}{q'_{o}} = \left[\frac{2\tilde{H}}{\pi H} \sin \frac{\pi H}{2\tilde{H}}\right] \qquad (10)$$

$$\frac{q'_{o(ave)}}{q'_{o(max)}} = \left[1 - \frac{2}{\pi} \left(\frac{X - 1}{X}\right)\right] \qquad (11)$$

APPENDIX IV

DERIVATION OF INTEGRAL ENERGY EQUATION FOR PROMPT GAMMA HEATING

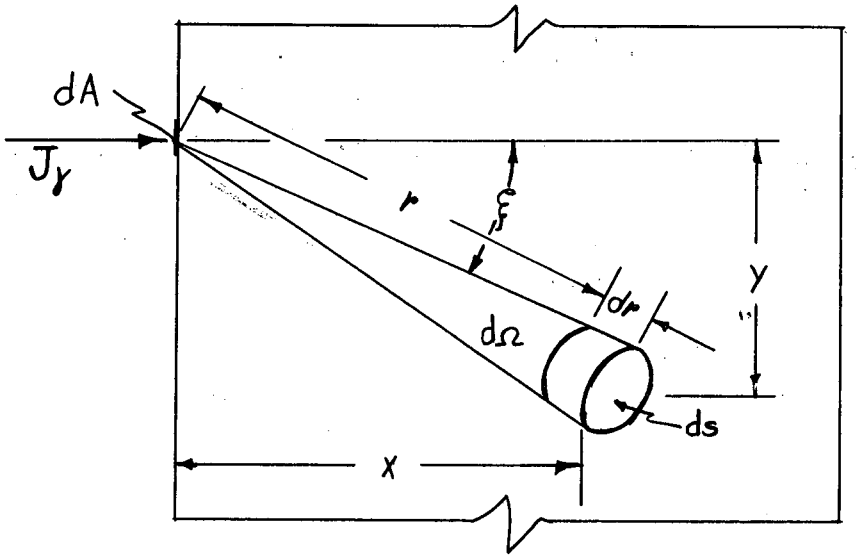

$$d^3N(0, E_n \xi) = J_\gamma (E_n)\, dA P_\Omega (\xi)\, d\Omega$$

$$= J_\gamma\, dA\, P_\gamma (E_n, 0)\, d E_n\, P_\Omega (\xi)\, d\Omega$$

$$\frac{d}{dr} \int_{E=0}^{\infty} E\, d^3N(r, E, \xi) = - \int_{E=0}^{E=\infty} E\, d^3N(r, E\xi) \left[\mu_a(E) + \sigma(E) + \mu_c(E) + f\mu_c(E) \right]$$

which is the change in total energy along dr due to absorption and compton scattering of the photons d^3N where, $\delta(E) \equiv$ average fraction of γ energy E that is deposited locally by a compton collision.

$f \equiv$ average fraction of the γ's with energy E which are scattered to energies $< E_o$, the cutoff energy for compton scattering.

Now $d^3N(r, E, \xi) = d^2N(r, \xi) P_\gamma(E, r)dE$ and furthermore, when the penetration distance is small and only a few photons are scattered from the beam

$$P_\gamma(E, r) = P_\gamma(E, 0)$$

thus

$$\frac{d}{dr} d^2N(r, \xi) \int_{E=0}^{\infty} E\, P_\gamma(E)dE = -d^2N(r, \xi) \int_{E=0}^{\infty} E\, \mu_e(E) P_\gamma(E)dE$$

where

$$\mu_e = \mu_t \left[\frac{\mu_a}{\mu_t} + \frac{\mu_c}{\mu_t} + \frac{f\, \mu_c}{\mu_t} \right]$$

since

$$\bar{E} = \frac{\int_{E=0}^{\infty} E\, P_\gamma(E)\, dE}{\int_{E=0}^{\infty} P_\gamma(E)dE} = \int_{E=0}^{\infty} E\, P_\gamma(E)\, dE$$

$$\bar{\mu}_e = \frac{\int_{E=0}^{\infty} \mu_e(E)\, E\, P_\gamma(E)\, dE}{\int_{E=0}^{\infty} E P_\gamma(E)\, dE} = \frac{1}{\bar{E}} \int_{E=0}^{\infty} \mu_e(E)\, E\, P_\gamma(E)\, dE$$

$$\frac{d}{dr}\, d^2N(r,\xi) = -d^2N(r,\xi)\, \bar{\mu}_e$$

on solving yields

$$d^2N(r,\xi) = d^2N(0,\xi)\, e^{-\bar{\mu}_e r}$$

$$\frac{d}{dr}\, d^2N(r,\xi) = -\bar{\mu}_e\, d^2N(0,\xi) e^{-\bar{\mu}_e r} \quad .$$

The change in heat generation in length dr is equal to the energy of the photons times the photons that give up their energy in dr .

$$dG = \frac{-\bar{E}\left\{\frac{d}{dr}\, d^2N(r,\xi)\right\} dr}{ds\, dr}$$

$$= \bar{E}\, \frac{\left\{\bar{\mu}_e\, d^2N(0,\xi) e^{-\bar{\mu}_e r}\right\}}{ds\, dr} dr \quad .$$

But

$$d^2N(0,\xi) = J_\gamma \, dA \, P_\Omega(\xi) \, d\Omega = J_\gamma \, dA \, \frac{I}{J} \, d\Omega$$

$$J_\gamma(E, A) = \int_\Omega I(E, A, \xi) d\Omega \quad .$$

From modified transport theory, (17)

$$I(E, A, \xi) = \frac{\cos \xi}{4\pi} \quad \frac{S(E)}{\mu_t} \quad (1 - e^{-\mu_t R_{max}})$$

$$R_{max} = \frac{b}{\cos \xi}$$

where b = thickness of source

$$J_\gamma \ (E, A) = \int_\Omega \frac{\cos \xi}{4\pi} \ \frac{S(E)}{\mu_t} \ (1 - e^{-\mu_t b/\cos \xi}) \, d\Omega$$

$$dA = 2\pi y \, dy \qquad d\Omega = \frac{ds}{r^2} \qquad \cos \xi = \frac{x}{r}$$

$$r^2 = y^2 + x^2 \qquad rdr = ydy$$

$$d^2N = \frac{x}{4\pi r} \frac{S}{\mu_t} (1 - e^{-\mu_t \frac{b}{x} r}) \, 2\pi y \, dy \, \frac{ds}{r^2}$$

$$dG = \bar{E} \bar{\mu}_e \frac{\frac{x}{4\pi r} \frac{S}{\mu_t} (1 - e^{-\mu_t \frac{b}{x} r}) e^{-\bar{\mu}_e r} \, 2\pi y \, dy \, \frac{ds}{r^2}}{ds \, dr} dr$$

$$G = \int_{r=x}^{\infty} \frac{S \bar{E}}{2 \mu_t} \bar{\mu}_e x \frac{(1 - e^{-\mu_t \frac{b}{x} r}) e^{-\mu_e r}}{r^2} dr$$

letting $u = r/x$ this reduces to

$$G = \frac{S \bar{E} \bar{\mu}_e}{2 \mu_t} \left[E_2(\bar{\mu}_e x) - E_2(\mu_t b + \bar{\mu}_e x) \right]$$

where

$$E_2(\bar{\mu}_e x) = \int_1^{\infty} u^{-2} e^{-\bar{\mu}_e x u} \, du \quad .$$

APPENDIX V

CAPTURE GAMMA HEATING IN ALUMINUM

Assume that the aluminum fuel element housing is an infinite flat plate of solid aluminum

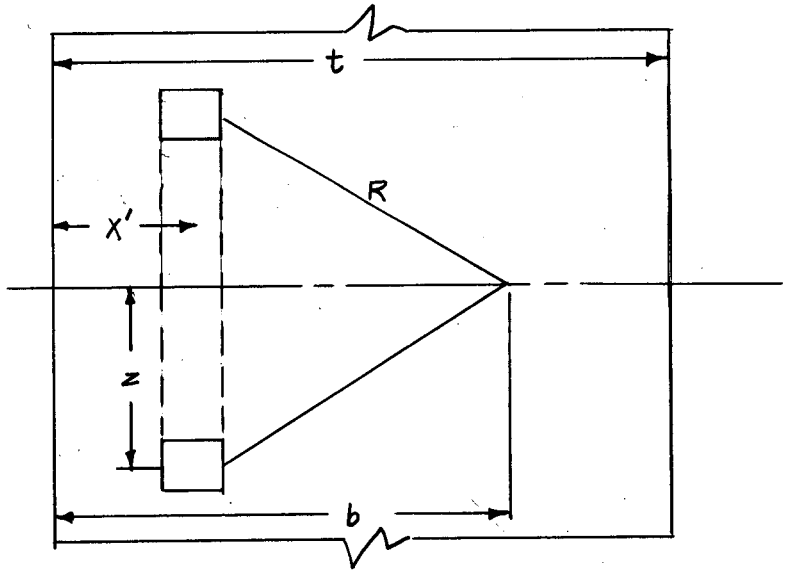

The equation for heat generation in a plane located distance b from one surface is given by

$$G(b) = \frac{N_\gamma \Sigma_a}{2} \int_E \int_Y \int_{x'} Ba(E, \mu_t R) \frac{e^{-\mu_t R}}{R^2} \mu_e(E) P(E) dE \phi(x') y \, dy \, dx' \quad (1)$$

After making the necessary geometric substitutions and by considering only one energy increment ΔE about E, equation (1) becomes

$$G(b) = \frac{N_\gamma \Sigma_a \mu_e E}{2} \left[\int_{R=b}^{R=\infty} \int_{x'=0}^{x'=b} Ba(\mu_t R)\, e^{-\mu_t R}\, \phi(x')\, \frac{dR\, dx'}{R} + \right. \tag{2}$$

$$\left. \int_{R=(t-b)}^{R=\infty} \int_{x'=b}^{x'=t} Ba(\mu_t R)\, e^{-\mu_t R}\, \phi(x')\, \frac{dR\, dx'}{R} \right]$$

where the first integration is over x', holding R constant.

A linear buildup, B_a, was assumed, taking the form

$$B_a = 1 + m(E)\, \mu_t(E)\, R \quad . \tag{3}$$

The thermal neutron flux shape was assumed to be

$$\phi = \phi_1 \left[1 - \frac{X - 1}{X} \sin \frac{\pi x'}{t} \right] \tag{4}$$

where ϕ_1 is the maximum flux at the edge of the fuel annulus.

After making the substitutions, the equation becomes

$$G(b) = N_\gamma \Sigma_a \mu_e E \phi_1 \left\{ \int_{R=b}^{R=\infty} \int_{x'=0}^{x'=b} \left[1 + m\mu_t R\right] \frac{e^{-\mu_t R}}{2R} \left[1 - \left(\frac{X-1}{X}\right) \sin \frac{\pi x'}{t}\right] + \right. \tag{5}$$

$$\left. \int_{R=(t-b)}^{R=\infty} \int_{x'=b}^{x'=t} \left[1 + m\mu_t R\right] \frac{e^{-\mu_t R}}{2R} \left[1 - \left(\frac{X-1}{X}\right) \sin \frac{\pi x'}{t}\right] \right\} dr\, dx' \,.$$

Equation (5) may be rewritten as

$$G(b) = N_\gamma \Sigma_a \mu_e E \phi_1 I(b, E) \,. \tag{6}$$

Upon integration

$$I(b, E) = \frac{1}{2} \left[b + \frac{t}{\pi} \left(\frac{X-1}{X}\right) \left(\cos \frac{\pi b}{t} - 1\right) \right] m e^{-\mu_t b}$$

$$+ \frac{1}{2}\left[b + \frac{t}{\pi}\left(\frac{X-1}{X}\right)\left(\cos\frac{\pi b}{t} - 1\right)\right]\int_{\mu_t b}^{\infty} e^{-(\mu_t R)}\,\frac{d(\mu_t R)}{(\mu_t R)}$$

$$+ \frac{1}{2}\left[(t-b) - \frac{t}{\pi}\left(\frac{X-1}{X}\right)\left(\cos\frac{\pi b}{t} + 1\right)\right] m e^{-\mu_t (t-b)}$$

$$+ \frac{1}{2}\left[(t-b) - \frac{t}{\pi}\left(\frac{X-1}{X}\right)\left(\cos\frac{\pi b}{t} + 1\right)\right]\int_{(t-b)\mu_t}^{\infty} e^{-(\mu_t R)}\,\frac{d(\mu_t R)}{(\mu_t R)} \quad . \qquad (7)$$

The energy spectrum for capture gammas in aluminum is as follows[18]

Energy interval (Mev)	0 - 1	1 - 3	3 - 5	5 - 7	7 - 7.7 (max)
Photon/100 capture	?	13	77	21	35

Values of m[19]

E (Mev)	2	4	6	7.5
m	.85	.55	.40	.33

APPENDIX VI

HEAT PRODUCTION IN INTERIOR MODERATOR

1. Prompt Gamma Heating

   a. Gamma current

$$\text{fission rate} = 3.1 \times 10^{10} \text{ fissions/watt-sec} \times P(\text{Mw})\ 10^{6} \text{watts/Mw}$$

$$= 3.1 \times 10^{16} P \text{ fissions/sec}$$

$$\text{core volume} = (91.44 \text{ cm})(55^2 - 40^2)$$

$$= 4.085 \times 10^{5} \text{ cm}^3$$

$$\frac{\text{fissions}}{\text{cm}^3\text{-sec}} = \frac{3.1 \times 10^{16} P}{4.085 \times 10^{5}} = 7.589 \times 10^{10} P$$

$$\text{energy from prompt gammas} = 7.5 \text{ Mev/fission}$$

$$S_v = \text{volume source strength} = 7.5 \times 7.589 \times 10^{10} P$$

$$= 5.692 \times 10^{11} P \text{ Mev/cm}^3\text{-sec}$$

   b. Relaxation length

$$\text{Volume U/element} = 7.97 \text{ cm}^3$$

$$\text{Volume U + Al/element} = 1664 \text{ cm}^3$$

$$\text{Volume Al/element} = 1556.03 \text{ cm}^3$$

$$\text{Volume core} = 4.085 \times 10^{5} \text{ cm}^3$$

$$\text{Volume cell} = 6808 \text{ cm}^3$$

$$\text{Volume Al/cell} = \text{Volume of cell} - \text{Volume of element}$$

$$= 6808 - 4160 = 2648 \text{ cm}^3$$

$$\text{Total Al volume} = 4204.03 \text{ cm}^3$$

Volume H_2O/element = 2496 cm^3

Volume fractions:

Al	4204.03/6808	= .6175
H_2O	2496/6808	= .3666
U	7.97/6808	= .00117

Assuming 3 - 5 Mev

	$u\ cm^{-1}$	λ_{cm}	Volume Fraction / λ
H_2O	.034	29.41	.01247
D_2O	.0374	26.74	.01371
Al	.084	11.90	.05189

$$\therefore \frac{1}{\lambda_c} = .0656$$

for b = 15 cm

$\bar{\mu}_e$ = .0242

μ_t = .0656

$$G = 1.05 \times 10^{11} P(Mw) \left[E_2(\bar{\mu}_e x) - E_2(\mu_t b - \bar{\mu}_e x) \right] .$$

Results are plotted on Figure 1 as a function of the distance into the moderator.

$$G = 1.63 \times 10^3 \text{ Btu/hr-ft}^3/\text{Mw} \left[E_2(\bar{\mu}_e x) - E_2(\bar{\mu}_t b - \bar{\mu}_e x)\right] .$$

Total heat in watts,

$$Q = 2\pi H \int Gr \, dr$$

$$= 5.72 \times 10^2 \, P(\text{Mw}) \, .$$

2. Heating Due to Elastic Collisions

a. Total Heat

$$G_{ne} = \int_{E_o}^{\infty} \delta_{ne} E_n \Sigma_{ne} \phi_n \, d E_n$$

$$P = \int \omega \Sigma_f \phi_n \, d^3 r$$

$$\phi_n = \frac{3.1 \times 10^{10}}{.0455 \text{ cm}^{-1}} \frac{\text{fissions}}{\text{watt-sec}} \frac{P(\text{Mw}) \, 10^6}{\int d^3 r}$$

$$Q_{ne} = \int G_{ne} \, d^3 r$$

$$= \delta_{ne} E_n \Sigma_{ne} \frac{3.1 \times 10^{16} \, P}{.0455}$$

$$\alpha = \frac{M-1}{M+1} = \frac{1}{3} \qquad \delta_{ne} = \frac{1 - \alpha}{2} = \frac{1}{3}$$

$$N = 3.3 \times 10^{22} \text{ atoms/cm}^2 \qquad \sigma\,(7 \text{ Mev}) = 4.1 \times 10^{-24} \text{ cm}^2$$

$$Q_{ne} = 1/3(7)\ (3.3 \times 10^{22})(4.1 \times 10^{-24})\ \frac{(3.1 \times 10^{16})P}{.0455}\ (1.603 \times 10^{-13} \text{ watts/sec})$$

$$= 3.4 \times 10^{4}\ P(\text{Mw}) \text{ watts.}$$

b. Power density distribution

Assume $\phi_n = \phi_{12max}\, e^{-\Sigma_f r}$

$$\phi_{12max} = \frac{\phi_{12max}}{\bar{\phi}_{12}}\ \bar{\phi}_{12}\ \frac{\bar{\phi}_{32}}{\bar{\phi}_{12}}\ \frac{\bar{\phi}_{12}}{\bar{\phi}_{32}}$$

$$\frac{\phi_{12max}}{\bar{\phi}_{12}} = K_1 \qquad \frac{\bar{\phi}_{12}}{\bar{\phi}_{32}} = K_2 \qquad K = K_1 K_2$$

$$P = \bar{\phi}_{32}\, \omega\, \Sigma_f\, V$$

$$G_{ne} = \delta_{ne}\, E\, \Sigma_{ne}\, \frac{K}{V\omega}\, \frac{P}{\Sigma_f}\, e^{-\Sigma_f r}$$

$$G_{ne} = 1/3(7 \text{ Mev})(3.3 \times 10^{22} \text{ atoms/cm}^2)\ \frac{(4 \times 10^{-24} \text{ cm}^2)PK\ 3.1 \times 10^{10}\ \frac{\text{fiss}}{\text{watt-sec}}}{(4.085 \times 10^{5} \text{cm})(.0455 \text{ cm}^{-1})}\ e^{-\Sigma_f r}$$

$$= 5.265 \times 10^{3}\ PK\ e^{-\Sigma_f r}\ \frac{10^6 \text{ watts}}{\text{Mw}}\ 1.52 \times 10^{-16} \text{Btu/Mev} \times \frac{1 \text{ cm}^3}{3.53 \times 10^{5} \text{ ft}^3} \times 3600 \text{ sec-hr.}$$

$$= 81.56\ P(\text{Mw})\ K\ e^{-\Sigma_f r} \text{ Btu/hr-ft}^3 .$$

3. Neutron Capture Heating

$$G_{nc} = \int_{E_o}^{\infty} \delta_{nc} E_n \Sigma_{nc} \phi_n \, d E_n$$

$$P = \int \omega \Sigma_f \phi_n \, d^3 r$$

$$Q_{nc} = \frac{3.1 \times 10^{10}}{.0455 \text{ cm}^{-1}} \frac{\text{fissions}}{\text{watt-sec}} \frac{P(\text{Mw}) \, 10^6}{\int d^3 r}$$

$$Q_{nc} = \int G_{nc} \, d^3 r$$

$$= \delta_{nc} E_n \Sigma_{nc} \frac{3.1 \times 10^{16} \, P}{.0455}$$

$$\delta_{nc} = \frac{m}{\mu_t m} = \frac{1}{3}$$

$$\Sigma_{nc} = 8.5 \times 10^{-5} \text{ cm}^{-1} \quad E_n = 8 \text{ Mev}$$

$$Q_{nc} = 1/2(8 \text{ Mev})(8.5 \times 10^{-5}) \frac{(3.1 \times 10^{16} P)}{.0455} (1.603 \times 10^{-13} \text{ watts-sec/Mev})$$

$$Q_{nc} = 37 \, P(\text{Mw}) \text{ watts} \, .$$

APPENDIX VII

HEAT PRODUCTION IN SHIM TUBES

1. Boron capture γ-particles:

$$\frac{\text{Volume of B}}{\text{Total Volume}} = \frac{.0151}{1}$$

$$N = (.0151)\,\frac{(2.535)(6.01 \times 10^{23})}{5} = 4.6 \times 10^{21}\ B\ \frac{\text{nuclei}}{cm^3}$$

$$\Sigma_a = N\sigma = 755 \times 10^{-24}\ cm^2 \times 4.6 \times 10^{21} = 3.475\ cm^{-1}$$

$$G = 3.3 \times 10^{15}\ \frac{n}{cm^2\ sec} \times \frac{2.314\ Mev}{n\ capture} \times 3.475\ cm^{-1} = 2.654 \times 10^{16}\ \frac{mev}{cm^3\ sec}$$

$$2.654 \times 10^{16}\ \frac{mev}{cm^3\ sec} \times 1.52 \times 10^{-16}\ \frac{Btu}{Mev} \times 3.532 \times 10^{-5}\ \frac{ft^3}{cm^3} \times \frac{3600\ sec}{hr} = .513\ \frac{Btu}{hr\text{-}ft^3}$$

This flux corresponds to a power level of 368 MW and yields 1.39×10^{-3} Btu/hr-ft^3/MW.

2. Boron Capture γ-rays:

Source is .48 Mev γ's $\frac{\text{Btu}}{\text{hr-ft}^3\text{/MW}}$

$$G = 3.3 \times 10^{15} \frac{n}{cm^2\text{-sec}} \times \frac{.48 \text{ Mev}}{\text{n-capture}} \times 3.475 \text{ cm}^{-1} = .5504 \times 10^{16} \frac{\text{Mev}}{cm^3 \text{ sec}}$$

$$.5504 \times 10^{16} \frac{\text{mev}}{cm^3 \text{ sec}} \times 1.52 \times 10^{-16} \frac{\text{Btu}}{\text{Mev}} \times 3.532 \times 10^{-5} \frac{ft^3}{cm^3} \times \frac{3600 \text{ sec}}{\text{hr}} = .106 \frac{\text{Btu}}{\text{hr-ft}^3}$$

$$= 2.88 \times 10^{-4} \frac{\text{Btu}}{\text{hr-ft}^3/\text{MW}} .$$

3. Elastic Collisions:

$$G_{ne} = \int_{E_o}^{\infty} \delta_{ne} E_n \quad \Sigma_{ne} \phi_n \, d E_n .$$

Let $\phi_n = 3.3 \times 10^{15} \frac{n}{cm^2\text{-sec}}$

$$E_n = 2 \text{ Mev} .$$

Assuming mixture of boric acid:

molecular weight boric acid = 61.84

molecular weight B = 10.82 .

at 99°C solubility = 20 gm $\frac{\text{boric acid}}{100 \text{ gm } H_2O}$

$$20 \text{ gm} \times \frac{10.82}{61.84} = .035 \frac{\text{gm B}}{\text{gm } H_2O}$$

$$\frac{.035 \times \frac{1}{2.32} \frac{gm}{cm^3}}{cm^3\ H_2O} = \frac{.0151\ cm^3 B}{cm^3\ H_2O} .$$

$\therefore$ consider tube to contain 100% D_2O

$$\delta_{ne} = \frac{1-a}{2} = \frac{1}{2} \qquad a = \frac{\mu - 1}{\mu + 1} = 0$$

$$N = 3.3 \times 10^{22} \frac{atoms}{cm^3}$$

$$\sigma_H = 2.9 \text{ barns}$$

$$\sigma_0 = 3.6 \text{ barns}$$

$$\Sigma_{ne} = 3.3 \times 10^{22} (5.8 + 3.6)(10^{-24}) = .31\ cm^{-1}$$

$$G_{ne} = \frac{1}{2}(2\ Mev)(.31\ cm^{-1})(3.3 \times 10^{15} \frac{n}{cm^2\text{-sec}})(1.52 \times 10^{-16} \frac{Btu}{Mev})(3.532 \times 10^{-5} \frac{ft^3}{cm^3})$$

$$(\frac{3600\ sec}{hr})$$

$$G_{ne} = .0198 \frac{Btu}{hr\text{-}ft^3} = 5.38 \times 10^{-5} \frac{Btu}{hr\text{-}ft^3/MW} .$$

Total heat developed in tube will be

from B capture - particles		.513
B capture γ's		.106
elastic collisions		.0198
	Total heating	.5388 Btu/hr-ft^3

or

$$1.46 \times 10^{-3} \ \frac{\text{Btu}}{\text{hr-ft}^3/\text{MW}} \ .$$

APPENDIX VIII

HEATING IN FUEL ELEMENT HOUSING

1. Prompt Fission Gamma Heating

Assume that the housing can be represented by a .5" thick plate

$$\text{Gamma volume source, } S_v = \text{fission rate} \times \frac{\gamma\text{'s}}{\text{fission}} \times \frac{1}{\text{core volume}}$$

Assume $7.5 \frac{\gamma\text{'s}}{\text{fission}}$ at $\frac{1 \text{ mev}}{\gamma}$

$$S_v = 3.1 \times 10^{10} \frac{\text{fission}}{\text{watt-sec}} \times P(MW) 10^6 \frac{\text{watt}}{MW} \times 7.5 \frac{\gamma\text{'s}}{\text{fission}} \times \frac{1}{2.50} \times 10^5 \text{ cm}^3$$

$$\text{Volume} = \text{No. of elements} \times \frac{\pi d^3}{4} \times L = 60 \times \pi \left(\frac{7.62}{4}\right)^3 91.5 = 2.50 \times 10^5 \text{ cm}^3$$

$$S_v = 9.30 \times 10^{11} \frac{\gamma\text{'s}}{\text{sec-cm}^3} P(MW)$$

for $\bar{\mu}_e = .0567$ and $\mu_t b = .984$

$$G = \frac{9.30 \times 10^{11}}{2} P(MW) \frac{.0567}{.0056} .679 = 2.779 \times 10^{11} P \frac{\text{Mev}}{\text{cm}^3\text{-sec}} = 4.23 \times 10^3 \frac{\text{Btu}}{\text{hr-ft}^3}$$

X cm	$E_2(\bar{\mu}_e x) - E_2(\mu_t b - \bar{\mu}_e x)$
.2	.79
.4	.75
.6	.73
.8	.69
1.0	.65
1.27	.63
Avg.	.679

The average over the double thickness times two is the heat density in the Al since it is exposed on both sides

$$G_{avg} = 8.46 \times 10^3 \frac{Btu}{hr\text{-}ft^3} /MW \quad .$$

2. Capture Gamma

Using equation 4; (Heat Production)

E_γ Mev	1 cm	3 cm	6 cm	7.5 cm
2	$.131 \times 10^5$	$.168 \times 10^5$	$.184 \times 10^5$	$.185 \times 10^5$
4	1.575	2000	2190	2.500
6	.626	.785	.831	.850
7.5	1.348	1.660	1.794	1.778
Total	3.680×10^5	4.613×10^5	5.019×10^5	$5.013 \times 10^5 \frac{Btu}{hr\text{-}ft^3}$

yields

$$G_{avg} = 4.8 \times 10^5 \frac{Btu}{hr\text{-}ft^3}$$

or

$$1.31 \times 10^3 \frac{Btu}{hr\text{-}ft^3/MW} \quad .$$

3. Elastic Collisions

$$G_{ne} = \int_{E_o}^{\infty} \delta_{ne} E_n \Sigma_{ne}(E_n) \phi_n(E_n) d E_n$$

$$\delta_{ne} = \frac{1 - \alpha}{2} = \frac{.0715}{2} \qquad \alpha = \frac{\mu - 1}{\mu + 1} = \frac{26}{28} = .9285$$

$$= .0358$$

$$\overline{\phi}_n = 3.3 \times 10^{15} \ *$$

$$E_{ne} = 2 \text{ Mev}$$

$$N = 6.2 \times 10^{22} \text{ neuts/cm}^3$$

$$\sigma(2 \text{ Mev}) = 3b$$

$$\Sigma_{ne} = 6.2 \times 10^{22} \times 10^{-24} \times 3$$

$$G_{ne} = (.0358)(2)(6.2 \times 10^{-2})(3)(3.3 \times 10^{15}) \frac{n}{cm^2\text{-sec}} \times 1.52 \times 10^{-16} \frac{Btu}{Mev}$$

$$\times \ 3.532 \times 10^{-5} \frac{ft^3}{cm^3} \times \frac{3600 \text{ sec}}{hr}$$

$$= 8.68 \times 10^{4} \frac{Btu}{hr\text{-}ft^3} = 2.36 \times 10^{2} \frac{Btu}{hr\text{-}ft^3/MW} \ .$$

---

* One should note that the fluxes used in the above calculations are only typical and depend on the fuel annulus, etc.

APPENDIX IX

SHIELDING

1. Gamma Shielding - Linear buildup factors

$$\text{Fission rate} = 3.1 \times 10^{10} \frac{\text{fissions}}{\text{sec}} P(\text{MW})\ 10^{6} \frac{\text{watts}}{\text{MW}}$$

$$= 3.1 \times 10^{16} P \frac{\text{fissions}}{\text{sec}}$$

Volume of core $= 4.95 \times 10^{5}$ cm^3 so that,

$$\frac{\text{fissions}}{\text{cm}^3\text{-sec}} = \frac{3.1 \times 10^{16} P}{4.95 \times 10^{5}} = 6.26 \times 10^{10} P \ .$$

The total energy from both prompt gammas and radiation accompanying radioactive decay of fission products is 12 Mev per fission. In addition there are 8 Mev per fission due to capture and decay gamma in the reactor, resulting in a total of 20 Mev produced per fission. The volume source strength is,

$$S_v = (20 \text{ Mev})(6.26 \times 10^{10} P) = 1.252 \times 10^{12} P \frac{\text{Mev}}{\text{cm}^3\text{-sec}} \ .$$

The equivalent isotropic surface source strength may be expressed as[20]

$$S_a = S_v \lambda = 1.252 \times 10^{12} \text{ P} \times 15.24 \text{ cm} = 1.908 \times 10^{13} \text{ P} \frac{\text{Mev}}{\text{cm}^2\text{-sec}} .$$

Required relaxation lengths,[23]

Material	Neutrons	Gammas
Ordinary concrete ρ=2.3 gm/cm^3	20 cms	17.6
Heavy Water	11.3	41.3
Steel	6.6	4.4

Considering the radiation as coming from an infinite plane source and a linear buildup factor

$$D = \frac{S_a}{2} e^{-r/\lambda} \quad (21) .$$

The attenuation of gamma radiation leaving the 200 cm reflector is,

$$D_1 = \frac{1.908 \times 10^{13}}{2} \text{ P } e^{-\frac{200}{41.3}} = .9546 \times 10^{12} \text{ P} \frac{\text{Mev}}{\text{cm}^2\text{-sec}}$$

or in rad/hr

$$.9546 \times 10^{12} \text{P}(.0205 \text{ cm}^2/\text{gm})_{\text{tissue}} \; 1.6 \times 10^{-6} \frac{\text{ergs}}{\text{Mev}} \; \frac{\text{rad}}{100 \frac{\text{ergs}}{\text{gm}}} \times \frac{3600 \text{ sec}}{\text{hr}}$$

$$= 1.42 \times 10^6 \text{ P r/hr} .$$

The dose at the surface of the steel is

$$D_2 = 1.42 \times 10^6 \, P \, e^{-r_3/4.4}$$

and that leaving the concrete is expressed as

$$D_3 = D_2 \, e^{-r_3/13.0} \, .$$

2. Prompt Fission Gammas - NDA buildup factors

The data for gammas per fission in discrete energy ranges reported by Gamble and Bell[22] is

Energy Mev	Photons/fission in the 1/2 Mev range centered on this energy	Groups N(E) photons/fission at E Mev/photon
1/2	3.1	3.2 at 1 Mev
1	1.9	
1 1/2	0.84	0.8 at 1.5 Mev
2	0.55	0.85 at 2.3 Mev
2 1/2	0.29	
3	0.15	0.15 at 3 Mev
3 1/2	0.062	
4	0.065	
4 1/2	0.024	0.2 at 5 Mev
5	0.019	
5 1/2	0.017	
6	0.007	
6 1/2	0.004	
Total	7.0 photons/fission 7.8 Mev/fission	7.8 Mev/fission

The above groups were used to reduce the number of sources considered. Consider a shield consisting of the following

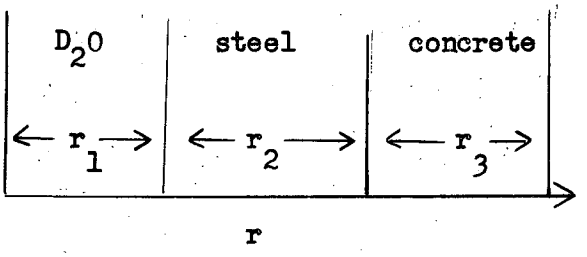

The dose at the outside of the concrete shield at a distance $r = r_1 + r_2 + r_3$ is

$$D(r) = \frac{S\,E_o}{4\pi r^2} (\mu_a)_{tissue}\, B_1(\mu_1 r_1)\, B_2(\mu_2 r_2)\, B_3(\mu_3 r_3)\, e^{-\mu_1 r_1} e^{-\mu_2 r_2} e^{-\mu_3 r_3} \times$$

$$\times \frac{1.6 \times 10^{-16}\ \text{ergs/Mev}}{100\ \text{ergs/gm}}\ \text{rad} \times \frac{3600\ \text{sec}}{\text{hr}} .$$

Now,

$$\frac{\text{fissions}}{\text{sec}} = 3.1 \times 10^{10}\ \frac{\text{fissions}}{\text{watt-sec}} \times 10^6\ \frac{\text{watt}}{\text{MW}}\ P(\text{MW}) = 3.1 \times 10^{16}\ P .$$

Volume of Reactor $= \pi(55^2 - 4.0^2)(91.44) = 4.085 \times 10^5\ cm^3$.

E(Mev)	Photons / Fission	Photons / sec	Mev / sec	$\mu_1 cm^{-1}$	$B_1(\mu_1 r_1)$	$\mu_2 cm^{-1}$	$B_2(\mu_2 r_2)$
1	3.2	9.92×10^{16} P	9.92×10^{16} P	15.6	53.5	.212	2.9
1.5	0.8	2.48×10^{16} P	3.72×10^{16} P	12.8	20.5	.185	2.6
2.3	0.85	2.64×10^{16} P	6.07×10^{16} P	10.1	11.5	.165	2.15
3	0.15	$.465 \times 10^{16}$ P	1.40×10^{16} P	8.8	7.7	.165	1.92
5	0.2	$.62 \times 10^{16}$ P	3.10×10^{16} P	6.6	4.3	.181	1.80

E(Mev)	μ_3 cm^{-1}	$(\frac{\mu - \sigma_s}{\rho})$ tissue $\frac{cm^2}{gm}$
1	.146	.03
1.5	.120	.0275
2.3	.095	.024
3	.084	.0225
5	.065	.019

Linear absorption coefficients and buildup factors for D_2O and F_e were taken from APEX-176[23], assuming $\mu_{D_2O} = 1.1\mu_{H_2O}$. Doses for various thicknesses of concrete are plotted for $r_1 =$ 200 cm, and $r_2 =$ 2, 10, and 20 cm respectively. Absorption coefficients as a function of energy for ordinary concrete of density 2.3 gms/cm^2 are plotted in CRR-578[24], p. 413. The composition is as follows:

Hydrogen	.52%
Carbon	.18
Silicon	28.1
Aluminum	7.51
Iron	2.8
Calcium	5.82
Sulphur	.24
Magnesium	.80
Sodium	2.10
Potassium	3.14
Oxygen	48.58

Dose buildup factors for concrete were computed from plotted parameters appearing in TID-7004[25], p. 423 and the relation

$$B_3(E_o, \mu_3 r_3) = A_1 e^{-\alpha_1 \mu_3 \gamma_3} + A_2 e^{-\alpha_2 \mu_3 r_3}$$

where A_1, α_1 and α_2 are functions of E_o. The results are plotted in Figure 53.

3. Neutron Shielding

Since each fission liberates 2.5 fast neutrons the fast-neutron volume source strength may be taken as

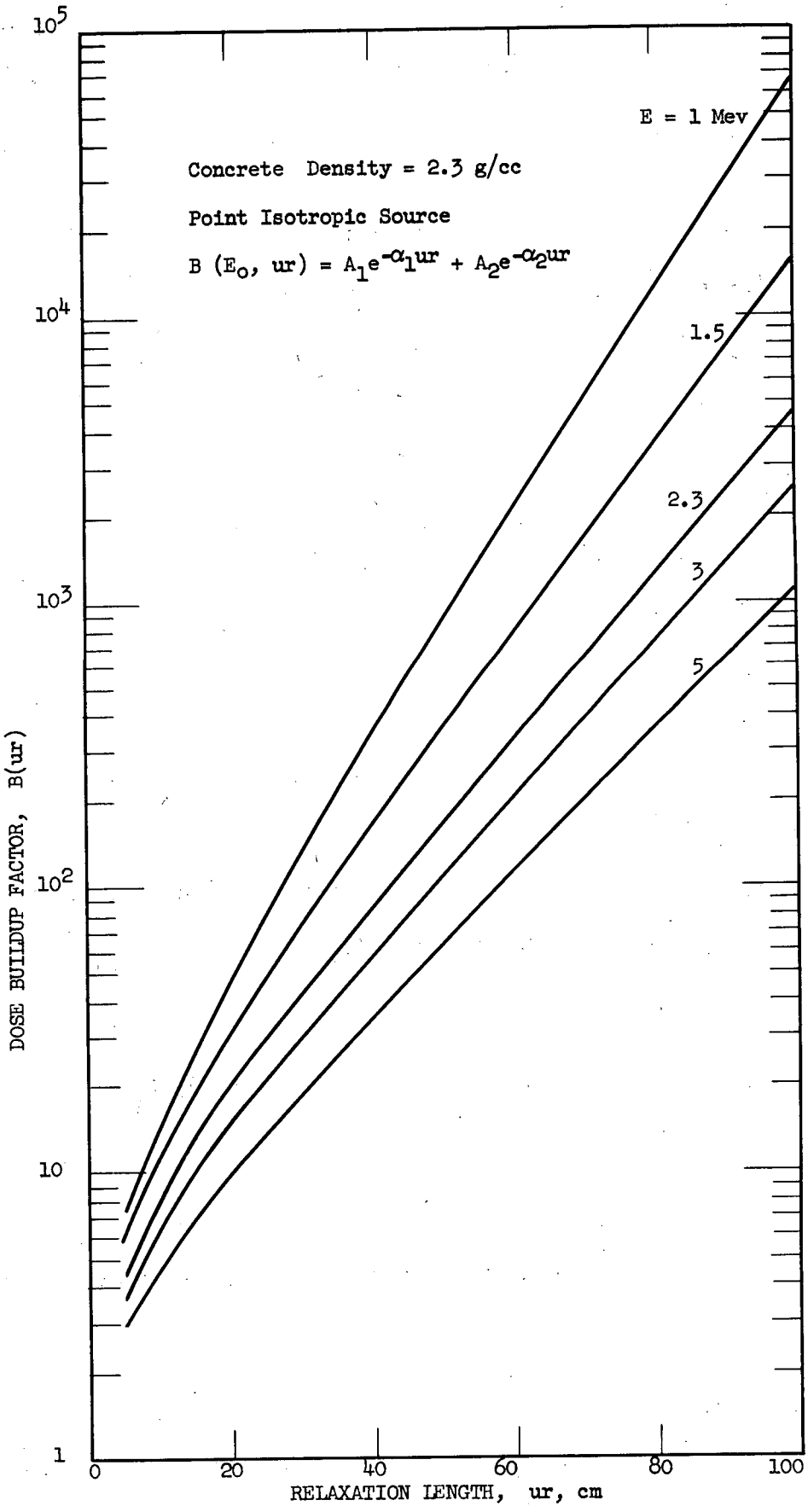

Fig. 53 DOSE BUILDUP FACTOR VS. RELAXATION LENGTH IN CONCRETE, FOR VARIOUS ENERGIES

$$S_v = 6.26 \times 10^{10} \, P \, \frac{\text{fissions}}{\text{cm}^3\text{-sec}} \times \frac{2.5 \text{ n}}{\text{fission}} = 1.568 \times 10^{11} \, P \, \frac{\text{n}}{\text{cm}^3\text{-sec}} \, .$$

The equivalent surface source strength is obtained by

$$S_a = S_v \lambda$$

$$= 1.568 \times 10^{11} \, P \times 11.3 \text{ cm} = 1.77 \times 10^{12} \, P \, \frac{\text{n}}{\text{cm}^2\text{-sec}} \, .$$

The fast neutrons leaving the 200 cm reflector is

$$D_1 = \frac{S_a}{2} e^{-r_1/\lambda}$$

$$= 1.77 \times 10^{12} \, P \, e^{-200/11.3} = 2.05 \times 10^{4} \, P \, \frac{\text{n}}{\text{cm}^2\text{-sec}} \, .$$

The dose at the surface of the steel is,

$$D_2 = 2.05 \times 10^{4} \, P \, e^{-r_2/16.6}$$

and that leaving the concrete

$$D_3 = D_2 e^{-r_3/15.1} \quad .$$

4. Secondary Gammas

The equivalent fast-neutron surface source strength leaving the reflector and entering the steel shield is $2(2.05 \times 10^4 P)\frac{n}{cm^2\text{-sec}}$. Each neutron produces one secondary gamma of 7 Mev energy in the steel. Assuming these leave the surface of the steel the thickness of concrete necessary to decrease the dose to .075 r/hr at 500 MW, is

$$.075 = 7 \text{ Mev } 2\left(\frac{7.05 \times 10^4}{2}\right)(500)\, e^{-r_3/13.0}\, .0205 \frac{gm^2}{gm}\, 1.6 \times 10^{-6} \frac{ergs}{mev} \times \frac{r}{100 \frac{ergs}{gm}} \times \frac{3600 \text{ sec}}{hr}$$

$$r_3 = 11.4 \text{ r cm} \quad .$$

Also each neutron may be assumed to produce a 4 Mev gamma originating 30 cm within the shield. The thickness of concrete required is

$$r_3 = 106.6 \text{ cm} \quad .$$

APPENDIX X

XENON INSTABILITY

1. The prompt neutron lifetime is

$$L = \frac{1}{\Sigma_a V(1 + M^2B^2)}$$

where

L = prompt neutron lifetime, seconds

Σ_a = macroscopic absorption cross section
= 5.95×10^{-2} cm^{-1}

V = neutron speed, 2.2×10^5 cm/sec.

M^2 = migration area = 190 cm^2

B^2 = geometric buckling = 1.66×10^{-3} cm^{-2} .

Using these values the prompt neutron lifetime of the HFRR is 6.0×10^{-5} seconds.

2. When ϕ is near 10^{14} neutrons/cm^2-sec, the period is given by the following expression[26]:

$$T = \sqrt{\frac{t_{eff}\ t_x}{Y}}$$

where

T = period, seconds

t_{eff} = $L_p + BkL_d$, effective neutron lifetime

= 9.45×10^{-2} sec.

t_x = $1/\sigma_x \phi$, xenon lifetime = 465 sec.

Y = iodine-135 yield = .056

L_p = prompt neutron lifetime = 6×10^{-5} sec

B = delayed neutron fraction = 7.55×10^{-3}

k = effective multiplication constant = 1.00

L_d = delayed neutron lifetime = 12.5 sec.

σ_x = xenon-135 absorption cross section

= 3.5×10^{-18} cm^{-2}

ϕ = neutron flux = 6.12×10^{14} neutrons/cm^2-sec.

Using these values, the period comes out to be 28 seconds.

3. The criterion derived by Ward[28] states that if $-A/K_1 < 1$ and $-A/K_2 < 1$ are true for a particular reactor, the reactor will not be subject to the constant power flux oscillation. In the above expression:

$$A \approx .035$$

$$K_1 = M^2(B_o^2 - B_1^2)$$

$$K_2 = M^2(B_o^2 - B_2^2)$$

where

M_2 = migration area = 190 cm^2

$B_o^2 = (\frac{\pi}{H})^2 + (\frac{2.405}{R})^2 = 1.195 \times 10^{-3}\ cm^{-2}$

$B_1^2 = 4(\frac{\pi}{H})^2 + (\frac{2.405}{R})^2 = 2.635 \times 10^{-3}\ cm^{-2}$

$B_2^2 = (\frac{\pi}{H})^2 + 2.53\ (\frac{2.405}{R})^2 = 2.289 \times 10^{-3}\ cm^{-2}$

H = extrapolated half height of the reactor

R = extrapolated radius of the reactor

then

$$K_1 = -.275 \text{ and } K_2 = -.208$$

and

$$\frac{-A}{K_1} = .127 \text{ and } \frac{-A}{K_2} = .157 .$$

Since both are less than 1.00 the reactor is stable by this criterion.

APPENDIX XI

TABLE OF NOMENCLATURE

Regions: 1 - Central Region

2 - Second region (annulus)

3 - Outer region.

Groups: 1 - Fast neutron energy

2 - Intermediate neutron energy

3 - Thermal neutron energy.

Note: In all two-digit subscripts, first number refers to group, second number to region.

av (or ave)	Subscript denoting a value averaged over geometry concerned.
B	Energy absorption buildup factor
B_i^2	Unreflected group i buckling
C_I	Iodine concentration, atoms/cm^3, subscript 0 refers to steady state value
C_X	Xenon concentration, atoms/cm^3, subscript 0 refers to steady state value
c_p	Specific heat at constant pressure, Btu/lb-degree F
D	Gamma dose, Mev/cm^2-sec or rad/hr. Neutron dose, neutrons/cm^2-sec
D	Diffusion coefficient, cm, subscripts denote group and region
E_o	Gamma energy, Mev
G	Specific rate of heat release, Btu/hr-ft^3
H	Actual half-length of reactor core, ft
$\tilde{H}$	Extrapolated half-length of reactor core, ft

h	Film coefficient of heat transfer, Btu/hr-ft^2-degree F
K	Thermal conductivity, Btu/hr-ft-degree F
l	Neutron lifetime, sec
M	Atomic mass of nucleus, amu
m	Atomic mass of neutron, amu
N_B	Boron concentration, atoms/cm^3, subscript 0 refers to time zero
N_F	Fuel concentration, atoms/cm^3, subscript 0 refers to time zero.
N_{FP}	Fission product pair concentration, atoms/cm^3
N_{Sm}	Samarium concentration, atoms/cm^3
N_{Xe}	Xenon concentration, atoms/cm^3
n	Group number
n_{th}	Group corresponding to thermal lethargy
P	Power, megawatts
P_o	Power density, watts/cm^3
Q	Heat generation or power density, Btu/hr-ft^3
q	Slowing down density, neutrons/cm^3-sec
q'	Heat flux in reactor core, Btu/hr-ft^2
q'_o	Heat flux at z = 0, Btu/hr-ft^2
$q'_{o'ave)}$	Average heat flux in radial direction for z = 0
$q'_{o(max)}$	Maximum heat flux in radial direction for z = 0
R_1	Region 1 thickness, cm
R_2	Region 2 thickness, cm
R_3	Region 3 thickness, cm
r	Distance from source to detector, cm
S_a (or S)	Isotropic surface source strength, Mev/cm^2-sec
S_v	Volume gamma source strength, Mev/cm^2-sec

T_i	Coolant temperature at inlet to fuel element, degrees F
T_o	Coolant temperature at outlet from fuel element, degrees F
t_1	Shell 1 thickness, cm, shell located between regions 1 and 2
t_2	Shell 2 thickness, cm, shell located between regions 2 and 3
u	Lethargy of neutrons
V	Velocity, ft/sec
W	Thickness of fuel plate, ft or in.
X	Ratio of maximum to minimum thermal flux in the fuel region
z	Distance upward from center of reactor core, ft
z_{max}	Distance from center of reactor core upward to point at which $T_{s_{max}}$ occurs
$\triangle P_E$	Pressure loss in exit from fuel element, psi
$\triangle P_I$	Pressure loss in entrance to fuel element, psi
$\triangle P_s$	Pressure loss in straight section of fuel element, psi
δ_{nc}	Average fraction of energy of incident particle that is released locally upon neutron capture
δ_{ne}	Average fraction of energy of incident particle that is released locally in an elastic collision
ϵ	Coolant gap width, ft or in.
λ_{Pm}	Promethium decay constant, sec^{-1}
λ_{Xe}*	Xenon decay constant, $sec^{-1} = \lambda_{Xe} + \sigma_a^{Xe} \phi$
μ	Viscosity, lb/hr-ft
$\bar{\mu}_e$	Photon energy absorption coefficient, cm^{-1}
$\bar{\mu}$	Average value of cosine of the scattering angle in the laboratory system
μ_a	Absorption cross section, cm^{-1}

μ_I	Fission yield of Iodine, atoms/fission
μ_{Pm}	Fission yield of Promethium, atoms/fission
μ_{Xe}	Fission yield of Xenon, atoms/fission
ν	Neutrons produced per fission
ξ	Average logarithmic energy decrement
ρ	Density, lb/ft^3 or gm/cm^3
Σ	Macroscopic cross section, cm^{-1}

Subscripts: a - absorption
f - fission
x - transfer

Superscripts: F - fuel
M - moderator
I - iodine
Sm - Samarium
U - uranium
X - xenon

Σ^T	Total cross section for a number of elements, cm^{-1}
σ	Microscopic cross section, barns, subscripts and superscripts as for macroscopic cross section above
τ	Slowing down length squared, cm^2
ϕ	Neutron flux, neutrons/cm^2-sec
$\overline{\phi}\Delta u$	Integrated flux or "weighting function"
ω	Conversion factor, fissions/watt-sec

TABLE 2

THREE GROUP CONSTANTS FOR VARIOUS MATERIALS

	D_2O	B_e	C	Al
N	.0332	.1229		
Σ_{a_1}	0	.0002343	0	.0002259
Σ_{a_2}	0	.0001389	.0000500	.001867
Σ_{a_3}	.0000642	.0009439	.000228	.0123'
Σ_{x_1}	.02752	.01888	.00924	.0002902
Σ_{x_2}	.01651	.01148	.00464	.003017
D_1	1.321	.6955	1.432	1.533
D_2	1.203	.5107	.942	3.713
D_3	.874	.4185	.945	4.262

TABLE 3

THREE GROUP CONSTANTS FOR VARIOUS DILUENTS IN D_2O

Diluents	B_e	B_e	Al	Al	Al
Volume %	70	50	70	50	30
Σ_{a_1}	.0001640	.0001171	.0001577	.0001129	.00006780
Σ_{a_2}	.00009719	.00006938	.001303	.0009334	.0005604
Σ_{a_3}	.0006605	.0004715	.008588	.006150	.003692
Σ_{x_1}	.02269	.02508	.006134	.01115	.01690
Σ_{x_2}	.01255	.01322	.006390	.009545	.01238
D_1	.8074	.9063	1.450	1.401	1.361
D_2	.6161	.7153	2.273	1.806	1.501
D_3	.4966	.5677	1.933	1.467	1.184
N_{D_2}	.0100	.0166	.0232	.0166	.00996
N_{Al}	0	0	.0181	.03015	.0421
N_{Be}	.0860	.0614	0	0	0

TABLE 4

THREE GROUP CONSTANTS FOR VARIOUS URANIUM CONCENTRATIONS

	H[c]	H	H		H		H
N_u[a]	$1x10^{-5}$	$2x10^{-5}$	$3x10^{-5}$	$4x10^{-5}$	$5x10^{-5}$	$6x10^{-5}$	$7x10^{-5}$
N_{Al}	.0255	.0255	.0255	.0255	.0255	.0255	.0255
N_{D_2O}	.0192	.0192	.0192	.0192	.0192	.0192	.0192
M/W	.73	.73	.73	.73	.73	.73	.73
Σ_{a_1}	.000117	.000138	.0001606	.0001826	.0002047	.0002255	.0002695
Σ_{a_2}	.00159	.002425	.002987	.003849	.00464	.004819	.005431
Σ_{a_3}	.00111	.0170	.0228	.02884	.0346	.04066	.0464
Σ_{x_1}	.01386	.01396	.01406	.001356	.01414	.01363	.01422
Σ_{x_2}	.01099	.01112	.0110	.01082	.01101	.01089	.01104
D_1	1.380	1.385	1.391	1.391	1.39	1.392	1.392
D_2	1.66	1.66	1.652	1.671	1.642	1.674	1.639
D_3	1.255	1.23	1.20	1.222	1.15	1.136	1.11
Σ_{f_1}	.0000480	.0000960	.000144	.0001928	.000240	.000288	.000336
Σ_{f_2}	.00132	.00264	.00395	.005975	.00659	.00789	.00923
Σ_{f_3}	.0122	.0244	.0366	.0496	.0610	.0744	.0854
WF[b]							

[a] Concentration in atoms per cm^3 x 10^{-24}

[b] Weighting functions used. See Table 1

[c] Indicates constants were hand calculated and therefore differ slightly from those prepared on group constant preparation routine.

Table 4 (Cont.)

N_u[a]	8×10^{-5}	9.18×10^{-5}	12×10^{-5}	13×10^{-5}	15×10^{-5}	17×10^{-5}	20×10^{-5}
N_{Al}	.0255	.0255	.0255	.0255	.0255	.0255	.0255
N_{D_2O}	.0192	.0192	.0192	.0192	.0192	.0192	.0192
M/W	.73	.73	.73	.73	.73	.73	.73
Σ_{a_1}	.0002693	.0002952	.0003570	.0003789	.0004228	.0004666	.0005324
Σ_{a_2}	.006214	.007036	.009003	.009700	.01109	.01249	.01458
Σ_{a_3}	.05248	.05945	.07612	.08203	.09384	.1057	.1234
Σ_{x_1}	.01369	.01372	.01380	.01382	.01389	.01394	.01402
Σ_{x_2}	.01094	.01097	.01104	.01106	.01110	.01115	.01121
D_1	1.391	1.390	1.388	1.388	1.387	1.385	1.384
D_2	1.673	1.672	1.670	1.669	1.667	1.667	1.664
D_3	1.092	1.067	1.012	.9935	.9592	.9272	.883
Σ_{f_1}	.000384	.000430	.000576	.000624	.000720	.000817	.000960
Σ_{f_2}	.01052	.01208	.0158	.01710	.01972	.0223	.02625
Σ_{f_3}	.0994	.1138	.1488	.1611	.1860	.211	.248
WF[b]							

Table 4 (Cont.)

N_u[a]	25×10^{-5}
N_{Al}	.0255
N_{D_2O}	.0192
M/W	.73
Σ_a	.0006420
$\Sigma_{a_2}^1$	.01807
Σ_a	.1530
$\Sigma_{x_1}^3$	.01415
Σ_{x_2}	.01131
D_1	1.381
D_2	1.660
D_3	.8178
Σ_{f_1}	.001201
Σ_{f_2}	.0329
Σ_{f_3}	.310
WF[b]	

TABLE 5

THREE GROUP CONSTANTS FOR VARIOUS METAL TO WATER RATIOS

AND VARIOUS URANIUM CONCENTRATIONS

N_u	9.18×10^{-5}	9.18×10^{-5}	12×10^{-5}	5.5×10^{-5}	7×10^{-5}	9.18×10^{-5}	10×10^{-5}
N_{Al}	.00547	.0139	.0139	.0341	.0341	.0341	.0341
N_{D_2O}	.0305	.0255	.0255	.0144	.0144	.0144	.0144
M/W	.10	.30	.30	1.30	1.30	1.30	1.30
Σ_{a_1}	.0002214	.0002524	.0003143	.0002462	.0002790	.0003628	.0003448
Σ_{a_2}	.006537	.006747	.008714	.004685	.005731	.007251	.007822
Σ_{a_3}	.05536	.05708	.07375	.03946	.04832	.06120	.06605
Σ_{x_1}	.0245	.01957	.01964	.009615	.009661	.00972	.009733
Σ_{x_2}	.01560	.01301	.01305	.008703	.008733	.008783	.00803
D_1	1.320	1.358	1.356	1.425	1.424	1.423	1.422
D_2	1.264	1.421	1.420	1.939	1.937	1.935	1.935
D_3	.8379	.9376	.8948	1.377	1.327	1.262	1.239
$D\Sigma_{f_1}$	.0004415	.0004415	.0005760	.000264	.000337	.000442	.000481
$D\Sigma_{f_2}$	.01207	.01207	.01580	.00724	.00921	.01208	.01315
$D\Sigma_{f_3}$	.1138	.1138	.1488	.06825	.0868	.1109	.1240
WF	WFB	WFB	WFB	WFB	WFB	WFB	WFB

TABLE 5 (Cont.)

N_u	15×10^{-5}
N_{Al}	.0341
N_{D_2O}	.0144
M/W	1.30
Σ_{a_1}	.0004544
Σ_{a_2}	.01131
Σ_{a_3}	.09560
Σ_{x_1}	.009854
Σ_{x_2}	.008910
D_1	1.420
D_2	1.930
D_3	1.115
Σ_{f_1}	.000720
Σ_{f_2}	.0197
Σ_{f_3}	.186
WF	WFB

TABLE 6

GROUP CONSTANTS FOR CONSTANT POWER BURNUP WITH BURNABLE BORON POISONS

N_u	9.18×10^{-5}	9.18×10^{-5}	9.18×10^{-5}	9.18×10^{-5}	9.18×10^{-5}	9.18×10^{-5}	9.18×10^{-5}
N_{Al}	.0255	.0255	.0255	.0255	.0255	.0255	.0255
N_{D_2O}	.0192	.0192	.0192	.0192	.0192	.0192	.0192
N_B	1.62×10^{-5}	1.94×10^{-5}	2.16×10^{-5}	2.7×10^{-5}	3.23×10^{-5}	3.766×10^{-5}	2.112×10^{-5}
M/W	.73	.73	.73	.73	.73	.73	.73
Σ_{a_1}	.0003048	.0003067	.0003080	.0003112	.0003143	.0003175	.0003695
Σ_{a_2}	.008313	.008566	.008739	.009165	.009582	.01000	.01067
Σ_{a_3}	.07029	.07243	.07390	.07751	.08106	.08464	.09024
Σ_{x_1}	.01372	.01372	.01372	.01372	.01374	.01374	.01380
Σ_{x_2}	.01098	.01098	.01098	.01098	.01099	.01099	.01104
D_1	1.390	1.390	1.389	1.389	1.389	1.389	1.388
D_2	1.671	1.671	1.671	1.671	1.671	1.671	1.669
D_3	1.031	1.024	1.019	1.008	.9977	.9871	.9701
Σ_{f_1}	.0004408	.0004408	.0004408	.0004408	.0004408	.0004408	.0005762
Σ_{f_2}	.01207	.01207	.01207	.01207	.01207	.01207	.01578
Σ_{f_3}	.1138	.1138	.1138	.1138	.1138	.1138	.1488
WF	WFB	WFB	WFB	WFB	WFB	WFB	WFB

TABLE 6 (Cont.)

N_u	12×10^{-5}	12×10^{-5}	12×10^{-5}	12×10^{-5}	12×10^{-5}	8.661×10^{-5}	8.142×10^{-5}
N_{Al}	.0255	.0255	.0255	.0255	.0255	.0255	.0255
N_{D_2O}	.0192	.0192	.0192	.0192	.0192	.0192	.0192
N_B	2.55×10^{-5}	2.82×10^{-5}	3.528×10^{-5}	4.21×10^{-5}	4.91×10^{-5}	1.522×10^{-5}	1.422×10^{-5}
M/W	.73	.73	.73	.73	.73	.73	.73
Σ_{a_1}	.0003721	.0003737	.0003779	.0003820	.0003862	.0002928	.0002809
Σ_{a_2}	.01101	.01122	.01178	.01232	.01287	.007874	.007433
Σ_{a_3}	.09317	.09498	.09972	.1043	.1090	.06990	.06659
Σ_{x_1}	.01380	.01381	.01381	.01381	.01381	.01371	.01369
Σ_{x_2}	.01104	.01104	.01104	.01105	.01105	.01096	.01095
D_1	1.388	1.388	1.388	1.387	1.387	1.390	1.390
D_2	1.669	1.669	1.669	1.669	1.668	1.672	1.672
D_3	.9617	.9567	.9440	.9319	.9198	1.033	1.043
Σ_{f_1}	.0005762	.0005762	.0005762	.0005762	.0005762	.0004159	.0003910
Σ_{f_2}	.01578	.01578	.01578	.01578	.01578	.01139	.01071
Σ_{f_3}	.1488	.1488	.1488	.1488	.1488	.1074	.1010
WF	WFB	WFB	WFB	WFB	WFB	WFB	WFB

TABLE 6 (Cont.)

N_u	6.61×10^{-5}	4.04×10^{-5}	1.55×10^{-5}	8.661×10^{-5}	8.142×10^{-5}	6.61×10^{-5}	4.040×10^{-5}
N_{Al}	.0255	.0255	.0255	.0255	.0255	.0255	.0255
N_{D_2O}	.0192	.0192	.0192	.0192	.0192	.0192	.0192
N_B	1.134×10^{-5}	$.6610 \times 10^{-5}$	$.2203 \times 10^{-5}$	2.03×10^{-5}	1.901×10^{-5}	1.512×10^{-5}	$.8813 \times 10^{-5}$
M/W	.73	.73	.73	.73	.73	.73	.73
Σ_{a_1}	.0002455	.0001874	.0001308	.0002959	.0002837	.0002478	.0001887
Σ_{a_2}	.006138	.004482	.002255	.008275	.007811	.006436	.004682
Σ_{a_3}	.05596	.03791	.02023	.07330	.06980	.05849	.03939
Σ_{x_1}	.01365	.01358	.1349	.01371	.01369	.01365	.01358
Σ_{x_2}	.01092	.01086	.01079	.01096	.01095	.01092	.01086
D_1	1.391	1.391	1.386	1.390	1.390	1.391	1.391
D_2	1.673	1.671	1.671	1.672	1.671	1.673	1.671
D_3	1.080	1.147	1.224	1.022	1.033	1.071	1.142
Σ_{f_1}	.0003174	.0001947	.00007498	.0004159	.0003910	.0003174	.0001947
Σ_{f_2}	.008695	.006031	.002454	.01139	.01071	.008695	.006031
Σ_{f_3}	.08195	.05009	.01922	.01074	.1010	.08196	.05009
WF	WFB	WF3	WF2	WFB	WFB	WFB	WF3

TABLE 6 (Cont.)

N_u	1.50×10^{-5}	8.661×10^{-5}	8.142×10^{-5}	6.61×10^{-5}	4.04×10^{-5}	1.50×10^{-5}	11.66×10^{-5}
N_{Al}	.0255	.0255	.0255	.0255	.0255	.0255	.0255
N_{D_2O}	.0192	.0192	.0192	.0192	.0192	.0192	.0192
N_B	$.2938\times10^{-5}$	3.533×10^{-5}	3.301×10^{-5}	2.632×10^{-5}	1.534×10^{-5}	$.5114\times10^{-5}$	1.545×10^{-5}
M/W	.73	.73	.73	.73	.73	.73	.73
Σ_{a_1}	.0001301	.0003048	.0002920	.0002545	.0001927	.0001314	.0003587
Σ_{a_2}	.002285	.009459	.008915	.007319	.005276	.002497	.009984
Σ_{a_3}	.02072	.08337	.07918	.06599	.04376	.02218	.08879
Σ_{x_1}	.01445	.01372	.01369	.01366	.01358	.01445	.01384
Σ_{x_2}	.01156	.01096	.01096	.01092	.01086	.01156	.01107
D_1	1.386	1.389	1.390	1.391	1.390	1.386	1.388
D_2	1.671	1.671	1.671	1.673	1.671	1.671	1.670
D_3	1.221	.9912	1.004	1.046	1.125	1.215	.9746
Σ_{f_1}	.00007257	.0004159	.0003910	.0003174	.0001948	.00007257	.0005599
Σ_{f_2}	.002375	.01139	.01071	.008695	.006031	.002375	.01534
Σ_{f_3}	.01860	.1074	.1010	.08195	.05009	.01860	.1446
	WF	WF2	WFB	WFB	WFB	WF3	WF2	WFB

TABLE 6 (Cont.)

N_u	10.96×10^{-5}	9.42×10^{-5}	6.84×10^{-5}	4.26×10^{-5}	1.75×10^{-5}	11.66×10^{-5}	10.96×10^{-5}
N_{Al}	.0255	.0255	.0255	.0255	.0255	.0255	.0255
N_{D_2O}	.0192	.0192	.0192	.0192	.0192	.0192	.0192
N_B	1.47×10^{-5}	1.247×10^{-5}	$.878\times10^{-5}$	$.5233\times10^{-5}$	$.1912\times10^{-5}$	2.061×10^{-5}	1.960×10^{-5}
M/W	.73	.73	.73	.73	.73	.73	.73
Σ_{a_1}	.0003435	.0003078	.0002491	.0001914	.0001350	.0003619	.0003458
Σ_{a_2}	.009515	.008187	.006097	.004529	.002392	.01039	.009823
Σ_{a_3}	.08482	.07402	.05679	.03921	.02220	.09225	.08810
Σ_{x_1}	.01382	.01377	.01367	.01357	.01343	.01387	.01382
Σ_{x_2}	.01105	.01101	.01094	.01084	.01076	.01108	.01107
D_1	1.389	1.389	1.391	1.390	1.386	1.388	1.388
D_2	1.670	1.671	1.673	1.671	1.671	1.669	1.670
D_3	.9865	1.019	1.077	1.143	1.215	.9648	.9769
Σ_{f_1}	.0005263	.0004523	.0003285	.0002053	.00008457	.0005599	.0005263
Σ_{f_2}	.01442	.01239	.008997	.006359	.002771	.01534	.01442
Σ_{f_3}	.1359	.1168	.08481	.05282	.02170	.1446	.1359
WF	WFB	WFB	WFB	WF3	WF2	WFB	WFB

TABLE 6 (Cont.)

N_u	9.42×10^{-5}	6.84×10^{-5}	4.266×10^{-5}	1.755×10^{-5}	11.66×10^{-5}	10.96×10^{-5}	9.42×10^{-5}
N_{Al}	.0255	.0255	.0255	.0255	.0255	.0255	.0255
N_{D_2O}	.0192	.0192	.0192	.0192	.0192	.0192	.0192
N_B	1.663×10^{-5}	1.171×10^{-5}	$.6977\times10^{-5}$	$.2549\times10^{-5}$	3.587×10^{-5}	3.412×10^{-5}	2.895×10^{-5}
M/W	.73	.73	.73	.73	.73	.73	.73
Σ_{a_1}	.0003103	.0002508	.0001926	.0001355	.0003708	.0003545	.0003176
Σ_{a_2}	.008515	.006328	.004692	.002458	.01159	.01097	.009486
Σ_{a_3}	.07681	.05875	.04037	.02263	.1025	.09783	.08507
Σ_{x_1}	.01378	.01369	.01357	.01343	.01391	.01388	.01382
Σ_{x_2}	.01102	.01095	.01085	.01077	.01112	.01110	.01105
D_1	1.389	1.391	1.390	1.386	1.388	1.388	1.389
D_2	1.671	1.673	1.671	1.671	1.669	1.670	1.671
D_3	1.011	1.070	1.138	1.213	.9371	.9499	.9859
Σ_{f_1}	.0004523	.0003285	.0002056	.00008491	.0005599	.0005263	.0004523
Σ_{f_2}	.01239	.008997	.006368	.002779	.01534	.01442	.01239
Σ_{f_3}	.1168	.08481	.05289	.02176	.1446	.1359	.1168
WF	WFB	WFB	WF3	WF2	WFB	WFB	WFB

TABLE 6 (Cont.)

N_u	6.84×10^{-5}	4.26×10^{-5}	1.75×10^{-5}
N_{Al}	.0255	.0255	.0255
N_{D_2O}	.0192	.0192	.0192
N_B	2.038×10^{-5}	1.214×10^{-5}	$.4437 \times 10^{-5}$
M/W	.73	.73	.73
Σ_{a_1}	.0002560	.0001956	.0001365
Σ_{a_2}	.007011	.005157	.002638
Σ_{a_3}	.06456	.04383	.02389
Σ_{x_1}	.01373	.01360	.01344
Σ_{x_2}	.01097	.01086	.01077
D_1	1.391	1.390	1.386
D_2	1.673	1.671	1.671
D_3	1.051	1.125	1.207
Σ_{f_1}	.0003285	.0002053	.00008467
Σ_{f_2}	.008997	.006359	.002771
Σ_{f_3}	.08481	.05282	.02170
WF	WFB	WF3	WF2

TABLE 7

THREE GROUP CONSTANTS FOR TEMPERATURE COEFFICIENT CALCULATIONS

N_u	9.18×10^{-5}	9.18×10^{-5}	9.18×10^{-5}	9.18×10^{-5}	9.18×10^{-5}	9.18×10^{-5}
N_{Al}	.0255	.0255	.0255	.0255	.0255	.0255
N_{D_2O}						
M/W	.73	.73	.73	.73	.73	.73
T, °C	30	50	100	150	200	250
Σ_{a_1}	.00029516	.00029516	.00029516	.00029516	.00029516	.00029516
Σ_{a_2}	.0070300	.0068770	.0066456	.0064497	.0062807	.0061331
Σ_{a_3}	.059985	.057172	.053152	.049911	.047286	.045050
Σ_{x_1}	.013770	.013691	.013280	.012719	.011955	.010977
Σ_{x_2}	.01102	.010965	.010709	.010353	.0098551	.0092106
D_1	1.3899	1.3947	1.4215	1.4595	1.5115	1.5838
D_2	1.6717	1.6801	1.7243	1.7869	1.8741	1.9989
D_3	1.0378	1.0572	1.1114	1.1771	1.2878	1.3934
Σ_{f_1}	.00044082	.00044082	.00044082	.00044082	.00044082	.00044082
Σ_{f_2}	.012064	.011792	.011321	.010942	.010595	.010284
Σ_{f_3}	.11372	.10838	.10075	.094611	.089654	.085434
	WF	WFB	WFB	WFB	WFB	WFB

TABLE 8

THREE GROUP CONSTANTS FOR TEMPERATURE COEFFICIENT CALCULATIONS

ASSUMING BORIC ACID HOMOGENIZED

T, °C	19.45	84.12	163.12	259.75
E_{th}	.02518	.03075	.03756	.04587
N_u	9.18×10^{-5}	9.18×10^{-5}	9.18×10^{-5}	9.18×10^{-5}
N_{Al}	.0255	.0255	.0255	.0255
N_D	.03134	.030522	.028464	.024554
N_o	.01921	.018691	.017431	.015057
N_B	2.7×10^{-5}	2.619×10^{-5}	2.4400×10^{-5}	2.1202×10^{-5}
N_H	.00708	.00686	.006398	.005560
Σ_{a_1}	.00031121	.00031072	.00030967	.00030775
Σ_{a_2}	.0093337	.0088280	.0082596	.0076263
Σ_{a_3}	.080220	.071974	.064009	.056310
Σ_{x_1}	.027403	.026682	.024996	.021846
Σ_{x_2}	.020524	.020080	.018905	.016589
D_1	1.3446	1.3678	1.4270	1.5536
D_2	1.4209	1.4671	1.5461	1.7415
D_3	1.0287	1.1032	1.2165	1.4114
Σ_{f_1}	.00044082	.00044082	.00044082	.00044082
Σ_{f_2}	.012075	.011452	.010849	.010270
Σ_{f_3}	.11391	.10292	.093089	.084569
	WF	WFB	WFB	WFB

REFERENCES

1. R. R. Bate, L. T. Einstein, and W. E. Kinney, "Description and Operating Manual for the Three Group, Three Region Reactor Code for the ORACLE", Oak Ridge National Laboratory, January 13, 1955, CF-55-1-76.

2. J. H. Alexander and N. D. Given, "The Eyewash Program for UNIVAC", Oak Ridge National Laboratory, September 6, 1955, ORNL-1925.

3. C. W. Nestor, Oak Ridge National Laboratory, Private Communication.

4. A. M. Weinberg, T. E. Cole, and M. M. Mann, "The Materials Testing Reactor and Related Research Reactors", Geneva Paper P-490, July 12, 1955.

5. BNL-325, "Neutron Cross-Sections".

6. RH-1, p. 23, McGraw-Hill.

7. H. H. Clayton, "Pile Instability Due to Poison", July, 1946, TP-141.

8. W. H. McAdams, Heat Transmission, Second Edition, p. 168, McGraw-Hill.

9. J. E. Cunningham, Metallurgy Division, Oak Ridge National Laboratory, Private Communication.

10. H. Hurwitz, Jr., KAPL-753, 1952, Classified.

11. L. C. Noderer, "Temperature Dependence of the Neutron Diffusion Coefficient in Heavy Water", ORNL-CF-54-4-142, April 20, 1954.

12. A. Radkowsky, "Temperature Dependence of Thermal Transport Mean Free Path", ANL-4476, p. 89, July 5, 1950.

13. B. I. Spinrad, and Katsumi Tamaka, "Multigroup Parameters and Critical Calculations in D_2O Moderated Systems", Reactor Science and Technology, TID-2014, p. 104.

14. W. E. Kinney, Oak Ridge National Laboratory, Private communication.

15. RH-1, Table 1.5.62, p. 575.

16. RH-1, Table 1.5.55, p. 572.

17. L. G. Alexander, ORSORT Notes, Oak Ridge National Laboratory, 1956.

18. NDA-10-99.

19. APEX-176.

20. S. Glasstone, Principles of Nuclear Reactor Engineering, p. 603, First Edition, D. Van Nostrand, 1955.

21. Ibid, p. 599.

22. Gamble and Bell, ORNL-1620.

23. J. Moteff, APEX-176, 1954.

24. Handbook of Shielding and Heat Production Calculations for NRU-Reactor, CRR-578, p. 413.

25. T. Rockwell, Nuclear Reactor Shielding Manual, TID-7004.

26. K. O. Donelian, and J. R. Menke, MONP 379 (Classified).

27. Reactor Handbook, Volume 1, Unclassified, p. 590 and 592.

28. A. G. Ward, "The Problem of Flux Instability in Large Power Reactors", CRRP 657.